Advanced Raman Spectroscopy for Bioprocess Monitoring

vorgelegt von

Dipl.-Wirt.-Inf.

Martin Kögler

geb. in Potsdam

von der Fakultät III – Prozesswissenschaften

der Technischen Universität Berlin

zur Erlangung des akademischen Grades

Doktor der Ingenieurwissenschaften

- Dr.-Ing. -

genehmigte Dissertation

Promotionsausschuss:

Vorsitzender: Prof. Dr. Juri Rappsilber

Gutachterin: Prof. Dr. Janina Kneipp

Gutachter: Prof. Dr. Peter Neubauer

Gutachter: Dr. habil. Michael Maiwald

Tag der wissenschaftlichen Aussprache: 23.01.2018

Berlin 2018

Abstract

The Raman -effect was discovered almost 90 years ago. It took a long time until the importance of Raman spectroscopy was fully understood and accepted for process industrial applications. Still today the usage is limited to a small application area. During the last decades advances in the production of spectroscopic components have reduced the complexity of the instrumentation and further mediated a persistent decline in costs, thus making this technology available for a broader audience. The basic components of a Raman spectrometer are a monochromatic light source, typically laser, a Raman probe with optical fibres, a spectrograph and a detector which is connected to a measurement- and control PC. Raman spectroscopy is increasingly becoming a choice as analytical tool in bioanalytics. Most of biological samples are handled in aqueous form which challenges many other analytical techniques (e.g., infrared spectroscopy). Raman and its enhancement techniques are able to measure quality and quantity of compounds in liquid phase with no or very little interference of water. The quantity of a compound can be determined by the peak-intensity and the quality by the position in the measured spectrum. Another advantage is that Raman spectroscopy does not rely on extensive sample preparation and measurements can be carried out non-invasively by placing an immersion probe with fibre optics directly in the liquid media. A Raman measurement is conducted fast, within milliseconds, and multiple relevant process parameters from the same sample can be measured at the same time. The measurements can be performed in continuous mode, i.e. one after the other or with a delay in-between. The operator can determine the measurement interval and in this way the development of a process can be observed online and in real-time. Further important advantages of spectroscopic methods over many other biochemical and physical measurement tools are the robustness as they do not require assays and they are rather unsusceptible against variations of pH, temperature changes, vibrations and other process parameters. If there is no coating, colour or special treatment of the glass, some Raman set-ups allow measurements directly through the glass into the liquid phase. This option enables real process measurements without the need to disturb or contaminate the analytes. These experimental set-ups are in the focus of this thesis.

Despite great advantages of spectroscopic methods, the utilization is often complicated since the threshold values are often above what is required for screening. Besides the lack of sensitivity of conventional Raman in bioprocess applications, the major drawback of this technique so far has been the disturbance of the broad fluorescence background especially in biological samples.

The main objective of this thesis was to find solutions for increasing the limit of detection (LOD) for biomolecules, being capable to detect them during the course of the process reliably and being able

to diminishing background signals induced by sample- and matrix-related auto-fluorescence. The proposed solutions are mainly surface enhanced Raman spectroscopy (SERS), time-gated (TG) Raman spectroscopy and the combination of both.

This thesis had a rather broad scope ranging from biofilm detection on water membrane filtration processes, over low-concentration bacteria detection with various enhancement options to finally follow the course of cell culture media development during cultivations. The aim of the thesis is to show that in challenging bioprocess-environments, Raman spectroscopy can detect weak signals over the background-noise from fluorescence in combination with SERS-enhancement-sensor techniques and with the time-gated Raman technology in particular.

Zusammenfassung

Der Raman-Effekt wurde schon vor fast 90 Jahren entdeckt. Anerkennung und Akzeptanz dieser Technologie für den Einsatz in der Verfahrenstechnik brauchten eine lange Zeit, wobei derzeit die Anwendungsbereiche noch sehr beschränkt sind. In den letzten Jahrzehnten haben technologische Fortschritte in der Produktion von optischen Komponenten, insbesondere von Lasern und Detektoren, die Komplexität von Raman-Spektrometern erheblich reduziert. Kostenreduzierung von Komponenten und Vereinfachung der Instrumente ermöglicht jedoch ein breiteres Anwenderfeld.

Die Hauptkomponenten eines Raman-Spektrometers sind eine monochromatische Lichtquelle, typischerweise Laser, eine Raman-Sonde mit Lichtleitern, ein Spektrograph und ein Detektor, der mit einem Mess- und Steuer-PC verbunden ist. Die Raman-Spektroskopie wird zunehmend als analytisches Instrument in der Bioanalytik eingesetzt. Die meisten biologischen Proben werden in wässriger Form behandelt, was viele andere analytische Techniken (z.B. Nahinfrarotspektroskopie) herausfordert. Raman und insbesondere die oberflächen-verstärkte Raman-Spektroskopie (SERS) sind in der Lage, organische und anorganische Verbindungen in flüssigen Proben ohne großen Einfluss der Wasserbanden zu charakterisieren. Unter konstanten Messbedingungen ermöglichen Raman und SERS auch die Quantifizierung von Komponenten in der Probe. Hauptsächlich ermöglicht SERS aber die Bestimmung von Komponenten in sehr geringen Stoffkonzentrationen. Die Quantität eines Stoffes kann durch die Peak-Intensität und die Qualität durch die Position der Peaks im gemessenen Spektrum ermittelt werden. Ein weiterer Vorteil ist, dass die Raman-Spektroskopie nicht eine umfangreiche Probenvorbereitung benötigt und Messungen nicht-invasiv durchgeführt werden können. Eine faseroptische Raman-Sonde (spezielle Tauchsonde) kann auch für den Einsatz direkt in flüssigen Medien benutzt werden. Eine Raman-Messung kann sehr schnell (innerhalb von wenigen Millisekunden) durchgeführt und es können mehrere relevante Prozessparameter gleichzeitig bestimmt werden. Die Messungen können kontinuierlich, nacheinander oder in bestimmten Zeitintervallen durchgeführt werden. Auf diese Weise kann die Entwicklung eines Prozesses online und in Echtzeit beobachtet werden. Weitere wichtige Vorteile spektroskopischer Methoden gegenüber vielen anderen biochemischen und physikalischen Messwerkzeugen sind die Robustheit, da sie keine speziellen Assays erfordern, und sie sind eher unempfindlich gegenüber Variationen von Prozessparametern wie z.B. pH, Temperaturänderungen, Druck und Vibrationen. Falls es keine Beschichtungen, Einfärbungen oder spezielle Behandlungen des Glases gibt, erlauben einige Raman-Aufbauten Messungen direkt durch Glas in das flüssige Medium, z.B. durch Glasbehälter oder Küvetten. Diese Optionen ermöglichen reale Prozessmessungen von Proben ohne die Notwendigkeit die

Analyten zu stören oder zu kontaminieren. Neben Durchflusszellen stehen diese experimentellen Aufbauten im Fokus dieser Arbeit.

Trotz großer Vorteile der Raman-Spektroskopie, ist die Realisierung robuster Messergebnisse oftmals kompliziert, da die Schwellenwerte der Stoffkonzentrationen von den meisten Analyten in Bioprozessen oft unterhalb der Nachweisgrenze liegen. Neben dem Mangel an hoher Empfindlichkeit von konventionellem Raman bei Bioprozessanwendungen war der größte Nachteil dieser Technik bisher die Störung des breiten Fluoreszenzhintergrundsignals, welches das eigentliche Raman-Signal zum Teil stark überlagert.

Das Hauptziel dieser Arbeit war es, Lösungen für die Verbesserung der Nachweisgrenze (Limit of Detection, LOD) für Biomoleküle zu finden, um in der Lage zu sein, den Prozessverlauf und einzelne Organismen zuverlässig charakterisieren zu können. Die vorgeschlagenen Lösungen sind vor allem die oberflächenverstärkte Raman-Spektroskopie (SERS), die zeitaufgelöste (time-gate, TG) Raman-Spektroskopie und die Kombination beider.

Diese Doktorarbeit bearbeitet ein recht breites Feld von Anwendungen, angefangen von Biofilm-Erkennung auf Filtermembranen bei der Trinkwasseraufbereitung, über die Erkennung von Bakterien in sehr geringen Konzentrationen mit verschiedenen SERS Nanopartikeln und Oberflächensubstraten bis zur Messungen der Zusammensetzung von Zellüberstandproben während einer kompletten Kultivierung. Das Ziel dieser Arbeit ist es, in unterschiedlichen Einsatzfeldern von Bioprozessen zu zeigen, wie weiterentwickelte Raman-Spektroskopische Methoden eingesetzt werden können, um die sehr geringen biochemischen Signale vom störenden Einfluss der Hintergrundsignale, insbesondere der Fluoreszenz, unterscheiden und charakterisieren zu können.

Preface and acknowledgements

List of publications

I   Chapter 3.1

Real-time Raman based approach for identification of biofouling, **Martin Kögler**, Bifeng Zhang, Li Cui, Yunjie Shi, Marjo Yliperttula, Timo Laaksonen, Tapani Viitala, Kaisong Zhang, Sensors and Actuators B 230 (2016) 411–421, (permitted post print).

https://doi.org/10.1016/j.snb.2016.02.079

II Chapter 3.2

Detection of Listeria innocua on roll-to-roll produced SERS substrates with gold nanoparticles, **M. Kögler** (eq.), S. Uusitalo (eq.), A.-L. Välimaa, A. Popov, Yu. Ryabchikov, V. Kontturi, S. Siitonen, J. Petäjä, T. Virtanen, R. Laitinen, M. Kinnunen, I. Meglinski, A. Kabashin, A. Bunker, T. Viitala and J. Hiltunen, RSC Adv., 2016, 6, 62981–62989, (permitted post print).

https://doi.org/10.1039/C6RA08313G

III Chapter 3.3

Bare laser-synthesized Au-based nanoparticles as non-disturbing SERS probes for Bacteria Identification, **Martin Kögler** (eq.), Yury V. Ryabchikov (eq.), Sanna Uusitalo, Alexey Popov, Anton Popov, Gleb Tselikov, Anna-Liisa Välimaa, Ahmed Al-Kattan, Jussi Hiltunen, Riitta Laitinen, Peter Neubauer, Igor Meglinski and Andrei V. Kabashin (Journal of Biophotonics – accepted manuscript, permitted preprint).

https://doi.org/10.1002/jbio.201700225

IV Chapter 3.4

Comparison of time-gated surface enhanced Raman spectroscopy (TG-SERS) and classical SERS based monitoring of Escherichia coli cultivation samples, **Martin Kögler,** Andrea Paul, Emmanuel Anane, Mario Birkholz, Alex Bunker, Tapani Viitala, Michael Maiwald, Stefan Junne and Peter Neubauer, (Biotechnology Progress – submitted manuscript, permitted preprint).

In all the publications listed here, I was responsible for the design and realization of the experimental work, interpretation of the results and did the main part of writing apart the paper: "Detection of Listeria innocua on roll-to-roll produced SERS substrates with gold nanoparticles" published in RSC (Uusitalo et al. 2016) and accepted manuscript: "Bare laser-synthesized Au-based nanoparticles as non-disturbing SERS probes for Bacteria Identification", where I equally shared the work with the first respectively second mentioned author.

Article I is reproduced by permission of Elsevier, Sensors & Actuators, B: Chemical, II is reproduced by permission of the Royal Society of Chemistry, III was submitted to the Journal of Biophotonics and permission for reproduction have been enquired and IV has been submitted to the Journal of Biotechnology Progress for which permission for reproduction have been enquired as well.

Author's contributions

I   The author had contributed in the original idea, performing the measurements, the design and implementation. The author contributed in the setting up of instrumentation, producing the gold nanoparticles and manufacturing of the designed flow-cell set-up. The author performed the data analysis and writing of the manuscript.

II The author and equally contributing second author conceived and performed the SERS measurements. The author has planned and performed the fabrication of the gold nanoparticles. Both, the author and equally contributing second author contributed in the data analysis and writing of the manuscript.

III The author and equally contributing second author conceived and performed the measurements. The author conceived SERS and Time-Gate Raman measurements as well in the bacterial research referred to it.

IV The author performed all measurements and reference analytics. The Author and the second author contributed in the data analysis and writing of the manuscript.

Contents

List of abbreviations and symbols

2D	Two-dimensional
3D	Three-dimensional
Ag	Silver
Ag NPs	Silver nanoparticles (AgNP)
ATR	Attenuate total reflection
Au	Gold
Au NPs	Gold nanoparticles (AuNP)
CARS	Coherent anti-Stokes Raman spectroscopy
CCD	Charge-coupled device
CMOS	Complementary metal–oxide–semiconductor
CSLM	Confocal scanning laser microscopy
CW	Continues wave
FTIR	Fourier transform infrared spectroscopy
HPLC	High-performance liquid chromatography
ICCD	Intensified Charged Coupled Device
ICORS	International Conference on Raman Spectroscopy
IR	Infra-red or infrared absorption spectroscopy
LabVIEW	Laboratory Virtual Instrument Engineering Workbench (software)
Laser	Light amplification by stimulated emission of radiation
LOD	Limit of detection
LSPR	Localised surface plasmon resonances
Nd:YAG	Neodymium-doped yttrium aluminium garnet
Nd:YVO$_4$	Neodymium-doped yttrium orthovanadate
NIR	Near infra-red
NMR	Nuclear magnetic resonance
NP	Nanoparticle
MATLAB	Matrix laboratory (software)
MVDA	Multivariate data analysis
PAT	Process analytical technology
PCA	Principal component analysis
PLSR	Partial least squares regression
R2R	Roll-to-roll
RS	Raman spectroscopy
SERDS	Shifted-excitation Raman difference spectroscopy
SERS	Surface-enhanced Raman Spectroscopy

SNR   Signal-to-noise ratio

TG   Time gating (time-gated Raman spectroscopy), abbreviated as TG-Raman

TG-SERS Time-gated surface-enhanced Raman Spectroscopy

VTT   Valtion teknillinen tutkimuslaitos, eng. Technical Research Centre of Finland

λ   Wavelength of the laser

cm^{-1} Raman shift (common expression for the shift from the excitation frequency, it does imply the $\Delta\ cm^{-1}$)

1.   Introduction

This thesis is covering conventional Raman using continuous wave (CW) laser excitation, SERS and time-gated Raman using pulsed laser excitation in combination for different project applications which are related to the detection of small biomolecules and the study of their growth-mechanisms in aqueous environments. Raman spectroscopy is a growing field with high importance in the area of process analytical technology. A major part of biotechnology is process analytical technology (PAT) with high importance for biopharmaceutical production. It has an increasing demand of monitoring in the area of quality by design (QbD) for the industrial scale especially in the pharmaceutical sector (Classen et al., 2016). Until now, Raman technology has not yet shown its full potential in process online monitoring, mainly due to auto-fluorescence of the measured sample which is the major disadvantage of this spectroscopic technology. Fluorescence is a specific form of photoluminescence (light re-emission of molecules after absorption of photons).

According a VTT-study, Raman spectroscopy is one of the most promising at-line and online PAT-tools in biopharmaceutical production, but it is often ruled out by the fluorescence problem (Streefland et al., 2013). Nevertheless, standard process Raman spectrometers possess the advantage that they can measure reliably and relatively fast changes of samples, e.g., culture broth in biotechnological and biopharmaceutical processes compared to other detection methods. The Raman effect is a weak optical phenomenon. From about 10^7 excited photons which excite a molecule there is one Raman photon (Smith and Dent, 2005). A major advantage of Raman spectroscopy is that it allows for measuring the quality and quantity of compounds in liquids where other optical methods often to fail, since the Raman signal has only little interference from water (Baranska, 2014; Smith and Dent, 2005). Raman spectroscopy needs an enhancement to compete with other biological detection methods if the concentration of compounds is low. Already in the 1970s, Martin Fleischmann's group observed an enormous enhancement of the Raman signal when pyridine molecules were adsorbed on a silver electrode surface (Fleischmann et al., 1974). Later this phenomenon was named as SERS (surface-enhanced Raman spectroscopy) after it was confirmed and described by several groups (Albrecht and Creighton, 1977; Jeanmaire and Van Duyne, 1977). SERS significantly enhances the Raman signal compared to the normal Raman signal and showed that it can be used for single-molecule detection (Kneipp et al., 1997; Smith and Dent, 2005). It brings nobel metallic nanoparticles or roughened metal structures to a dipolar localized surface plasmon resonance when in contact with molecules of interest (Li and Xu, 2016). SERS can clearly improve the limit of detection (LOD) and can also quench the auto-fluorescence to

some extended but not completely (Schlücker, 2014). However, the disturbance from background signals such as the auto-fluorescence makes the measurement often impractical and useless. Another advanced Raman spectroscopic technique for fluorescence suppression is time-gated Raman (TG) which enables the detection of the Raman signal before the stronger fluorescence and other disturbing signals, such as room light and cosmic rays arrive at the detector. This happens due to fast gating or in other words, short duty-cycle of detection. This principle is not particularly new but the implementation into a compact, portable and process spectrometer-based technology has just happened recently (Kostamovaara et al., 2013; Rojalin et al., 2016). The aim of the thesis is to show that in challenging bioprocess-environments, advanced Raman spectroscopy can detect weak signals over the background-noise from fluorescence in combination with SERS enhancement-sensor techniques and time-gated Raman technology in particular.

1.1 Raman spectroscopy set-up for bioprocess related measurements

A process Raman spectrometer generally consist of the following components: (1) light source, typically a monochromatic light source such as laser of a specific wavelength, (2) fibre-optical Raman probe which in some cases can be protected with special sleeves or a sealing to be directly immersed into the process, (3) spectrograph with suitable grating and optical components (filters) for the specific wavelength, (4) detector, (5) measurement and control-computer with spectroscopy software, (6) optical fibre cables up to several tens of metres and the (7) sample for inspection. This set-up is referred as "process Raman spectrometer" as shown in Fig. 1 in two configurations, (A) without a confocal microscope attached and (B) with a microscope attached by using an adapter.
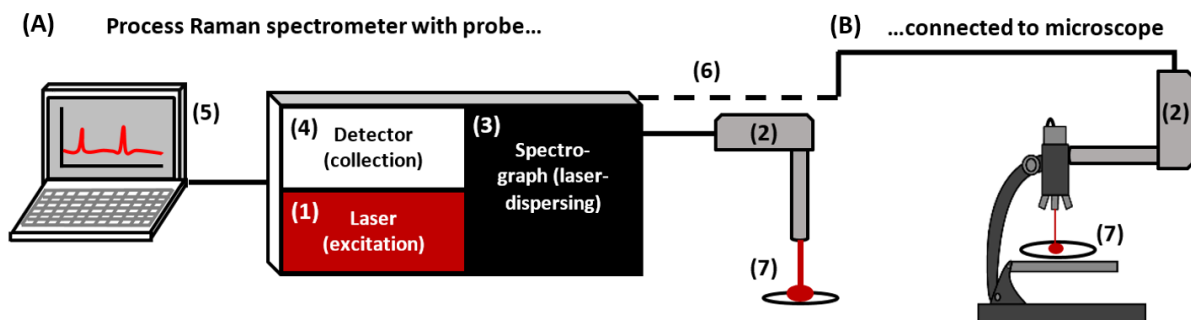
Figure 1 – Basic set-up of a process Raman spectrometer with (A) standard fibre-optical probe and with (B) same probe and adapter connected to a confocal microscope.

Fig. 1 symbolizes the set-up and requirements of parts used for a process Raman spectrometer (CW- and TG-Raman). The configuration (A) and (B) has been used for the studies shown in the Chapters 3.1 to 3.4. A hand-held Raman, i.e., used in field-measurements for forensics and military purposes does not differ much in comparison to the representation shown in Fig. 1A besides in size and its performance (Chalmers et al., 2012). Moreover the set-up of the measurement often differs depending on the task and analytes to be measured and it is important that a standard process Raman spectrometer can be adapted easily to any kind of measurement task. SERS can be even performed with a simple and low specification Raman spectrometer, as presented in Chapter 3.1 (Buckley and Ryder, 2017). If the measurement requires high spatial accuracy, only little effort is needed i.e., turning a process Raman spectrometer into a confocal Raman microscopy set-up with adding a commercially available adapter into the optical pathway, typically between ocular und lens-mount Fig. 1B. Often the same fibre-optical Raman probe is used. An additional advantage turning the process Raman spectrometer into a confocal set-up is (i) the option to perform spectral mapping within XY-plane and (ii) depth profiling with focal change of Z-direction which becomes useful for cell-analysis (Procházka, 2016). The focal point, respectively the spot-size with the confocal Raman set-up (Fig. 1B) is typically in the order of 10-20 fold smaller, depending on the chosen magnification lens, than with the default probing system not attached to the microscope (Fig. 1A). This is indicated in Figure 1 with the different size of the red dot on the sample. The difference of the focal spot size has an effect to the enhancement of the Raman signal with metallic nanoparticles in the SERS configuration, which is discussed in detail in Chapter 3.4. Furthermore, related to this fact, it is more difficult to use a dedicated Raman microscope for process-related set-ups. However, e.g., flow-cell measurements in connection to antibody-captured *Escherichia coli* bacteria studies have been reported (Knauer et al., 2012).

1.2 Raman, SERS and Time-Gated Raman in context for bioprocess measurement tasks

The Raman effect was named after the Indian physicist Sir C.V. Raman who received in 1930 the Nobel Prize in Physics for his work on inelastic light-scattering properties of matter (Krishnan and Shankar, 1981). Soon after the discovery and long before laser have been available, the Raman analysis of amino acids and related compounds was performed by John T. Edsall and published in 1937 (Edsall, 1937). The invention of laser by Charles H. Townes, Nikolay Basov, and Alexander Prokhorov who received the shared Nobel Prize in Physics in 1964 accelerated the development of Raman spectrometers (Procházka, 2016). Another major milestone in analytical research was the discovery of SERS. In 1974 Martin Fleischmann showed the feasibility for the Raman signal enhancement which is seen as the groundwork of SERS (Fleischmann et al., 1974). Like for Raman spectroscopy, it took still years that the potential of the SERS was employed using patterned and roughened surface structures, electrodes or colloidal nanoparticles for liquid analytes. The effect is related to the excitation of localized surface plasmon resonances (LSPR) and it enhances the classic Raman signal between 10^4-10^{10} fold when molecules of interest are in close proximity to metallic surfaces or nanoparticles (cf., Fig. 6). Besides the strong enhancement, SERS can quench fluorescence to some extent but high fluorescence is still limiting the adaptation (Dulkeith et al., 2005; Mayilo et al., 2009; Smith and Dent, 2005; Vielma and Leung, 2007). On the side of the development of detectors, the development of transistors paved the way for the enormous development of imaging devices. Willard Boyle and George E. Smith received in 2009 the Nobel Prize for Physics for their invention of the CCD of which the development started in 1969 (Smith, 2009). Scientific CCDs are the principal component of a common Raman spectrometer. Despite the ground-breaking invention of the CCD and the further device miniaturization of instruments it has been deprecated by modern CMOS-technology (Fossum, 1993; Hain et al., 2007). Recently modern CMOS SPAD (complementary metal–oxide–semiconductor single photon counting avalanche diode) technology had become available which further reduces size and complexity, i.e., no detector cooling is necessary but most importantly the sensitivity is increased compared to scientific CCD's and additionally the arrival times of the photons can be temporally discriminated. Originally SPAD-detectors have been used as single photon detecting and counting devices but modified, they enable the commercial use of the time-gating principle for Raman detection to mainly reduce the major error-source in Raman measurements, namely the sample-related auto-fluorescence (cf., Fig. 2), which will be further discussed in section 1.3 (Kostamovaara et al., 2013; Mogilevsky et al., 2012; Nissinen et al., 2011). Within this thesis the terms time-resolved and time-gated Raman will be used as synonyms.
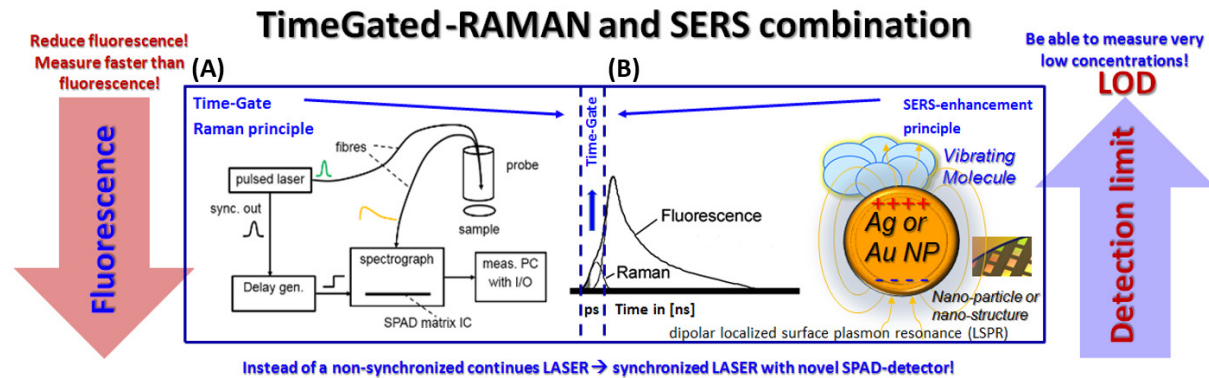
Figure 2 – Overview of Time-Gate Raman and SERS (TG-SERS) in combination to reduce the influence of fluorescence background signal and increase the Raman signal, achieving improved LOD. TG-SERS set-up includes: (A) pico-second pulsed laser excitation and time-gated SPAD detection with and (B) an area by area discrete scanning of the functionalized parts of the SERS.

Infra-red (IR) and Raman in visible and near-visible spectral regions are two important vibrational spectroscopies being able to detect molecular vibrations and to draw the chemical information of the analyte of interest. Besides providing characteristic information of spectral patterns (qualification), they enable the quantification of the amount from the analyte. This is because of the amount of the analyte is directly proportional to the concentration due to the Lambert-Beer law (Gordon, 1989). The concentrations of multiple components in samples of complex matrices are identifiable as long as the spectral peaks are not overlapping. However, both techniques, IR and Raman, provide a complementary view because of the different vibration of molecules and selection rules, hence the chemical information of a Raman spectrum is unique (Baia et al., 2008). A process Raman spectrometer allows the use of optical fibres up to several tens of metres for distance detection and the use of immersion probes enabling measurements directly in the liquid phase. This makes Raman more attractive for the observation of component and concentration changes in bioprocesses compared to NIR or MIR (Classen et al., 2016; Jestel, 2010; Lee et al., 2004; Smith and Dent, 2005).

1.3 Raman spectroscopy

1.3.1 Theoretical aspects

Samples at any state of aggregation can be analysed by RS. This depends on the cross-section and the amount of molecules in a given volume. In gasses the molecular cross-section is rather small and that is why RS is not much applied. Partly this has been overcome by specially developed gas-cells and techniques similar to radar such as the LIDAR (Philbrick, 1994; Smith and Dent, 2005). Despite this fact, most of process-related Raman applications focus on analysing solids and especially liquid samples. Typically RS is performed with the light excitation source being a monochromatic one. A stable laser without wavelength drift and steady intensity is a requirement, but RS can be performed with inexpensive LEDs as well, which in this case requires sharp optical bandpass or notch filters and the detection may be less efficient (Schmidt and Kiefer, 2013). RS provides similarly to IR spectroscopy the information about the scattering and rotation of molecules when they are excited by photons (cf., Fig. 3). However, the physical principle differs between Raman and IR absorption spectroscopy as well as the excitation of the sample, indicated in Fig. 3.

Compared to IR spectroscopy (FIR, NIR, MIR) RS has several advantages, the insensitivity to water and it can be applied for the measurement through containers, glass (if not coloured or coated) and even blisters and pills when making use of the spatially offset Raman spectroscopy (SORS) method (Matousek and Parker, 2007). The Raman effect can be briefly described by the frequency shift of an incoming incident photon. In other words, photons which make up light are either absorbed, scattered or passed through the sample without interaction. In case of interaction in form of absorption, the photon's energy equals the energy gap between the molecules ground state and its excited state. IR absorption spectroscopy measures this change. RS on the other hand measures the case that the photon interacts with the molecule and scatters inelastically from it. In the Raman case the photon does not have to match with the energy difference between the molecule's ground and excited stage which makes the fundamental difference to IR absorption spectroscopy (Smith and Dent, 2005). A profound consolidated mathematical description of the Raman effect is out of scope of this thesis. The interpretation of the molecular energy levels is well described in Perrin-Jablonski energy diagram, cf., Fig. 3.

6
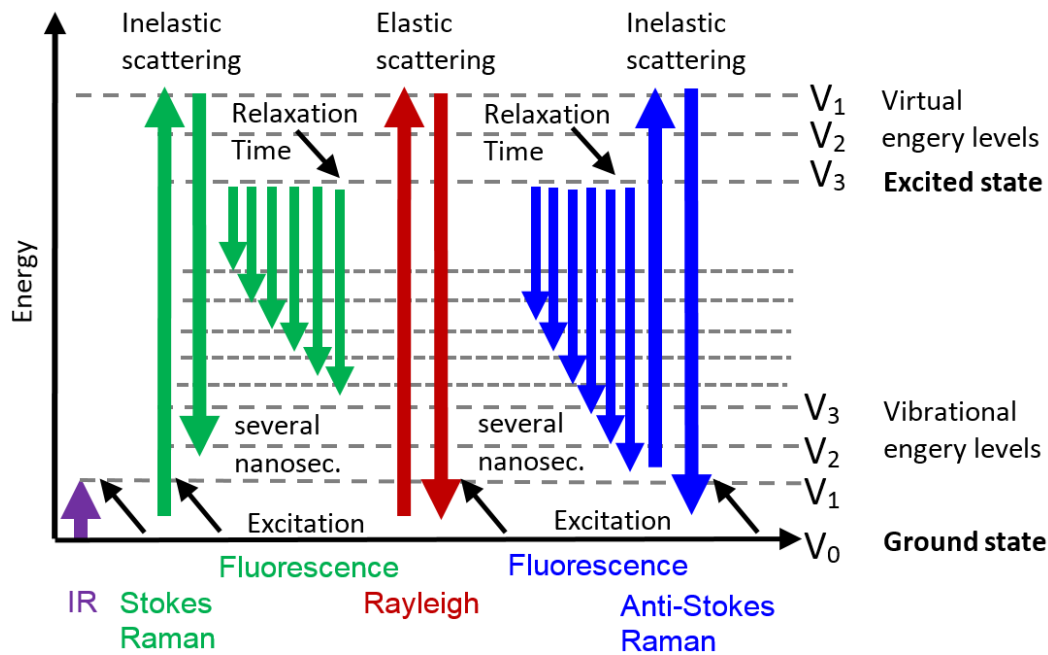
Figure 3 – Raman (Stokes and Anti-Stokes) scattering, Rayleigh scattering, fluorescence and infrared absorption (IR) as own interpretation of Perrin-Jablonski molecular energy levels.

Simplified, Raman scattering can be described with vibrational shifts. When photons interact with molecules most of the energy is scattered elastically and the energy is released without a frequency shift from the incoming energy (Rayleight scattering), only a small faction is scattered inelastically (Stokes and Anti-Stokes shift) which when generates Raman scattering. This can be described with vibrational shifts: V_1 = excited energy stage; V_0 = non-excited energy stage (cf., Fig. 3 and Fig. 4); V_s = wavelength shift; V_R^+ = Anti-Stokes shift Raman scattering and V_R^- = Stokes shift Raman scattering (Demtröder, 2007). If the incoming light V_1 (excited energy) equals V_0 and thus has the same wavelength, Rayleigh scattering appears and no wavelength shift happens, cf., Fig. 4. Very few photons, approximately only one from about 10^6–10^8 photons is scattered inelastically, representing that Raman scattering is a weak phenomenon (Smith and Dent, 2005). These photons cause a frequency shift at a different wavelength, either at V_R^- (molecule absorbs the photon and re-emits it at a lower energy than the absorb one) or V_R^+ (molecule loses energy and re-emits the photon at a higher energy than the absorb one). The resulting peaks are the energy loss of the photons as Stokes- and Anti-Stokes-shift, appearing with higher respectively lower frequency shift. RS typically does not consider Rayleigh scattering, on the other hand it is used as the start of the Raman spectrum. Commonly the Stokes shifted Raman molecules are considered in classical RS because their intensity is higher compared to Anti-Stokes shift due to increased probability of the molecule being at ground stage given by the Bolzmann-distribution

(Procházka, 2016). Otherwise Stokes and Anti-Stokes Raman spectra are symmetrical and have identical peaks. The high intensity laser line, the Rayleigh scattering and point of origin in the diagram is filtered out in most common Raman instruments, so that only the Stokes-shifted Raman, the shift from the laser excitation source towards the longer wavelengths is presented with the Raman spectrum as "Raman shift", written as "cm^{-1}" or "1/cm". It is typically shown with an off-set of a few hundred wavenumbers away from the excitation frequency. The off-set is due to the fact that common band-pass or laser-line filters in the collection optics are not able to perfectly remove the strong laser-line at $0\,\text{cm}^{-1}$. The Raman spectrum is generally displayed in a *XY*-diagram were the intensity of the spectrum represents the *Y*-value on the ordinate and the range of wavelength shift from the laser as Raman shifts on the abscissa as *X*-values. The reason that Raman spectra are often shown with high wavenumbers starting at the point of origin is a matter of a generally not respected convention.
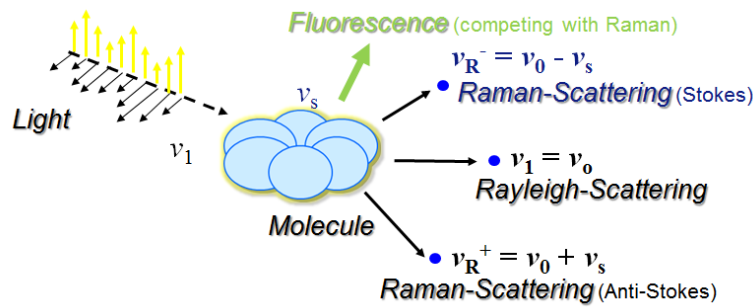
Figure 4 – Fundamentals of Raman scattering.

1.3.2 Influencing factors on Raman measurements

The intensity of the Raman signal (I) is proportional to the 4$^{\text{th}}$ power of the laser frequency (f^4), the intensity of the laser radiation (I_L), the amount of scattered molecules (N) and the polarizability change $\left(\delta_\alpha / \delta_\text{q}\right)$ as described in equation [Eq. 1].

$$I \sim f^4 \times I_\text{L} \times N \times \left(\frac{\delta_\alpha}{\delta_\text{q}}\right) \qquad \text{[Eq. 1]}$$

$$I \sim \left(\frac{1}{\lambda^4}\right) \qquad \text{[Eq. 2]}$$

The 4th power-rule describes that the efficiency of the Raman signal increases with the fourth power of the frequency of the incident light. Or in other words the Raman intensity is reverse proportional to

the 4th power of the excitation wavelength which is further symbolized in Fig. 5. Scattered Raman photons can be observed by collecting monochromatic light at an angle to the incident light, assuming that no absorption from other electronic transitions appears (Smith and Dent, 2005). Furthermore, the quality of the Raman signal detection is depended on several factors. The interference factors are: (1) fluorescence or photoluminescence, (2) surrounding lights, (3) shot noise which is sometimes also called detector noise and (4) cosmic rays. Fluorescence (1) and surrounding lights (2) appear as a broad interference, covering the whole range of the displayed Raman spectrum. Even though fluorescence is the main disturbing influence factor in RS, it can be avoided by several solutions. The measurement in another wavelength area, far away from the fluorescence-maximum at around 530 nm, e.g., in the UV-area will yield in fluorescence-free results. Because of:

$$E \ = \ h \ \times \ f = h \ \times \ \frac{c}{\lambda} \qquad\qquad \text{[Eq. 3]}$$

With (E) energy of the excitation radiation; (h) Planck constant; (f) frequency; (c) speed of light; (λ) wavelength (characterization of radiation).

Unfortunately, due to the 4th power-rule, the Raman sensitivity is extenuated in the UV region so that the return of Raman scattering is weak compared to the risk of sample degradation for organic materials (Blacksberg et al., 2016). The same applies to Raman measurements in the IR-region with common 1064 nm spectrometers which can be seen in Fig. 5. The best compromise with respect to common CCD detector sensitivity (quantum efficiency) seems the NIR spectral region, away from fluorescence maximum for Raman measurements around 785 nm as shown in Fig. 5.

Common Raman laser wavelengths in nanometers

λ_{exc} = 532 … 633 … 785 … 830 … 1064

High fluorescence   Low fluorescence

High sensitivity*   Low sensitivity*
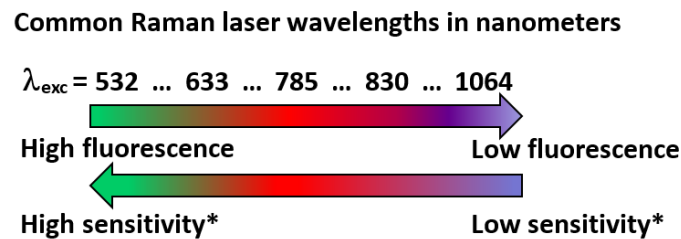
Figure 5 – Influence of fourth-power rule (*) and fluorescence with respect to common Raman excitation wavelengths.

Other solutions for minimizing the fluorescence influence are, e.g., (1) chemical sample bleaching, (2) frequency variable laser excitation sources, (3) the optical Kerr gate, (4) Streak-camera or gated ICCDs, (5) SERDS, (6) CARS, (7) SERS, and (8) time-gated Raman. The first solution (chemical sample bleaching or photobleaching) is a well-established laboratory practise to destroy chromophores irreversibly which often make up fluorescence in a sample over a time-frame of several minutes (Golcuk et al., 2006). This may only work for certain samples and it induces changes of the chemical property. The risk is that the sample might be degenerated or burned and thus is not applicable for biological samples. The second solution takes into account the 4th power-rule of equation [Eq. 2] and the relation between fluorescence and Raman sensitivity as shown in Fig. 5. A frequency tuneable laser excitation source is used in combination with optical components which are suitable for a broad wavelengths range. The drawback is that typically the sensitivity maximum, or rather the quantum efficiency of common CCD-detectors (characteristic curves are available from each vendor) which are suitable for Raman detectors is in a wavelength range between 500 and 850 nm (Coles et al., 2017).

The third solution solves the fluorescence problem by applying short temporal gates and consists of a high-speed optical shutter, but the equipment has huge space requirements, cf., Chapter 1.5.1. The forth solution includes the streak-camera principle, a high-speed multi-channel detector original meant for imaging purpose, an intensified and gated CCD (ICCD) in combination with a mode-locked laser. The disadvantages here are the high supply voltage above 1000 V to be able to form a pulse to be fed for the gating purpose, high instrumentation costs and additionally the other background noise originating from heat due to electron-multiplication of the detector which limit the SNR and disturb the measurements. SERDS a differential technique based on periodical wavelength modulation, taking into account that fluorescence is slower than the modulation as a fifth solution is very promising since it does not require a drastic change of standard components of a common Raman spectrometer (Sowoidnich and Kronfeldt, 2012). As an example fluorescence-free Raman spectra were observed

from high-fluorescent extra-terrestrial samples by modifying a standard Raman microscope with a tuneable microsystem diode laser to perform SERDS (Böttger et al., 2017). Coherent anti-Stokes Raman spectroscopy (CARS) as a sixth solution makes use of two pulsed laser sources where, e.g., a UV-laser enhances the fluorescence-free Raman signal (Rodriguez et al., 2006). The seventh (SERS) and eighth solution (TG) are integral part of this thesis, so the main focus within this thesis was in the individual and combined use of these techniques, thus they are described in more detail in the following sections. Generally for Raman, unlike for many other techniques, there is no need for sample preparation or optical transparency (Baranska, 2014). A stable Raman instrument set-up is compulsory prior any measurement, involving a short moment of time spent (unlike for TG-Raman) to cool CCD-based systems to operational detector cooling temperature (commonly between -20 to -60°C) and to check the laser-power output on Raman probes or microscope-lenses. Other influencing factors besides from software and hardware of the data acquisition instrument itself are: the adjustment of the focus onto the sample (tight/inside focus to the same, off-the-focus conditions), if there are fingerprints on the sample-containing glass cuvette which could cause fluorescence or other contaminants on the sample-carrier, the length and condition (bending radius or accidental fingerprints on fibre-tips) of the optical fibres or objectives in case of a microscope set-up (dirt on the lens), the stability of the laser, no drift in the excitation wavelength causing spectral drifts, and the laser power itself. In short, these adjustments and spectral calibrations are required in order to carry out good measurements in practise.

1.4 SERS

1.4.1 General overview

Surface-enhanced Raman spectroscopy as indicated by the name is an extension of RS. SERS has boosted the analytical research in large scale as cross-disciplinary analytical technique. It is at the moment dominating the field of Raman spectroscopy research in general, and has since its discovery increased exponentially based on the number of publications from 40 years ago until today (Cialla et al., 2012; Graham et al., 2017). Any Raman or Raman related conference such as International Conference of Raman Spectroscopy (ICORS) are dominated by new topics in SERS research. This has been achieved by a strong, broad and consequently growing international community pioneered by prof. Fleischmann, prof. Tian, prof. Moskovits, prof. Van Duyne, prof. Kneipp and prof. Popp. The success of SERS is mainly due to (1) the enormous enhancement of the Raman signal by millionfold when Raman active molecules are close to a metallic SERS active surfaces or colloids (Haynes et al., 2005); (2) the possibility to quench the disturbing fluorescence to some extend which was confirmed by Gersten–Nitzan model

and the Mie scattering theory (Cardinal et al., 2017; Geddes, 2017); (3) depending on the Raman configuration and laser excitation different kind of metallic enhancement materials such as silver, gold, or copper at visible light with huge potential on substrates but also in colloidal form and aluminium, platinum, palladium at UV spectral range (with limited applicability) can be used, enabling this technique to be applied in almost any kind of Raman set-up (Cardinal et al., 2017); (4) reduced photodecomposition and photobleaching of the sample compared to RS (Kneipp et al., 1997) and (5) even very inexpensive substrates such as paper-based ones (C. H. Lee et al., 2011). As a consequence, research areas of SERS are very broad: physics, chemistry, biophysics, biomedical, biopharmaceutics, bioanalytics, life science, forensic science, biophotonics, environmental and pollution detection, nanoscience and nanoparticle research, food- and safety, biofilm/biofouling detection and last-mentioned biotechnology. The latter four areas are part of this thesis with the focus on the detection of bacteria and conditional change of their surroundings.

1.4.2 Mechanisms of the enhancement

The enhancement of the Raman signal can be described by two proposed mechanisms, the electromagnetic (EM) enhancement mechanism and the charge transfer mechanism (CTM) which are important for understanding the relation between light and metallic nanostructures responsible of the LSPR (Cardinal et al., 2017). These nanostructures may be colloidal nanoparticles in solutions or on roughened and patterned surfaces, cf., Fig. 6. Commonly more accepted is EM due to the involvement of just photons and nanostructures (Schlücker, 2014). EM shall be considered as synonym of LSPR. An EM enhancement takes place when molecules are in close proximity to metal nanostructures and photons excited from the laser source are interacting with both the molecules and the nanostructure. This causes an electromagnetic resonance in such a way that firstly a local field enhancement of the laser occurs due to the polarizability of the metal nanostructure, and secondly the molecules re-emit this energy as electromagnetically amplified Raman signal. (Baia et al., 2008; Smythe et al., 2009). In short, EM amplifies both excitation and emission of the radiated Raman signal, cf., Fig. 6 (Cardinal et al., 2017).

(A) LSPR on NP

Monochromatic light

Nanoparticle which re-emits radiation at same frequency as incoming ω_{inc}

Electromagnetic wave Excitation

ω_{inc} angular frequency

E_0 amplitude

AgNP or AuNP

NP in matrix

Charge separation

(B) LSPR on patterned surface

Stokes $\omega_{inc} - \omega_{vib}$
Rayleigh ω_{inc}
Anti-Stokes $\omega_{inc} + \omega_{vib}$

Vibrating Molecule

incoming ω_{inc}

outgoing $\omega_{inc} - \omega_{vib}$

LSPR-supporting metal nanostructure

Figure 6 – SERS effect as LSPR on (A) nanoparticle and on (B) supported metal surface (adapted with permission of Schlücker 2014).

The enhancement by CTM describes the enhancement through a chemical first adsorbate layer process as the adsorption of the molecule onto the roughened surface or nanoparticle (NP), which then further forms an adsorbate-metal complex. This assay changes the molecule's polarizability and thus enhances the Raman radiation (Baia et al., 2008; Cardinal et al., 2017). There are attempts to unify both proposed mechanisms (Lombardi and Birke, 2008).

Generally the enhancement is (1) distance dependent (NP colloids or patterned surfaces need to be in close proximity to molecules, namely in nanometre-scale distance; cf., Fig. 7) and depends on the orientation of the molecule (Schlücker, 2014); (2) relies on the match of laser excitation wavelength (Chase and Parkinson, 1991); (3) dependent on specific roughness, shape, size of the nanostructures which may result in a so called "hot spot" (Camesano, 2014; Nuutinen, 2014). This situation may occur when, e.g., two nanoparticles (NPs) are apart only a few nanometres and a boosted enhancement takes place due to the coupled LSPR of the molecules in the gap between the NPs, which is depicted in Fig. 7 (Šmídová, 2012).
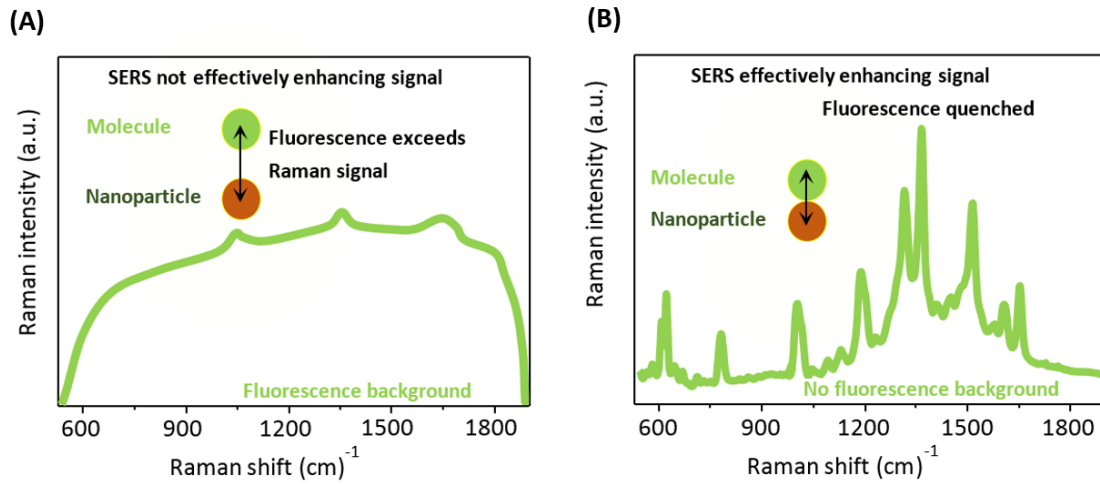
Figure 7 – SERS major advantage – distance dependency (A) molecule and NP colloid in far proximity without fluorescence quenching; (B) molecule and NP colloid in close proximity with fluorescence quenching and Raman signal enhancement.

Figure 7 denotes the major advantage of SERS compared to normal Raman scattering, which is the ability to quench the fluorescence depended on the above mentioned enhancement conditions and mainly the enormous boost of the Raman signal over the fluorescence.

Under some circumstances it may allow for single-molecule detection and an enhancement factor (EF) of ~10^{11} to 10^{14} can be achieved (Kneipp et al., 1997). The experimental enhancement factor or "analytical enhancement factor" (AEF) can be calculated by the product of the ratio between SERS and Raman Intensity (measured counts of Raman signal in stable condition) and the ratio of the measured concentration of SERS and Raman molecules, equation [Eq. 4] – (Habouti et al., 2010):

$$\text{AEF} = \left(\frac{I_{\text{SERS}}}{C_{\text{SERS}}}\right) \times \left(\frac{C_{\text{Raman}}}{I_{\text{Raman}}}\right) \qquad \text{[Eq. 4]}$$

In addition to SERS the CTM mechanism supports the resonance Raman spectroscopy (Thomsen and Reich, 2000).

1.4.3 Bioprocess related SERS substrates

Raman enhancement substrates respectively nanostructures for SERS can be either used for quantitative signal analysis with a high degree of reproducibility or for the detection of low concentration analytes with a maximum of sensitivity but rather poor reproducibility. According Procházka (2016), three categories of SERS substrates can be defined: (i) solutions of NPs, (ii) immobilized and assembled NPs on solid surfaces and (iii) nanostructures directly built on surfaces. How well a specific method performs can be depict from Table 1. It summarizes advantages and disadvantages of the different NP- and nanostructure types, and provides an overview which is based on Brown and Milton's table and further adapted from Procházka with permission (Brown and Milton, 2008; Procházka, 2016). Gold and silver, partially also copper as enhancement material are dominating because they generate optical conductive resonance, thus enhance Raman in the visible- and NIR-range and can be easily chemically synthesised (Li et al., 2017). Results in Chapter 3.2 shows how size distribution, uniformity, shape and material (chemically synthesised Au and Ag NPs and bare laser-synthesized) have a significant influence on the enhancement of the SERS signal. The enhancement effect of photo lithographically produced nanostructures was tested primarily and in combination of different NPs. Problems of biocompatibility and nanotoxicity are discussed and a solution, the bare laser-synthesized Au NPs for bacteria detection is presented in Chapter 3.3. Even though Ag NPs provide a stronger SERS-signal enhancement compared to Au NPs, nanotoxicity plays an important role (Alkilany and Murphy, 2010; Zeman and Schatz, 1987). Furthermore, due to slower aggregation and reaction with oxygen and increased biocompatibility, Au NPs are more stable and suitable for bioanalytical applications compared to Ag NPs, which is demonstrated in Chapter 3.1 (Cui et al., 2013; M. Fan et al., 2011; Hong and Li, 2013).

Table 1 – Performance comparison for different SERS methods.

	Method (NP or nanostructure)	Category	Sensitivity (enhance-ment)	Toxicity for cells	Reproducibility of measure-ments	Ease and cost of prepara-tion
1	Free chemically synthe-sized colloidal Au NPs	solution	good	moderate	poor	very good
2	Free chemically synthe-sized colloidal Ag NPs	solution	very good	high	poor	very good
3	Free bare laser-synthe-sized colloidal Au NPs	solution	moderate	low	moderate	good*
4	Templated Au NPs (evaporated superna-tant)	Solu-tion/solid	good	moderate	moderate	good
5	Unstructured metal sur-face	solid	poor	moderate**	poor	very good
6	Chemically roughened surface	solid	moderate	moderate**	moderate	very good
7	Lithographically pro-duced surfaces	solid	very good	moderate**	very good	good*
8	3D structured surfaces	solid	very good	moderate**	very good	poor

Ranking: very good, good, moderate, poor; good* = costs depend on production quantity (3 and 7); moderate** = toxicity depends on the used surface material Ag or Au (5 − 8) for enhancement (adapted from Brown and Milton 2008, and Procházka 2016 with permission).

1.5 Time-gated Raman spectroscopy

1.5.1 General overview

A major problem for RS and the detection of organic molecules is the often swamped or obscured Raman signal by fluorescence background (Zhang et al., 2010). The reason is the lower cross-section of Raman scattering compared to that of fluorescence (Matousek et al., 2001). However, this problem occurs especially with biological samples and contaminations. When using common CW-laser excitation at the a wavelength close to the fluorescence maximum, cf., Fig. 5, the sample-related auto-fluorescence radiation can be several orders of magnitude higher than that of Raman radiation (Holma et al., 2017). A selection of possible solutions to this problem are already mentioned in section 1.3.2. A comprehensive overview of all possible fluorescence suppression methods can be found in the state-of-the-art review of Dong Wei *et al*. Wei and co-workers divide these methods into three categories: (1) Time-Domain Methods; (2) Frequency-Domain Methods and (3) Wavelength-Domain Methods. Additionally spectral post-processing computational methods of fluorescence background removal can help to extract the obscured Raman signal since fluorescence background signal is much broader than Raman peaks. These methods are specifically polynomial fitting and wavelet transformation, further discussed in section 1.6 (Wei et al., 2015).

Time-resolved or time-gated (TG-) Raman in particular is an innovative solution since it can detect the Raman signal before the fluorescence arrives at the detector in "time-gating" principle. It belongs to the time-domain methods of fluorescence rejection which has its roots in the 1980ies. At that time it required a tremendous apparatus (Petrich et al., 1987). Earlier time-domain methods that have reached meaningful temporal resolution for fluorescence rejection, as optical Kerr gate (ps class) or fast gated ICCDs (100 ps class temporal resolution) have been based on components that are either physically too large or too expensive to be applied for commercially produced Raman instruments. Fluorescence can be efficiently rejected by applying the TG principle, based on the different temporal behaviour of Raman (less than one picosecond response time) and fluorescence signals (sample-depended time constant of the exponential decay is typically a few thousand picoseconds long) as shown in Fig. 8. Furthermore, Fig. 9A shows the laser excitation, the Raman response and the fluorescence signal. A common CCD-based CW-excitation Raman system measures in temporal regimes of seconds to minutes and the signal response is a convolution of both Raman and fluorescence signals. This can be seen in Fig. 9B and 9C with the extended delay time. In contrary to CW-Raman systems, the application of the TG principle is a pump/probe system in which the output of a pulsed laser excitation is

divided into two beams (Smith and Dent, 2005). Most of the excitation is fed to the Raman probe to excite the sample and the rest of the divided beam is fed to trigger the detector. Triggering allows a synchronization of laser and detector which enables the TG-principle, cf., Fig 2A. The measurement of the Raman signal can be completed during the period of the short laser pulse and most of the fluorescence is blocked out from the recorded spectrum since the lifetime of the fluorescence signal is longer than that of the Raman signal, comparing different gating-intervals in Fig. 9A and B (Blacksberg et al., 2016; Holma et al., 2017; Nissinen et al., 2017, 2011). Since one cycle of TG-Raman measurement (e.g., one picosecond gate) is not enough to record all Raman scattered photons with a sufficient SNR (cf., [Eq. 5]), the gate is opened and closed periodically within the short duty-cycle (time intervals of 250 microseconds are typical) to accumulate the return signal of a user-defined multitude of laser pulses. The laser pulse itself has a temporal width of around 100 picoseconds. In this way the probability of the rise-time of the fluorescence signal is decreased. Furthermore this benefits the baseline of the recorded Raman signal because the pure Raman scattering, resulting in an improved SNR compared to CW-Raman without or with reduced fluorescence is recoded. The temporal gating time to record the Raman scattering can be set depending on the sample-related fluorescence rise-time and decay-time, cf., Fig 9B and C. The number of Raman photons as well as the fluorescence photons are related to the shot noise as indicated in the equation [Eq. 5]. Furthermore, the total amount of Raman signal is the sum of the denominator under the square root.

$$\text{SNR} = \frac{N_{\text{Raman}}}{\sqrt{(N_{\text{Raman}} + N_{\text{Fluorescence}} + N_{\text{Dark count rate}})}} \qquad \text{[Eq. 5]}$$

Kostamovaara and co-authors have demonstrated with an example of highly fluorescent olive oil that when shortening the time gate, the detection probability for fluorescence is significantly decreased (Kostamovaara et al., 2013).

When choosing a specific time-gate (temporal position) with a specific width, e.g., shortly after the laser pulse but before the rising edge of the Raman and fluorescence signal, most of the fluorescence will be rejected. For highly fluorescent samples there will be always residual fluorescence in the chosen time-gate, e.g., this was observed with yellow fluorescence protein (YFP) sample, cf., Fig 8.

(A)

(B)
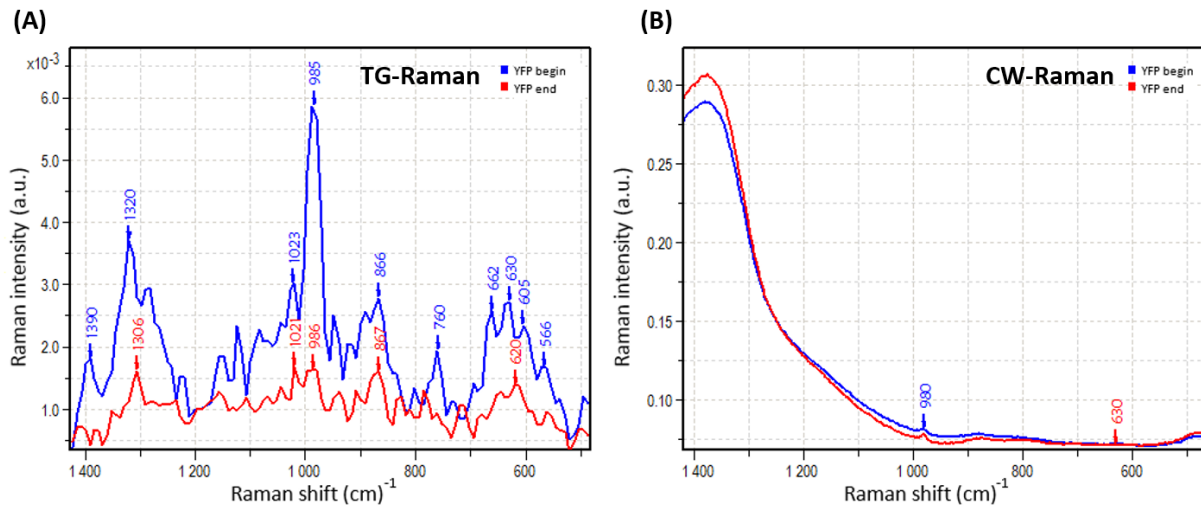
Figure 8 – Difference of fluorescence masked Raman signal between (A) TG-Raman at λ_{exc} = 532 nm and (B) CW-Raman at λ_{exc} = 785 nm from two YFP-samples at different stages of the cultivation.

Figure 8 shows on the example of YFP how the fluorescence suppression with TG-Raman works in practise comparing to CW-Raman. In 8A many peaks can be identified which are related to the broth of YFP, whereas in B only the strongest peaks around 980 and 630 cm^{-1} can be identified. Some residual fluorescence is still present in 8A. In 8B can be seen that from 1000 cm^{-1} onwards the auto-fluorescence broadens the overall signal and displaces the third strongest peak from the YFP sample, visible in 8A, to be unknowable.

However, a good practise to achieve the best possible SNR with TG-Raman, is the option to collect with an adequately wide gate interval first the Raman signal and sequentially the fluorescence signal while balancing the ratio of Raman and fluorescence photons. (Nissinen et al., 2017).

Another option is to set an additional time-gate which only collects fluorescence photons temporally after the Raman photons. Together with the information of the shape, decay time and the amount of the residual fluorescence it is further possible to subtract the fluorescence background signal from the Raman signal, resulting in a baseline corrected more readable Raman signal (Kostamovaara et al., 2013). The substation of residual fluorescence was first applied in a study of Rojalin and co-workers who tested the time-gated prototype Raman system with different kind of pharmaceutical compounds. They also applied the simple subtraction algorithm of the residual fluorescence resulting in an improved detection (Rojalin et al., 2016).
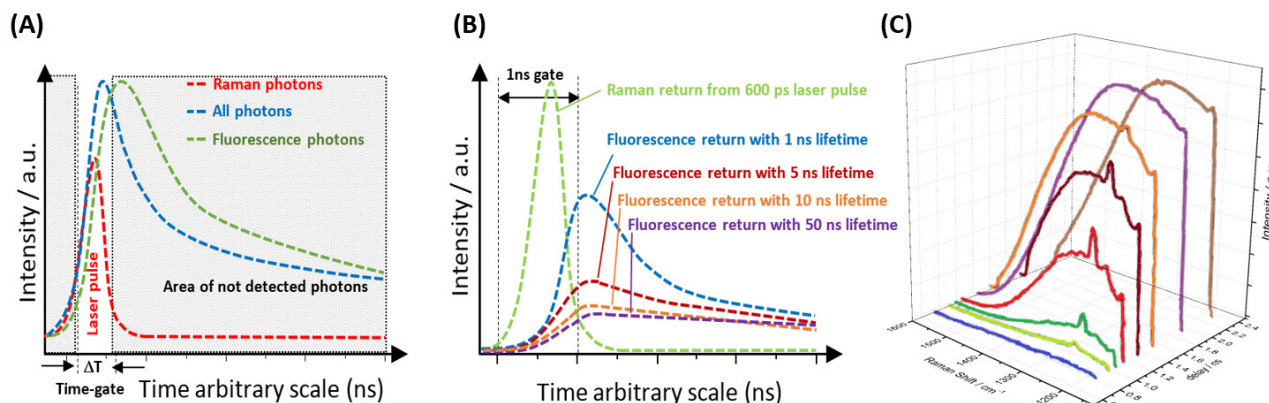
Figure 9 – Illustration of Raman and fluorescence at times shortly after laser excitation: (A) Temporal behaviour of laser, Raman and fluorescence; (B) Lifetime of sample specific fluorescence, adapted with permission of Blacksberg *et al.* 2016; (C) Effect of different gating times.

Figure 9 denotes the effect of the time-gating principle. Fig. 9A shows the time-window of the laser pulse with a return of Raman photons within the gate. Assuming that highly fluorescent sample is being measured, the signal return of all photons (blue curve) will have a stronger intensity. The fluorescence part of the signal, generated from the same laser pulse (green curve) is temporally shifted which is partly already outside the detector gate. The SPAD-detector has short dead-times. This is the time where fluorescence background is at the maximum out of the gate (shaded area in Fig. 9A, adapted from Holma et al. 2017 and not detected until the next laser pulse launches and the measurement cycle is repeated to fetch mainly the Raman signal. Fig. 9B shows different fluorescence lifetimes from different samples (adapted with permission from Blacksberg et al. 2016 and Fig. 9C the effect of different time-gates of one sample (Martyshkin et al., 2004). It can be seen that in the example of Fig. 9C a gating-time around 1 ns is optimal (red curve), including most of the Raman signal but extended gates (>1 ns e.g., violet or brown curve) will show only fluorescence which equals the signal measured with conventional continues wave Raman spectrometers. A commercial time gated process Raman instrument, "TimeGated 532" with fluorescence rejection as fibre-optical system (standard Raman probes of several metres in length), is available by the Finnish start-up company Timegate Instruments Oy. The excitation in the instrument is produced with a pulsed micro-chip Nd:YVO$_4$ of a 100 ps class picosecond 532 nm microchip laser, developed at optical research center (ORC) in Tampere University of Technology and produced by another Finnish start-up company. Temporally short Raman pulses (around 100 picoseconds and temporally longer fluorescence with an exponential decay time of a few to tens of 1000 picoseconds for most organics are able to be measured, resulting from pulsed excitation which is then spectrally dispersed by a spectrograph and detected with a 128 × 8 CMOS SPAD

array chip. (Timegate Instruments Oy, 2015). The representation of the three dimensional spectral data in Fig. 9C represents the raw data of the Timegate post-processing software , i.e., signal intensity versus Raman signal wavenumbers versus time delay information. A short time delay interval or a single spectrum at a specific delay time can be selected as the final measurement data.

1.5.2 Core components of TG-Raman

1.5.2.1 Picosecond pulsed laser

A picosecond pulsed laser is required to perform Raman measurements based on the TG-principle. The kind of pulsed laser, e.g., crystal and pump-mode used like Nd:YAG or Nd:YVO$_4$, is not the priority as long as it produces a stable out-put, narrow enough with a specific pulse-width (100 to 350 ps have been demonstrated) to trigger and operate the gate needed for time-gating (Nissinen et al., 2011). As described in Chapter 1.5.1, the pulsed laser excitation is divided into two beams of which most of the signal is used to stimulate and detect the Raman signal.

1.5.2.2 CMOS-SPAD detector

The standard CMOS fabrication process allows for an inexpensive production of compact and integrated high-speed electronic circuit boards such as single photon avalanche diodes (SPADs) even as arrays (Hallman, 2015). Due to the extreme sensitivity a primary application of CMOS SPADs has been time-of-flight (TOF) for the purpose of range finding and LIDAR systems (Hallman et al., 2012). TOF technology has also been used for cell viability and density measurements in bioreactors (Brognaux et al., 2013) but a less sensitive photomultiplier tube (PMT) is used as detector instead of a SPAD. CMOS SPAD detectors have several advantages over the more common CCD detectors: They are (1) more suitable for TG than CCD detector due to temporal behaviour. The advanced sensitivity (2) compared to most other detection principles is achieved by operating the SPAD close to the "break-down" voltage in the so called "Geiger mode" which in principle enables single photon detection sensitivity. This cannot easily be realized with CCD or PMT detectors and they are not able to measure fast transitions of very low intensities like the SPAD (Zappa et al., 2007). Other advantages over common CCD detectors are the lower manufacturing costs (3), less complexity (4), more integrated with less space requirements (5), less power consumption (6) and no cooling is required.

The SPAD-technology is under constant development. It has evolved from single-pixel Raman CMOS-SPAD detection system to recently achieved 256 × 16 SPAD array detector. The measurement time is decreased to as low as 151 picoseconds across the whole SPAD-array (Holma et al., 2017). The current limitation is still the dimension of the array which is smaller than a quarter of conventional scientific

CCD detectors. The spectral resolution is sacrificed by the amount of available pixels of the detector. To overcome this limitation, a micro lens array on top of the sensor can help to concentrate light onto the detector and thus increase the spectral resolution, which has also been implemented on conventional CCDs (Pan et al., 2008).

1.6 Data analysis methods for Raman spectra from bioprocesses

1.6.1 Purpose of data pre-treatment

Mathematical pre-treatment of spectroscopic data is an extensive topic which can in the context of this thesis only be considered superficially. Generally, the aim is to minimize the influence of irrelevant information.

Especially in Raman spectra of biological and other high content samples, a huge background noise is present resulting from the Raman scattering of the multi-component mixture, and is often overlaid by fluorescence emission. Moreover, due to the culture dependent increase of cells and exudates, a pronounced variance of the matrix affecting both the chemical (e.g., number and concentration of components) and physical properties (e.g., changes in opaqueness or viscosity) of the samples. The sources of noise in the spectrum are already discussed in equation [Eq. 5] and their impact to the real Raman signal is significant.

In addition, systematic errors which may occur as a consequence of misalignment of the Raman spectrometer (wavelength shift can be noticed), such as back-scattering from highly reflecting surfaces, intensity shifts caused by a defocussed sample or sample evaporation during the measurement process will cause difficulties for data evaluation. Another source of error arises from traces of room light penetrating the coverage of sample chambers contributing to a broad background noise in the recoded spectrum with common CW-Raman spectrometers. It shall be noted that in rare case oscillation of the excitation laser source may occur causing either a noisy spectrum (fluctuation of wavelengths) or a featureless spectrum (fluctuation of intensity – Paschotta, 2004).

Relevant information for bioprocesses are often found in the so-called fingerprint region, having Carbon-Carbon and Carbon-Nitrogen vibrations between 650–1600 cm^{-1} and in the double-bond region (C=O and C=C) around 1600–1800 cm^{-1} (Chen et al., 2010; Smith and Dent, 2005). Furthermore, typical spectral features are observed in the CH-region around 2700–3000 cm^{-1} which marks the upper detectable spectral area of most spectrometers. This region is often used as internal standard since the

intensity of the Raman bands here is roughly proportional to the 'biomass' (Bocklitz et al., 2011). However, one should bear in mind that with NIR excitation detectors are not operating in the most sensitive range. For data pre-treatments, fingerprint- and CH- region are often treated separately since the area in between, the N=C=N region (1800–2700 cm^{-1}) has often little information from organic substances (Himmelsbach et al., 2001; Jun et al., 2011).

However, the main characteristics are firstly the qualification as band position (Raman Shift) and peak shape, and secondly, the quantification which equals to the concentration as detected photons on the detector, excluding the noise, cf., [Eq. 5]. As a third and fourth measure comes the frequency shift (strain/temperature or pH) and the line width (structural disorder) which can impact the Raman spectrum (David, 2012; Lin et al., 2016). As the process time is consecutively increasing, Raman band shifts may appear and disappear with the variation of substrates and products in the sample matrix (cf., Chapter 3.4).

Depending on the purpose, i.e., qualitative or quantitative evaluation, different pre-treatments will be used. The basis for the quantitative analysis of Raman spectra is to achieve ideally a linear correlation between spectral features and concentration of analytes. The quantitative Raman spectra analysis can be performed either by univariate or (peak height and ration) or multivariate analysis. The latter typically uses many spectral variables to acquire quantitative data from the spectra (Sparén et al., 2009; Strachan et al., 2007).

1.6.2 Common pre-treatment methods

An important step in data pre-treatment is the baseline-correction of the spectrum. Several approaches can be used to perform this procedure which attains an adjustment of the spectrum in horizontal direction. Besides least-square, spline and Whittaker, most prominent is polynominal fitting. An estimation of curvature caused by the noise is approximated onto the raw-spectra and consequently straightened to a baseline, typically the Raman intensity of zero-level for the lowest signal (Afseth and Kohler, 2012; Dyar et al., 2015; He et al., 2014).

Baseline correction can be also performed by Savitzky–Golay algorithm in combination with the first derivative, generally used to reduce spectral noise by polynominal smoothing (Kessler, 2007).

Next to baseline correction normalization of spectra is an important aspect that allows to correct for intensity variation of spectra. Among the various normalization filters, vector normalising is another important data pre-treatment, typically performed by analysing multiple spectra to compensate dif-

ferences in intensities of spectra (Baranska, 2014). Intensity values of these spectra are rescaled between a minimum value (e.g., the baseline 0) and a maximum value (often 1) by performing it with mean value of all spectra among the vector length. This does not change the peak positions in the spectra but as a result, the intensities of different spectra are normed within this interval (0–1 respectively min/max) to each other (Schmid, 2009).

1.6.3   Multivariate Data Analyses

Both Raman and the surface-enhanced Raman spectra contain a multitude of spectral information resulting in a huge amount of data. The aim of multivariate data analysis (MVDA) respectively chemometric strategies (Rajalahti and Kvalheim, 2011) is to extract the relevant information from the data (Chalmers et al., 2012). When MVDA techniques are applied, it is feasible to significantly increase the selectivity of the information which is at first glance hidden in the spectra (Kessler, 2013). Chemometric methods such as Principal Component Analysis (PCA) and Partial Least Squares (PLS), have demonstrated their superior performance when analysing large amount of spectroscopic information (Baranska, 2014). The main benefit is that they enable process trajectory exploration, outlier detection, interference compensation and noise reduction, thus they possess efficient and robust calibration models (van den Berg et al., 2013).

Additionally, partial least square regression (PLSR), which is a standard method in the evaluation of NIR-spectra, is particularly useful, especially when predicting unknown amounts of components in spectral data (X variables) with the help of reference data (Y as target variables) from other analytical techniques (Kessler, 2007). Cross-scale PLSR modelling from Raman data was applied, e.g., on mammalian- and E. coli cell cultures (Clementschitsch et al., 2005; Mehdizadeh et al., 2015) and for stable prediction of different compounds in supernatants from complex fermentation samples (Paul et al., 2016). Furthermore, successful SERS measurements in combination with PCA analysis of the data was demonstrated for fast qualitative observation of changes in cultivation media even at storage condition, (Calvet and Ryder, 2014). Raman and SERS in combination as methods for quantification of antibiotics with the help of PCA was already confirmed to be feasible one decade ago (Clarke et al., 2005).

2. Aim

The aim of this thesis was to develop different kinds of approaches to apply time-gated Raman and SERS for background fluorescence rejection, for improved investigation of bacteria and cell-culture media. The explicit aims can be characterised as follows:

I. The creation of an SERS online sensor platform – from gold nanoparticles (Au NPs) immobilized onto membrane filtration surfaces, enabling the detection of biofilms such as *Brevundimonas dimiuta* bacteria and small molecules of adenine in very low concentrations at initial adhesion phase with a low-specification Raman spectrometer.

II. The detection of *Listeria innocua* bacteria with the improvement of LOD using SERS nanoparticles (different size and shape of Au NPs) and SERS patterned structure (specially designed Au-patterned-structure) in combination, enabling a low-cost dual-SERS sensor while testing time-gated- with other CW-Raman set-ups for low concentration bacteria detection.

III. The development of novel non-chemically synthesised ligand-free (bare) hybrid Au-Si nanoparticles with controlled content of Au in their composition (30–100 %) as mobile SERS probes in the tasks of bacteria detection (*Listeria innocua* and *Escherichia coli*) with CW-Raman and time-gated Raman.

IV. The investigation of temporal changes of cell-free supernatant *Escherichia coli* samples during the course of a cultivation as performance test for different spectroscopic set-ups with SERS and without SERS using classical Raman and time-gate Raman technologies.

3. Methods and approaches

3.1 Real-time Raman based approach for identification of biofouling

The Chapter is directly adopted from the correspondent publication.

Authors: Martin Kögler[a,b,d,*] , Bifeng Zhang[b] , Li Cui[b,**] , Yunjie Shi[c] , Marjo Yliperttula[a] , Timo Laaksonen[a] , Tapani Viitala[a] , Kaisong Zhang[b].

[a]Drug Research Program, Faculty of Pharmacy, Division of Pharmaceutical Biosciences, University of Helsinki, P.O. Box 56, 00014 Helsinki, Finland

[b]Key Laboratory of Urban Pollutant Conversion, Institute of Urban Environment, Chinese Academy of Sciences, Xiamen 361021, P. R. China

[c]DSXDSYS-R&D-Design and Manufacturing Company, Xiamen 361021, P. R. China

[d]Laboratory of Bioprocess Engineering, Institute of Biotechnology, Technische Universität Berlin, Ackerstr. 71–76, D-13355 Berlin, Germany

3.1.1 Abstract

This study describes a proof-of-concept for a compact real-time surface-enhanced Raman spectroscopy (SERS)-online sensing approach for detection of biofouling in drinking water membrane filtration. In this study we created a custom-designed flow-cell that mimics a cross-flow membrane filtration system. This enables one to measure changes in surface-foulants, such as *Brevundimonas dimiuta* (BD) bacteria and adenine, under conditions that are similar to conventional membrane filtration systems. For measurements we used a common portable Raman spectrometer with a laboratory Raman probe in combination with a specially developed gold nanoparticle (Au NP) SERS sensing area on filter-membranes. This allowed real-time detection of low concentrations of surface-foulants immediately after inoculation into an ultra-pure water reservoir under pressure-driven filtration conditions. We compared these online results with static measurements from an offline, sample-taking approach, using a confocal Raman laboratory-microscope. The developed Au NP SERS sensing-area on the membranes proved to be stable over a long period of surface fouling investigations and to suppress the strong interfering Raman signal originating from the composition layer of most filtration membranes.

3.1.2 Introduction

Membrane technology is globally a key technology for water management and it is rapidly gaining industrial popularity. A major challenge in using membrane technology is membrane fouling (Mänttäri and Nyström, 2000), especially biofouling. It causes a decrease in filtration capacity, increases filtration time and reduces the lifetime of membranes (Belfort, G.; Pimbley, J. M.; Grainer, A.; Chung, 1993; Fane and Fell, 1987; Flemming et al., 2007; Kallioinen et al., 2006). Only a few bacteria can initiate the formation of a mature biofilm, which goes on to develop further layer by layer, into bacterial communities (Chen et al., 2014; Cui et al., 2011; Flemming et al., 2007; Lamsal et al., 2012; Papukashvili, 2009). Therefore, once an undesired adhesion of bacteria has occurred, it is difficult to completely remove the biofilm formed. Because biofouling occurs just on the surface of membranes, a real-time monitoring solution that does not disturb the performance of membrane filtration systems would be desirable (Krause et al., 2008; Tung et al., 2012).The flux-decline and increase of trans-membrane pressure can be used as an initial indication of membrane fouling (Guo et al., 2012; Wett, 2005). Usually, the membranes are cleaned regularly to remove potential foulants and when their performance is deteriorated they need to be replaced (Ivleva et al., 2010; Wett, 2005). In order to avoid excessive chemical cleaning and replacement of membranes it would be necessary to identify biomolecules and differentiate fouling types (Chen et al., 2014; Guo et al., 2012; Li et al., 2003; Sim et al., 2013). An optimum solution would be real-time monitoring of the membrane surface which can reduce the environmental impact and may be economically more feasible compared to the membrane replacement strategy (Flemming et al., 1997; Nguyen et al., 2012). There are many approaches to measure fouling formation in real-time. Promising optical methods are, e.g., attenuated total reflection (ATR), confocal scanning laser microscopy (CSLM), Fourier transform infrared spectroscopy (FTIR), photo-sensors and bioluminescence (Guo et al., 2012; Janknecht and Melo, 2004). When online observation is of importance, real-time Raman spectroscopy has been found particularly useful, though some challenges remain in its applicability (Abu-absi et al., 2011; Gil, 2005; Stillhart et al., 2013; Willemse-Erix et al., 2009; Xie et al., 2004). Furthermore, Raman with SERS enhancement allows real-time observation due to its ability to identify the chemical information, especially the differentiation of fouling types and their changes over time. Real-time observation of early-stage biofouling development and its mechanisms using, e.g., standard process Raman detection without SERS enhancement is challenging. The main challenges are the interfering Raman scattering and the background fluorescence originating from the layer-composition of the membranes used for membrane-filtration which obfuscate the weak signal from the surface-foulants (Boccaccio et al., 2002; Khulbe and Matsuura, 2000; Zhao et al., 2013). Surface-enhanced Raman spectroscopy (SERS) is a promising technique that allow non-invasive and in-situ studies of the

growth of the bacteria fouling layers on membrane surfaces. This has for the first time been reported in our previous study (Cui et al., 2011) and has since then been recognized as a characterization technique for biofouling investigations (Nguyen et al., 2012). One of the advantages of SERS is that it can easily be applied on surfaces. SERS also overcomes the limit of detection (LOD) especially in aqueous solutions, and it gives an enhancement of about 10^6 in scattering efficiency compared to normal Raman scattering (Smith and Dent, 2005). Another key benefit of applying SERS compared to normal Raman spectroscopy is its ability to suppress the interfering Raman scattering originating from the layer-composition of most membranes, as demonstrated in this study. There are, however, several challenges related to real-time biofouling detection in cross-flow filtration systems, particularly in those that mimic industrial conditions. Firstly, the cross-flow velocity over the observed membrane makes it difficult to immobilize the SERS nanoparticles – required to enhance the weak Raman scattering – reliably to the membrane surface. Secondly, the pressure of water which is pumped through the system is high and vibrations caused by the water circulation pump can disturb the focusing of the probing system. Nevertheless, studies on biofouling behavior need to address these challenges for the applications to be suitable for industrial settings.

In this study we demonstrate a proof-of-concept solution for the use of online SERS measurements in conditions mimicking cross-flow membrane filtration. We have developed a novel solution for preparing pressure and water-flux resistant SERS sensing areas consisting of colloidal gold nanoparticles on filter-membranes and integrated them into filtration processes for online monitoring. The Raman signal enhancement and stability of the set-up were tested over an extended period. The fabrication technique of SERS substrates plays an important role in the performance of SERS (Chen et al., 2014; Efeoglu and Culha, 2013; M. Fan et al., 2011). The shape and size of the used Au NPs should be optimized in order to fit the pore size of specific membranes. Here we use a similar kind of approach for the mechanical attachment of Au NPs to the membrane surfaces as described in our earlier study for silver nanoparticles (Ag NPs – Cui et al., 2011). The porous and heterogeneous structure of many common membrane types (cf., Table 1) is beneficial for this type of SERS-sensing area immobilization and makes it stable for high cross-flow velocities and throughputs. Even though Ag NPs provide a stronger SERS signal enhancement (Zeman and Schatz, 1987), we used Au NPs in this study because they are more stable compared to Ag NPs and they are non-toxic for bacteria, which is important especially in the early-stage of monitoring biofilm development (Cui et al., 2013; Hong and Li, 2013).

Real-time SERS investigations in this study focused on finding a robust method to sense biofilm fouling. This method could help improving cleaning and pre-treatment schemes (Schneider et al., 2005). Within

this study we use the terms real-time and online as synonyms and the results are compared to a static offline, sample-taking approach.

3.1.3 Material and methods

3.1.3.1 Synthesis of gold nanoparticles

Colloidal Au NPs with an average dimension of about 120 nm at the longest side of the cross-section in an oval shape were synthesized by following the Frens-method (Frens, 1973). Concisely, 100 mL of 0.01 % (wt/vol) HAuCl4 aqueous solution was heated to boil under vigorous and continuous stirring, followed by the immediate addition of 0.6 mL of 1% (wt/vol) trisodium citrate solution. The solution was kept boiling for about 1 h until the color changed to light ruby red. The final Au NP-solution was prepared by centrifugation at 3500 rpm for 5 minutes (Eppendorf 5430R centrifuge) and subsequently followed by the removal of the supernatant. The final dark ruby red Au NP-solution with a concentration of about 5400 mg L^{-1} was used for the SERS substrate development. The biocompatibility and size-distribution have been described in our previous research (Cui et al., 2013).

3.1.3.2 Membrane and substrate preparation

The highly concentrated Au NP-solution (10 µL) was filtrated directly onto membranes and dried quickly under an applied mechanical pressure consequently immobilizing the Au NPs within the top-part of the membrane layer making them stable against elution (Cui et al., 2011). An even circular visible area was formed right on the top-layer of the membrane as a SERS sensing area. The Au NP SERS-sensing-area was prepared on various commercial and home-made membranes with different pore sizes and compositions (Table 2). The immobilization of the Au NPs on membranes used for cross-flow filtration was done just before the membranes were placed into the flow-cell. The Au NP SERS sensing-area was visible as an evenly ruby red colored circular detection area as shown in Fig. 1A.

3.1.3.3 Foulant samples

Biofilm model-bacteria *Brevundimonas dimiuta* (BD) were extracted from a drinking water pipeline as described earlier (Chen et al., 2014; L Cui et al., 2015). Pure adenine (Sinopharm Chemical Reagents Co., Ltd, China), a readily available small water soluble molecule (135.13 g/mol) was used since adenine and adenosine have been identified to contribute to SERS spectra of biofilms.
Foulant samples.

3.1.3.4 Bacteria adhesion process on membranes with and without SERS substrate

Commercial NF90 polyamide nanofiltration (NF90), mixed cellulose ester (MCE) microfiltration and home-made polysulfone (PS) ultrafiltration-membranes with and without the Au NP SERS sensing-area were prepared for monitoring bacteria adhesion. The home-made PS ultrafiltration-membranes were used in the online flow-cell and long-term substrate-performance-measurements (3.3 and 3.4). The applicability of the developed Au NP SERS sensing-area on membranes was tested offline on commercial NF90 and MCE-membranes.

Adhesion during filtration

In order to demonstrate and compare the bacteria adhesion process during filtration, *B. dimiuta* (BD) bacteria were cultivated directly on NF90 nanofiltration-membranes by using a cross-flow filtration equipment which is described elsewhere (L Cui et al., 2015). The membranes were sampled at cultivation times of 6 hours (Lag-phase), 16 hours (Log-phase) and 26 hours during the end of the stationary phase.

Adhesion during static cultivation

In order to demonstrate the adhesion of BD onto the Au NP SERS sensing-area under static cultivation conditions MCE-membranes were prepared as described in section 3.1.3.2 for biofouling tests on the substrate. For the sake of comparison, a static cultivation of BD on MCE-membranes without the Au NP SERS sensing-area was evaluated by pipetting a droplet of 10 µL Au NP solution on the biofouled membrane. The droplet was allowed to air-dry for about 1 hour before the SERS analysis. BD was grown overnight in about 1 mL of solution and resuspend with Phosphate-buffered saline (PBS). Subsequently, it was mixed with 100 mL of 1/500 Lysogeny broth (LB) nutrition-enriched media to form a diluted bacteria culture. A small piece, approximately 6 mm in diameter, of MCE-membrane with and without the Au NP SERS-sensing-area was placed into 12-well plates containing 2 mL diluted bacteria culture in each well. Both membrane samples were taken out for SERS analysis.

3.1.3.5 SEM imaging

Structural analysis of the surface fouling and consistency of the Au NP SERS sensing-area of the membrane samples were studied by recording scanning electron microscopy images (SEM, Hitachi S-4800 device). Prior to SEM analysis, the samples were sterilized and fixed for a couple of hours in a bath of 2.5% glutaraldehyde in 0.1 M PBS (phosphate buffer saline) followed by critical point drying-treatment

(CPD, Autosamdri-815B, Series A by Tousimis) as described previously (Chen et al., 2014; L Cui et al., 2015).

3.1.3.6 Flow-cell construction

A special table-sized sensing system consisting of an ultra-pure water reservoir, connected to a continuously operated AC-pump which pumped the water through the flow-cell with the membrane and sensors, was constructed. The set-up was built to operate the water flow in closed-loop at a constant pressure and flow-rate (Fig. 10).
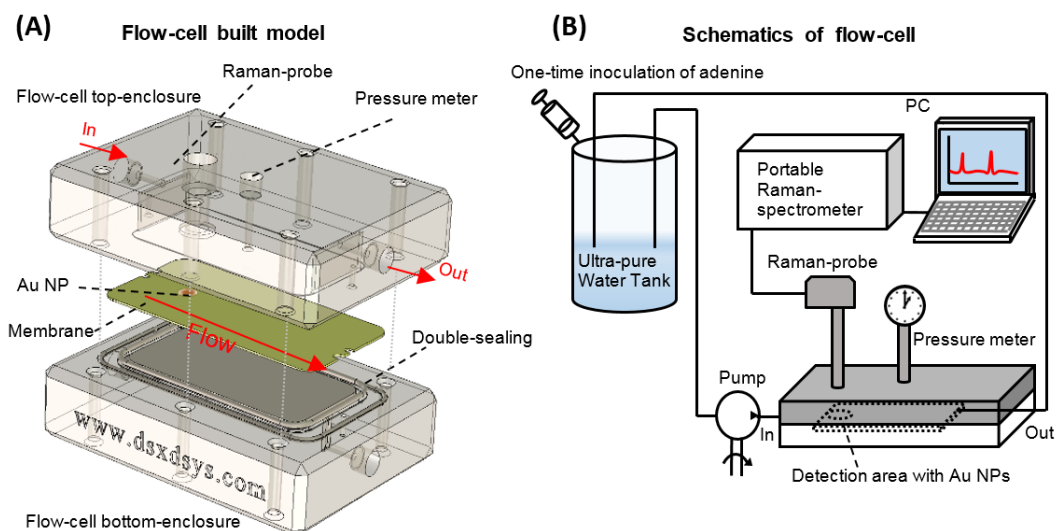
Figure 10 – (A) 3D-CAD-design of the built flow-cell model as a disassembled view for clarification of the layout. (B) Schematics of the flow-cell built for SERS online-detection as proof-of-concept with continuous flow-rate and constant pressure monitoring.

3.1.3.7 Modelling of flow in the flow-cell

The fluid-flow inside the flow-cell was modelled using Comsol Multiphysics software version 5.0. The fluid-flow was simulated as a laminar flow with no-slip wall boundary conditions and compressible flow conditions. The inlet and outlet flow-rate was set to 1.5 m s^{-1} and pressure at the inlet was set to 2 bar (29 PSI), based on the experimental set-up. The shear stress was calculated by multiplying the shear rate obtained from the Comsol modelling by the dynamic viscosity of water at the wall boundaries.

3.1.3.8 Measurement configuration and SERS analysis

A portable Raman spectrometer (B&W Tek, model BWS415, i-Raman 785S) at 785 nm CW-laser excitation, with maximum power of 320 mW at the laser-spot and a laser-spot-size of approximately 85 µm

at the membrane sample was used for the Raman spectra real-time identification. The detection was done through a quartz-glass window without coating using a standard Raman laboratory-probe (BWTek-BAC100) in close proximity with the specified focal distance of 8.1 mm. For online measurements, the BWSpec -measurement-software (B&W Tek) was used as data acquisition with reduced laser power of about 200 mW. The collected data was subsequently compared with the offline Raman data (sample-taking approach) from the Raman microscope-analysis. A signal integration time of 5 seconds was used in combination with 5 averages with the measurement-software in the online and in the offline set-up as well.

Performance-tests with adenine inoculated in an ultra-pure water reservoir were implemented into the experimental set-up which included membranes with the developed Au NP SERS sensing-area. Raman-offline-measurements were performed with a high-performance confocal Raman scanning-microscope (Horiba LabRAM ARAMIS operated by LabSpec-software, version 5.0) with a 600 g mm^{-1} grating and external 632.8 nm helium–neon CW-laser excitation. An Olympus 50x objective focused the laser beam with about 70 μW, a focal distance of approximately 8 mm and a numerical aperture of NA = 0.55 from the filter-membrane samples. SERS measurements were pre-processed with Matlab-software 2014 (The MathWorks) using Signal-Processing Toolbox and curve-plotting options.

3.1.4 Results and discussion

3.1.4.1 Eliminating the Raman signal interferences from filter-membranes with Au NPs

The size of SERS nanoparticles should be optimized to fit the individual pore-size of the selective top-layer of the filter-membranes. The SERS nanoparticles should preferably be immobilized just within the top membrane layer of the detection area in order to be able to detect fouling as the "First-layer-effect" causing surface-bound species to dominate the Raman spectra (Kennedy et al., 1999). If the SERS nanoparticles for some reason, e.g., due to their too small size, penetrate through the first layer to the next membrane layer, the SERS enhancement might decrease (Tian et al., 2007). This consequently increases the interfering Raman signal originating from the membrane. On the other hand, a too scarce immobilization of the SERS nanoparticles within the top membrane layer causes a decrease in SERS enhancement, because SERS enhancement decreases exponentially with respect to the distance between the nanoparticles (Bell and Sirimuthu, 2006). The SERS Au NP sensing-area was prepared on all together six different non-fouled filter-membranes (cf., Table 2). Before preparing any SERS Au NP sensing-area on the filter-membranes the level of the interfering Raman signals originating from the membrane-composition of the different pure non-fouled filter-membranes was determined with a confocal Raman scanning-microscope. The interfering Raman signals from the membranes were

then classified as strong, moderate or weak interference. The first two filter-membranes (1) and (2) in Table 2 are nanofiltration-membranes made from polyamide. The first layer in these membranes is a thin piperazinamide-based selective layer. The second layer below is a thicker ultrafiltration layer (UF-layer) (Sperling et al., 2008), and the third layer is a nonwoven (polypropylene) layer. These polyamide-based filter-membranes had strong interfering Raman signals with sharp and narrow peaks over the whole fingerprint region. This is also exemplified by the Raman spectrum of the NF90 membrane in Fig. 12A. The third filter-membrane (3) in Table 2 is a pure home-made polysulfone-membrane manufactured at the Key Laboratory of Urban Pollutant Conversation, IUE in Xiamen, China. The pure PS-membrane also displayed a strong interfering Raman signal as shown in the Raman spectrum in Fig. 12B. The other membrane types in Table 2, i.e., (4)–(6), are commercially available microfiltration-membranes composed of polyvinylidene-fluoride, mixed cellulose ester and polycarbonate, respectively. These microfiltration-membranes showed weak to moderate interfering Raman signals. The Raman spectrum of the MCE-membrane is shown in Fig. 12C. The pore sizes of the filter-membranes in Table 2 increases in the order from (1) to (6).

Table 2 – Comparison of the level of the interfering Raman signal of different pure non-fouled filter-membranes determined with a confocal Raman scanning-microscope.

Membrane type	Filtration type	Selective layer	Dominating composition	Level of inter-fering Rama signal
1. NF90 (Dow, USA)	nano	UF-layer	polyamide	strong
2. NF270 (Dow, USA)	nano	UF-layer	polyamide	strong
3. PS (home-made)	ultra	UF-layer	polysulfone	strong
4. PVDF (0.1 μm, Millipore, USA)	micro	MF-layer	polyvinylidene fluoride	weak
5. MCE (0.1 μm Millipore, USA)	micro	MF-layer	mixed cellulose ester	weak
6. PC (0.22 μm Millipore, USA)	micro	MF-layer	polycarbonate	moderate

The SERS sensing area on all the tested membranes in this study was prepared by immobilizing the same amount of the self-synthesized Au NPs of ca. 120 nm in diameter on the filter-membranes. Fig. 11 shows, as an example, SEM images of a clean non-fouled MCE-membrane before and after immobilization of the Au NPs, as well as the concept of the SERS Au NP sensing-area on the membrane surface. The clean MCE-membrane displays clearly visible pores in the size range of 200–300 nm and smaller. The SEM image of the SERS Au NP sensing-area shows that the NPs have formed a densely packed even layer on top of the membrane. The fact that the Au NP layer does not show any larger pores or cracks verifies that the Au NPs are immobilized within the topmost layer of the membrane

and do not penetrate through the membrane during immobilization. The close proximity to the top-layer of the membrane surface and the densely packed layer of the Au NPs, both illustrated in Fig. 11, should ensure SERS enhancement of the signal caused by foulants during the filtration process (Tang et al., 2009). The immobilization of the synthesized Au NPs on all the filter-membrane surfaces almost completely quenched the strong interfering Raman signal originating from the membrane-composition. Fig. 12 shows the elimination effect of the Au NP SERS sensing-area on the interfering Raman signal from pure and non-fouled NF90, PS and MCE-membranes. The red and blue spectra in Fig. 12 show the Raman signal without and with the Au NP SERS sensing-area, respectively. It is quite clear that the influence of the membrane-composition on the Raman-spectra would interfere the detection of any potential fouling event on the membrane surface without the Au NP SERS sensing-area. Furthermore, Fig. 12 also confirms that no strong interfering bands originating from the membrane-composition appear in the Raman spectra when applying the Au NPs SERS sensing surface on the membranes. This verifies the "First-layer-effect" and allows the detection of any fouling event. The NF90, PS and MCE-membranes were chosen for further fouling studies because they represent membranes used for different types of filtration processes (i.e., nanofiltration, ultrafiltration and microfiltration, respectively).
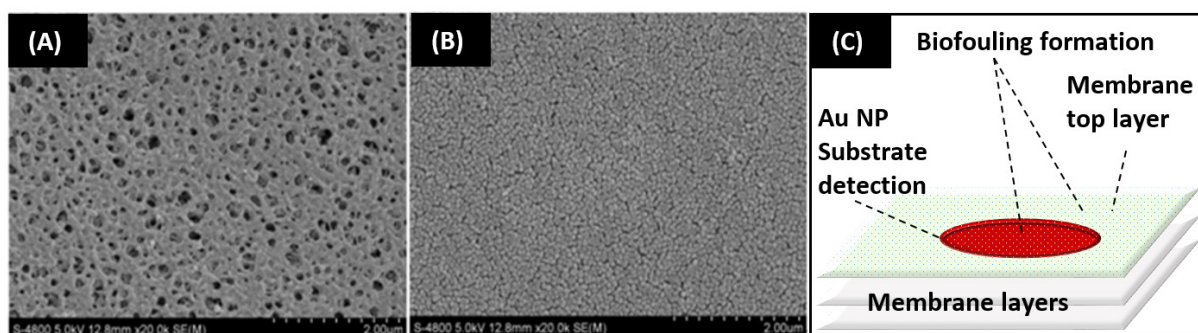
Figure 11 – Scanning electron microscope images of clean non-fouled MCE-membrane before (A) and after (B) immobilization of SERS Au NPs. The concept of the SERS Au NP sensing-area on the membrane surface is shown in (C).
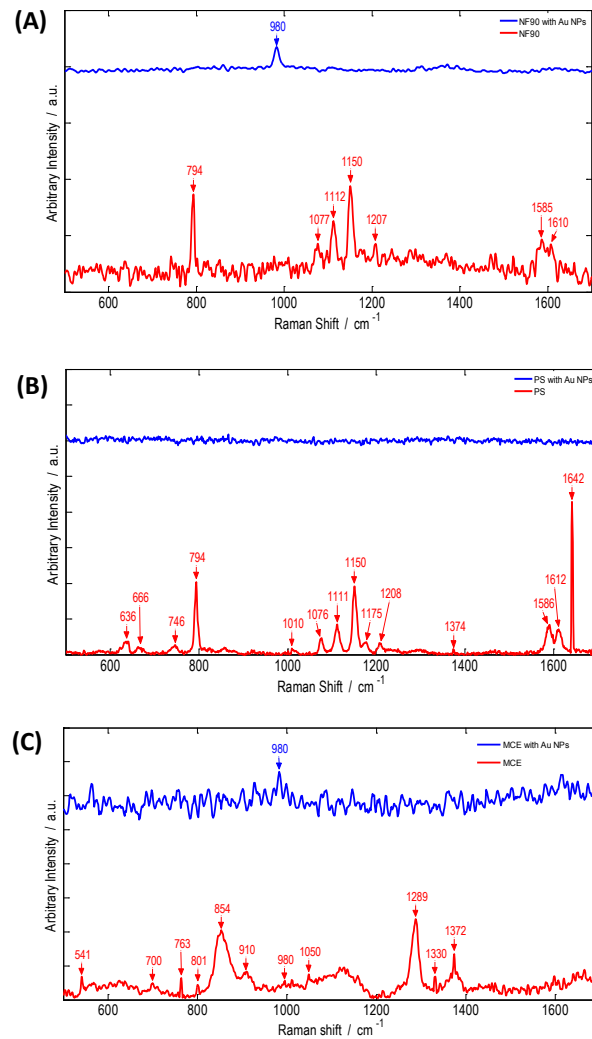
Figure 12 – Elimination effects of Raman signal interference of the membranes by Au NPs. Normal Raman spectra (red spectra) and SERS spectra measured from the SERS Au NP sensing-area (blue spectra) separated with an off-set on (A) – NF90, (B) – PS and (C) – MCE-membranes.

3.1.4.2 Fluid flow simulations of the flow-cell

The modeling of the flow conditions in the flow-cell was performed in order to ensure that the overall flow conditions in the flow-cell are homogenous, and that the inlet and outlet ports of the flow-cell do not disturb the flow-dynamics of the system. A 3D representation with accurate measurements of the flow-cell was constructed using the built-in tools of the Comsol software. Simulation results of the flow conditions in the flow-cell are shown in Fig. 13. The fluid flow at the bottom of the flow-cell has a fairly constant flow-rate and a low shear stress (< 1 Pa). Most of the stress is taken by the vertical parts of the flow-cell, which also distribute the flow evenly across the membrane. Simulations with turbulent

flow conditions were also calculated, but led to virtually the same results. These results indicate that the membrane samples do not experience very high fluid stresses and should be stable for online detection with SERS.
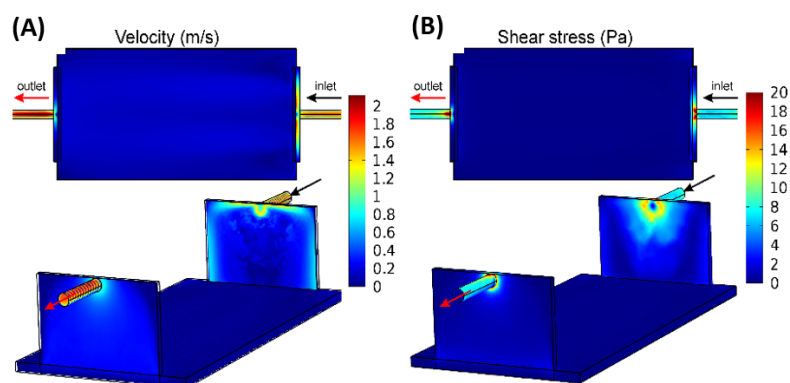
Figure 13 – Comsol simulation results: (A) Fluid flow velocity profile inside the flow-cell shown as a top-view and as an isometric 3D projection. (B) Wall shear stresses inside the flow-cell shown as a top-view and as an isometric 3D projection.

3.1.4.3 Online and offline fouling measurements with adenine

Online fouling measurements with adenine concentration of 10^{-4} M were performed on PS-membranes with Au NP SERS sensing-area by using the flow-cell-setup described in section 3.1.3.6 (Online SERS). The online measurements were performed under similar conditions as the fouling measurements with adenine on PS-membranes with Au NP SERS sensing-area in a cross-flow filtration system (Offline SERS). Fig. 14A shows the comparison of the raw SERS data obtained from the online (blue spectra) and offline (red spectra) fouling measurements with adenine. By focusing the laser on top of the Au NP substrate it was possible to detect all characteristic Raman bands of adenine with high accuracy in the SERS online configuration, as shown by the blue spectra of the SERS online measurements in Fig. 14A. Contrary to the online measurements, which were performed in a rough environment with high flow-rate and pressure, the Raman microscope used for subsequent SERS offline measurements with limited laser power shows significantly lower intensities of the Raman spectra of adenine. The difference in Raman signal intensities between the online and offline measurements is mainly attributed to the difference in the used laser power for the measurements, i.e., approximately 200 mW (60 % of laser power) for the online measurements and around 70 µW for the offline measurements. Therefore, Fig. 14B also shows for easier comparison both SERS data after normalization by limiting the spectral data into an interval from 0 to 1, scaling by multiplying with a factor to equalize the intensity-level of both curves, smoothing by adding a Gaussian filter and baseline-level-correction by apply-

ing a polynomial fit over the spectral data-range. The normalized online SERS spectra of adenine meas-
ured with the portable Raman spectrometer are slightly noisier with less detail compared to the nor-
malized offline SERS spectra obtained with the Raman microscope. This is attributed to the better sig-
nal-to-noise ratio (SNR) of the stationary Raman microscope measurements. Overall, these results
show that the developed Au NP SERS sensing-area works well with both a portable Raman spectrom-
eter and with reduced excitation energy exemplified by the Raman microscope measurements. To our
understanding similar SERS online results have not been reported earlier and they provide robust evi-
dence for the successful realization of the proof-of-concept for a compact real-time SERS online sens-
ing approach for monitoring small molecular foulants on filtration membranes.
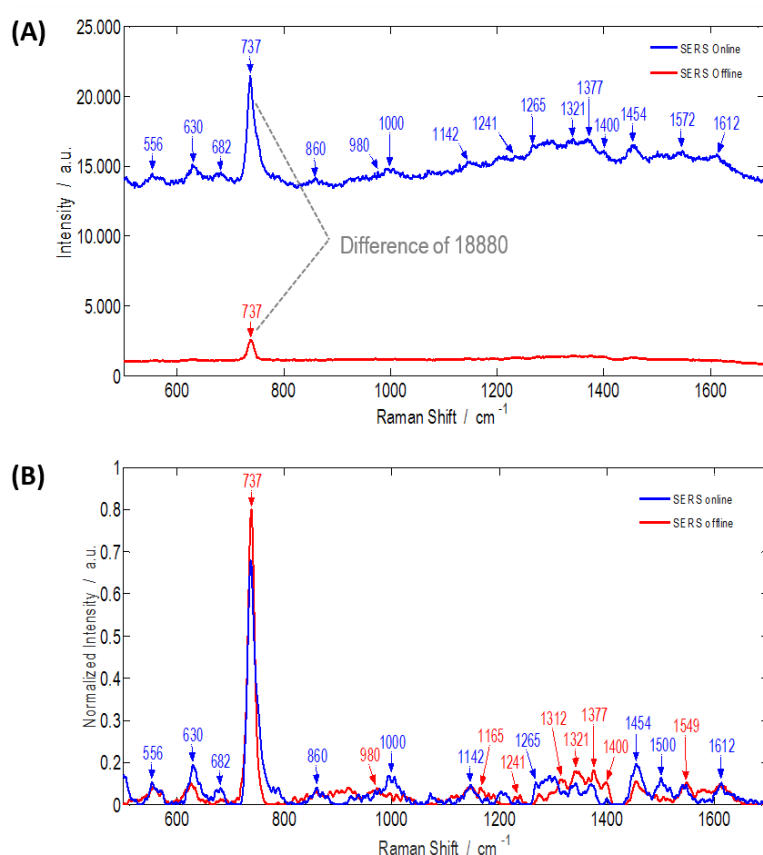
Figure 14 – Detection of Adenine with online (blue curve) and offline SERS (red curve) by using Au NP
SERS sensing-area on PS-membranes. (A) Raw SERS measurement data without off-set. (B) Normalized,
scaled, smoothed and baseline-corrected SERS measurement data.

In comparison, Li and Fang (Li and Fang, 2007) have achieved similar results with an offline configura-
tion using a roughened silver electrode modified with silver nanoparticles by using magnetron sput-

tering for SERS attachment and similar adenine concentration levels of 10^{-4} M. Fig. 14B also demonstrates that there are no major differences in the quality of the normalized Raman spectra for adenine between the online and offline SERS measurements on PS-membrane surfaces, with the exception of the peak centered at 737 cm^{-1} corresponding to the DNA-base (adenine ring breathing), which has a slightly stronger intensity in the offline SERS results. These results confirm the robustness of the developed Au NP SERS sensing-area for online-measurements during harsh conditions in the filtration process.

3.1.4.4 Long-term SERS sensing area performance

The long-term performance-tests of the Au NP SERS sensing-area on PS ultrafiltration-membranes up to 13 days were carried out only with the offline configuration using the confocal Raman microscope. The Au NPs were first filtrated on the surface of the ultrafiltration PS-membranes as a SERS sensing area. The PS-membranes with Au NP SERS sensing-area were then immersed in different concentrations of adenine (10^{-4}, 10^{-5}, 10^{-6}, and 10^{-7} M) and SERS spectra were measured after different immersion times: immediately after immersing, after 24 hours, 7 days and 13 days. Fig. 15 shows the raw SERS data, shifted with off-set for clearer presentation without normalization or baseline correction, and a different colour for each adenine concentration. The SERS spectra measured immediately after immersing the PS membranes in the adenine solutions show that the minimal LOD achieved at this point was 10^{-7} M (Fig. 15A). The concentration-level is linearly dependent to the intensity of characteristic adenine-peaks, showing that SERS can be used as quantitative analysis. The subsequent measurements on the same Au NP SERS sensing-area after 7 days of immersing the PS-membranes in the adenine solutions show that the LOD of adenine remains unchanged during this period (Fig. 15B). Fig. 15C shows that after 7 days, the peak around 737 cm^{-1} related to the adenine ring breathing was decreasing. This could be explained by a weakening of the adhesion of adenine molecules competing with reorganization and concentration reduction of the SERS sensing-area over the time. At the same time, the peak around 980 cm^{-1} was increasing which may be due to compounds embedded in the Au NPs during synthesis that are exposed on the sensing surface due to reorganization of the Au NPs (Cui et al., 2015 – Fig. 15C). Fig. 15D demonstrates finally that a long-term performance of the developed Au NP SERS sensing area is possible up to 13 days.
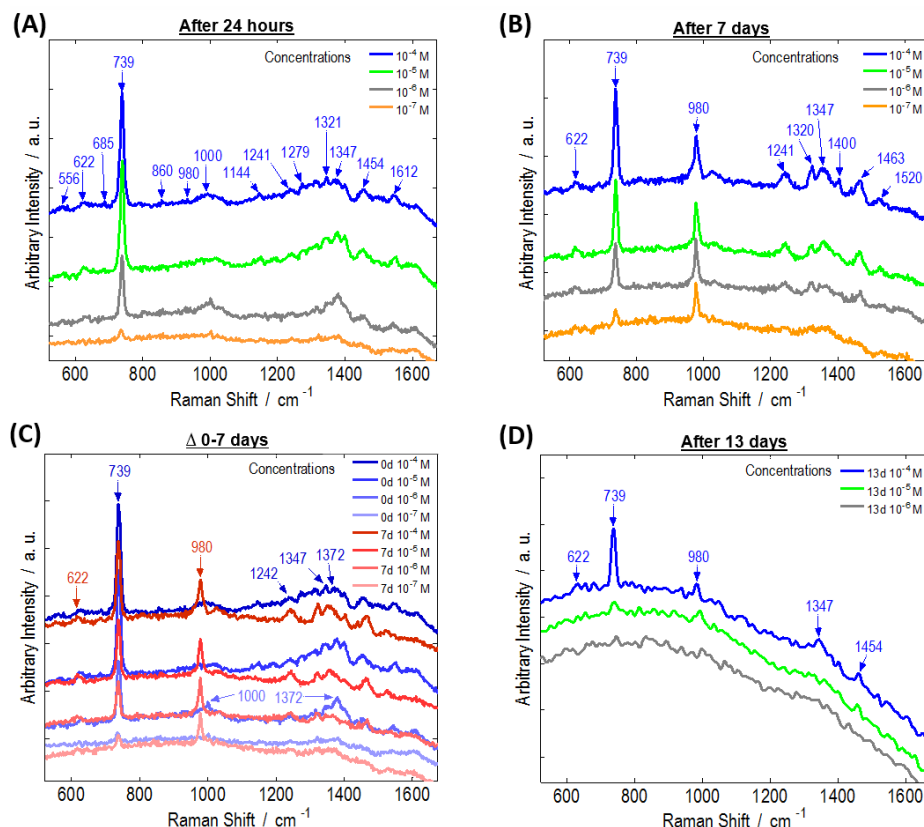
Figure 15 – Long-term stability test of Au NP SERS sensing-area during immersion in adenine solutions of different concentrations. SERS spectra after 0 days (A), after 7 days (B), band changes after 7 days compared to 0 days (C) and after 13 days (D).

3.1.4.5 Biofilm growth on the developed Au NP SERS sensing surfaces

In our previous study with Ag NPs we have observed a steady growth and good distinguishability of the rod-shape-like bacteria *B. dimiuta* (BD) after about 24 hours (Chen et al., 2014). Hence, in order to examine whether the Au NPs affect the biofilm growth behavior over extended time period the growth effects of the same bacteria on NF90 membrane surfaces with and without Au NP SERS sensing-area were measured. Mono-species biofilms of *B. dimiuta* (BD) were cultivated on the NF90-membranes in cross-flow filtration conditions and sampled at three different time points during the cultivation, i.e., 6, 16, and 26 h. SEM images of the BD fouled membranes pieces at 6, 16, and 26 hours are shown in Fig. 16. The SEM images clearly show that the Au NP SERS sensing-area does not prevent the adhesion and development of the BD-biofim. Unfortunately, the SERS spectra of the same samples were masked by a strong interfering fluorescence, possibly generated by some unknown residual components in the filtration system.
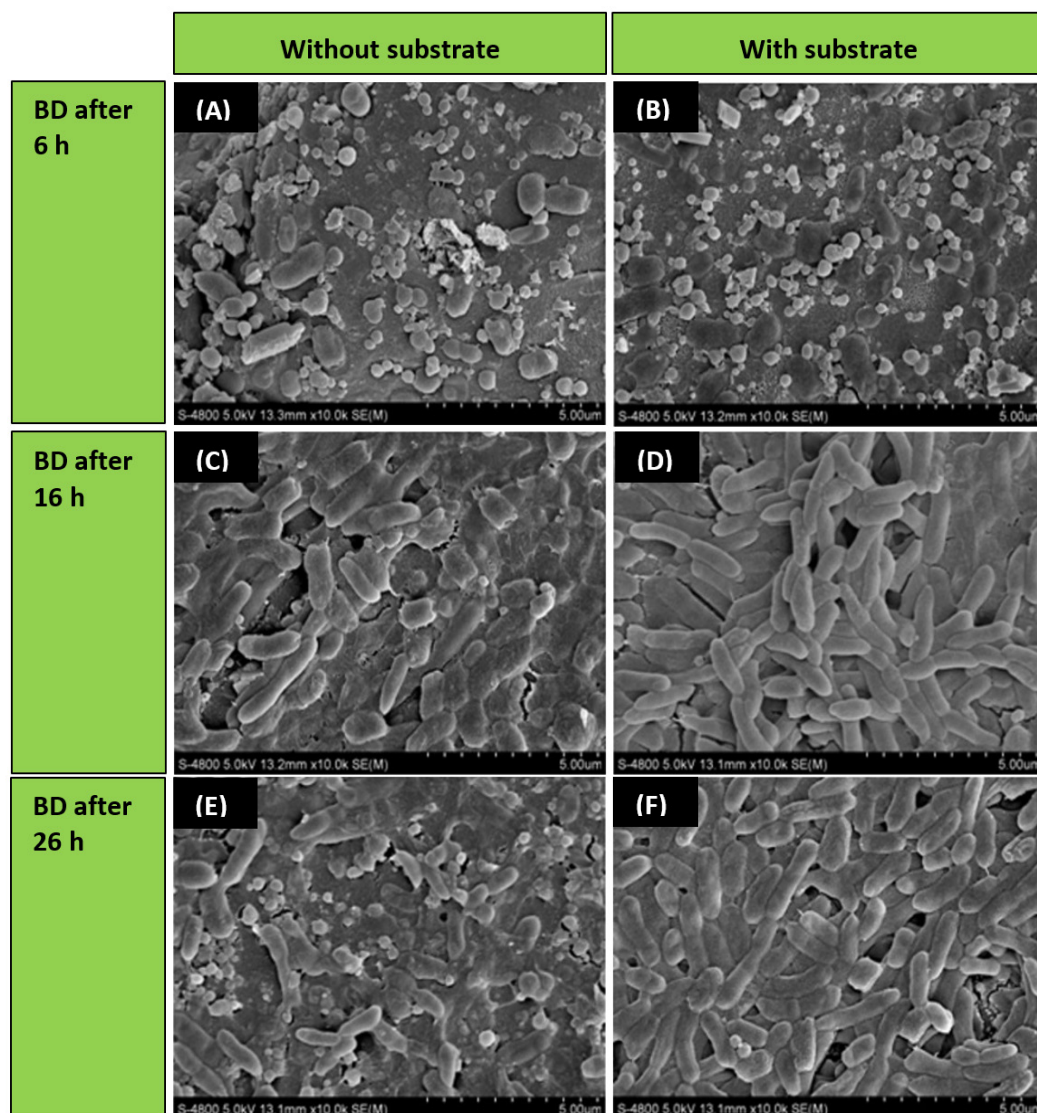
Figure 16 – SEM images of BD adhesion on NF-membrane without (left column; A, C, E) and with (right column; B, D, F) Au NP SERS sensing-area at different sampling times 6 h (A and B), 16 h (C and D) and 26 h (E and F). BDs are visible as rod-shaped depositions.

Static cultivation of the BD-biofilm was performed in a six-well plate in order to compare the growth of the BD-biofilm on the Au NP SERS sensing-area under static and dynamic growth conditions. MCE membranes with Au NP SERS sensing-area immersed into pure LB nutrition-medium without inoculating bacteria were also prepared and their SERS spectra were measured as a reference and compared with the BD biofilm. From Fig. 17A can be observed that the SERS spectra of BD biofilm and LB are identical which is due to the adsorption of LB first onto Au NP SERS substrate of MCE membrane before the actual bacterial attachment. Because of the short-distance SERS enhancement effect, substances adsorbed only in close proximity of the SERS substrate get enhanced, which here shows the SERS signal of LB (Chen et al., 2014).

тo demonstrate whether bacteria without LB (BD in PBS) can get enhanced by the developed SERS substrate, BD in PBS was dropped onto Au NP SERS substrate on MCE-membrane. As shown in Fig. 17B we were able to observe the SERS signal of BD, demonstrating that Au NP SERS sensing-surface can successfully enhance the Raman signal of bacteria. The SERS spectra in Fig. 17B shows typical SERS bands of bacteria, including 1000 cm^{-1}, 1251 cm^{-1}, 1446 cm^{-1}. Furthermore, the SERS spectra in Fig. 17B still displays a significant interfering fluorescence. However, the SERS intensity from the BD is slightly higher than that of the pure LB-media, demonstrating the contribution of the SERS signal from BD. It also seems that the interfering fluorescence actually originates from the pure LB-media. Despite of these challenges, the Au NP SERS sensing-surface developed here seems to be a highly viable approach for biofilm detection and can in the future be further optimized to improve the detection sensitivity of biofilms.
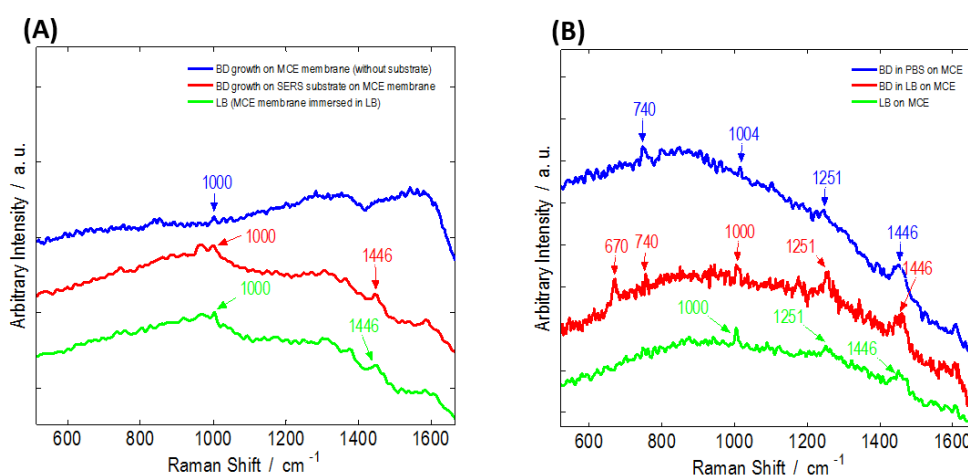
Figure 17 – (A) Raw SERS spectra of BD formed on SERS substrate immobilized on MCE membrane (red), SERS spectra of BD grow on MCE-membrane without SERS substrate (blue) and LB as reference (green) separated with off-set. (B) SERS spectra of BD in PBS drop on Au MCE membrane (blue), immersed in static pure LB media (red) and LB as reference (green).

3.1.5 Conclusion

In this study we propose a proof-of-concept design which can be scaled for other membrane-filtration techniques. This concept of online-sensing solution offers a significant advantage over traditional sample-taking methods, especially for detecting surface-foulants in water filtration processes during early-stage biofouling. One of the main advantages is the elimination of the contamination risk due to interruptions. The results also show that the developed Au NP SERS sensing-area is suitable as a SERS sensor in an online-process with high water-flux and pressure. However, the potential influence of the SERS

sensing area on the membranes' filtration efficiency, as well as the measurement conditions in terms of adjustments of the laser power and focus need to be further investigated (Cialla et al., 2012; Nuntawong et al., 2013). Although according to the Gersten-Nitzan (Dulkeith et al., 2005; Paquet-Mercier et al., 2013; Wang et al., 2010), Au NPs may quench the interfering fluorescence background, it still remains to be an issue which can be seen especially in the bacteria detection results of this study. A potential solution for the fluorescence suppression may be the use of time-gated Raman detection system instead of a classical CCD detection (Kostamovaara et al., 2013; Rojalin et al., 2016).

A novel setup consisting of a table-sized SERS online sensing system for membrane filtration with a portable Raman spectrometer and a commercial Raman probe with little space requirements was used in this study for the first time. It is capable of observing fouling growth through a glass window in real-time. The developed stable Au NP based SERS sensing area was shown to suppress the interfering Raman spectra originating from the membrane itself, whereas surface-bound species such as small molecular and biofoulants dominate the acquired SERS signal. Based on these initial results an online biofouling detection approach in membrane filtration processes may be possible with readily available, relatively low-cost instrumentations. The experimental set-up of the online SERS detection reported here could further be tested with other online measurement systems to confirm the occurring changes in real-time. The results of this study provide new insights into membrane technology targeted for biofouling real-time monitoring in water filtration processes.

Acknowledgments

3.2 Detection of *Listeria innocua* on roll-to-roll produced SERS substrates with gold nanoparticles

The Chapter is directly adopted from the correspondent publication (Uusitalo et al. 2016).

Authors: Martin Kögler[b,g](eq.), Sanna Uusitalo[a](eq.), Anna-Liisa Välimaa[c], Alexey Popov[d], Yury V. Ryabchikov[e,i], Ville Kontturi[f], Samuli Siitonen[f], Jarno Petäjä[a], Tiina Virtanen[h], Riitta Laitinen[c], Matti Kinnunen[d], Igor Meglinski[d], Andrei Kabashin[e], Alex Bunker[b], Tapani Viitala[b] and Jussi Hiltunen[a]

[a]VTT Technical Research Centre of Finland, Kaitoväylä 1, 90590 Oulu, Finland

[b]Drug Research Program, Faculty of Pharmacy, Division of Pharmaceutical Biosciences, University of Helsinki, P.O. Box 56, 00014 Helsinki, Finland

[c]National Resources Institute Finland (LUKE), Bio-based Business and Industry. University of Oulu, P. O. Box 413 (Paavo Havaksen Tie 3), FI-90014, Finland

[d]Optoelectronics and Measurement Techniques, Faculty of Information Technology and Electrical Engineering, University of Oulu, Finland

[e]Laboratoire Lasers, Plasmas Procédés Photoniques, Aix-Marseille University (AMU), 163 Avenue de Luminy, Case 917, 13288 Marseille Cedex 09, France

[f]Nanocomp Oy Ltd, Ensolantie 6, 80710 Lehmo, Finland

[g]Laboratory of Bioprocess Engineering, Institute of Biotechnology, Technische Universität Berlin, Ackerstr. 71–76, D-13355 Berlin, Germany

[h]Lappeenranta University of Technology, School of Engineering Science, Research Group of Membrane Technology, P. O. Box 20, FI-53851 Lappeenranta, Finland

[i]P. N. Lebedev Physical Institute of Russian Academy of Sciences, 53 Leninskii Prospekt, 119 991, Moscow, Russia

3.2.1 Abstract

The rapid and accurate detection of food pathogens plays a critical role in the early prevention of foodborne epidemics. Current bacteria identification practices, including colony counting, polymerase chain reaction (PCR) and immunological methods, are time consuming and labour intensive; they are not ideal for achieving the required immediate diagnosis. Different SERS substrates have been studied for the detection of foodborne microbes. The majority of the approaches are either based on costly patterning techniques on silicon or glass wafers or on methods which have not been tested in large scale fabrication. We demonstrate the feasibility of analyte specific sensing using mass-produced, polymerbased low-cost SERS substrate in analysing the chosen model microbe with biological recognition. The use of this novel roll to-roll fabricated SERS substrate was combined with optimised gold nanoparticles to increase the detection sensitivity. Distinctive SERS spectral bands were recorded for *Listeria innocua* ATCC 33090 using an in-house build (785 nm) near infra-red (NIR) Raman system. Results were compared to both those found in the literature and the results obtained from a commercial time-gated Raman system with a 532 nm wavelength laser excitation. The effect of the SERS enhancer metal and the excitation wavelength on the detected spectra was found to be negligible. The hypothesis that disagreements within the literature regarding bacterial spectra results from conditions present during the detection process has not been supported. The sensitivity of our SERS detection was improved through optimization of the concentration of the sample inside the hydrophobic polydimethylsiloxane (PDMS) wells. Immunomagnetic separation (IMS) beads were used to assist the accumulation of bacteria into the path of the beam of the excitation laser. With this combination we have detected *Listeria* with gold enhanced SERS in a label free manner from such low sample concentrations as 10^4 CFU ml^{-1}.

3.2.2 Introduction

Foodborne diseases represent a serious public health issue. The incidence of epidemics related to food pathogens has increased significantly due to the greatly accelerated range and speed of distribution that has resulted from the increasingly global trade network for food products (Law et al., 2015). For this reason, food safety authorities around the world have realized the need for a strict regulatory framework, including an exhaustive food testing regime (Gandhi and Chikindas, 2007; Gasanov et al., 2005). Traditional methods for the detection of bacteria, include direct culture and colony counting, polymerase chain reaction (PCR) and immunological methods. These are all extremely labour intensive and time consuming; (Law et al., 2015; Mungroo et al., 2015; Velusamy et al., 2010; Zhao et al., 2014)

the extent to which a rapid and efficient food testing regime can be achieved using the currently available methodologies is limited. Raman spectroscopy is a promising new methodology for bacteria detection, with many advantages including identification of the specific species of the bacteria, rapid detection, multiple simultaneous analyses and being label free (Boyaci et al., 2015; Harz et al., 2009; Lu et al., 2011a, 2011b; Wang et al., 2015). The identification of the species of bacteria through Raman spectroscopy is achieved through the detection of organic molecules on the surface of the bacterial membrane and wall. Their chemical structure provides a specific fingerprint of the bacterium that shows up in the Raman spectrum (Harz et al., 2009). The detection of a small concentration of bacteria with conventional Raman spectroscopy can demand a level of sensitivity greater than what it is capable of. The usual lowest detected bacterial concentration being around 10^8 CFU ml^{-1} (Lu et al., 2011b; Smith and Dent, 2005; Wang et al., 2015) Regulatory agencies demand finding a single cell in 25 g of food and such low concentrations require a brief pre-enrichment step to reach a more detectable level of 10^4 to 10^5 CFU ml^{-1}(Gasanov et al., 2005). The conventional Raman spectroscopy cannot reach this level and the signal thus needs to be amplified. This can be achieved through the use of noble metallic materials, for example gold or silver, to trigger localised surface plasmons (Anker et al., 2008). Surface Enhanced Raman Scattering (SERS) is a special type of Raman spectroscopy, where irregular or patterned metal substrates or metal nanocolloids of different shape and size can be used for the signal enhancement (Anker et al., 2008; Bantz et al., 2011; Bibikova et al., 2015; Nie and Emory, 1997). Typically the best enhancement effect is achieved with silver induced SERS (Liu et al., 2007). However, the use of silver has some drawbacks. As a substance it is antimicrobial and thus affects the sample under inspection. It is chemically quite reactive and the stability and reproducibility of the silver substrates and colloids (Ag NP) can also be an issue (Anker et al., 2008; Bantz et al., 2011) Gold is preferred in microbe detection as it is stable, non-toxic and has the optimal excitation wavelength in the near-infra red region, reducing auto-fluorescence issues generated by the microbes. Among the foodborne pathogens *Listeria monocytogenes* is the most common culprit in causing death due to food poisoning. The fatality rate for *L. monocytogenes* infection is relatively high, ranging from 20 to 30 % (Mungroo et al., 2015). *L. monocytogenes* is an especially difficult pathogen to control, as a result of its tolerance to a wide range of temperatures and pH conditions. The detection of *Listeria* spp. with SERS has been studied previously with different SERS enhancers including different SERS substrate (Grow et al., 2003; Mungroo et al., 2015) approaches and SERS colloid (Chen et al., 2015; M. Fan et al., 2011; Green et al., 2008; Kairyte et al., 2012; Liu et al., 2007; Luo and Lin, 2008) research. The SERS substrates have several advantages over the colloids; these include more consistent patterns without unforeseen aggregation and the ability to act as a base for the entire analysis chip. On the other hand, colloids can reach better sensitivity and be preferable when there is a need to detect features in the region of a larger organism

like bacteria. The direct detection of bacteria in food is difficult due to background signals and requires the disintegration of the solid food containing the bacteria, e.g., by mechanical methods, followed by culturing of the bacteria at elevated temperatures in the food matrix to accelerate the bacteria growth to a detectable level. Weidemaier et al., (Weidemaier et al., 2015) has studied the detection of *L. monocytogenes* inside the food matrix with the help of immunomagnetic beads and nanoparticle SERS tags with antibodies, as they point out, the method is sensitive to the extent to which the magnetic particles can be concentrated within the area of the laser beam and care must be taken to succeed with reproducible pelleting of the magnetic particles. A more common method for bacteria detection is to remove the bacteria from the food matrix, often with immunocapture and subsequently pre-enrich the concentration before detection (Zhao et al., 2014). Although the pre-enrichment technique requires culturing this can be used as a normalising factor for the state of the pathogen. The growth of Listeria at different temperatures, for example 4, 25, or 37 °C, produces bacteria with different amount of flagella and a different level of virulence. This affects the spectral fingerprint of the bacteria; in order to obtain reproducible spectra for bacteria, the same growing conditions in addition to detection processes are required (Efrima and Zeiri, 2009; Grow et al., 2003). In previous research, it has been shown that it is possible to differentiate bacteria through SERS analysis (Efrima and Zeiri, 2009; Knauer et al., 2010; Premasiri et al., 2005; Zhou et al., 2014). Preliminary results also indicate that SERS can be used for identifying bacteria and spores even at a strain level (Efrima and Zeiri, 2009; Grow et al., 2003). Usually this requires a high concentration of bacteria. With low concentration the assistance of immunocapture may be needed for the separation of different bacteria. The genus *Listeria* consists of fifteen species from which only *Listeria monocytogenes* is pathogenic to humans (Weller et al., 2015). Immunocapture by current commercially available antibodies can seldom distinguish between the *Listeria* species. There are studies focussing on the production of high quality antibodies only for *L. monocytogenes* (Mendonça et al., 2012). The presence of non-pathogenic *Listeria* such as *Listeria innocua* may, however, indicate also contamination with *L. monocytogenes* (Mendonça et al., 2012). Furthermore, as the morphologic structure of *L. innocua* is similar to *L. monocytogenes* and their Raman/SERS spectra are quite similar, *L. innocua* can be used as a model for *Listeria* detection (Green et al., 2008). The detection of Listeria with SERS has been previously studied by several research groups. The majority of studies have focussed on the detection of *Listeria* at high concentration, 10^8 to 10^{10} CFU ml^{-1} (C. Fan et al., 2011; Kairyte et al., 2012; Liu et al., 2009, 2007; Luo and Lin, 2008; Mendonça et al., 2012; Mungroo et al., 2015) and many have used chemometric analysis for the separation of Listeria spectra from the spectra of other pathogenic bacteria (C. Fan et al., 2011; Liu et al., 2009, 2007; Mungroo et al., 2015). Fewer studies have focussed on lowering the detection limit of the SERS proce-

dure for Listeria detection than on the acquisition of representative spectra. Chen et al. have developed a method for detection of *L. monocytogenes* and *L. innocua* by in situ synthesis of silver nanoparticles (Chen et al., 2015). The limit of detection for the model sample *L. innocua* was found to be 10^3 CFU ml^{-1}. The assay for bacteria detection was, however, performed for bacteria in pure water and required an extra incubation step with the silver colloids and two washing steps after the incubation. The objective of this study was to develop a simplified and affordable method for label-free detection of *Listeria* with high sensitivity that is possible to perform on a structured SERS substrate. The conventional way for fabricating structured SERS substrates is to use methods such as spin-coating, dip coating, chemical vapour deposition, electrochemical synthesis, electron beam lithography and (Chen et al., 2012; Chung et al., 2011; Galarreta and Norton, 2011; Huebner et al., 2012). However, they are not optimised for manufacturing single use chips in terms of throughput volume or cost. There are also many methods such as liquid–liquid interface formation, pulsed laser deposition on microscope slides and reduction of gold chloride III in natural rubber membranes which have been only tested in lab scale as batch fabrication (Cabrera et al., 2012; Hoppmann et al., 2014; Smyth et al., 2013; Suzuki et al., 2004). The fabricated sensor areas are often small and the fabrication methods are difficult to transfer into high volume production required of truly disposable sensor chips. Our approach is to fabricate the structured SERS substrates on polymer webs in large scale with UV imprint lithography. This enables the fabrication of large sensor surface areas which can be easily cut into smaller SERS substrates (Oo et al., 2013; Uusitalo et al., 2015). The fabricated SERS substrates are coated with a thin layer of gold by evaporation before integration of hydrophobic sample wells. This SERS platform is suitable for low cost high volume production and is practical for one-time use, which diminishes the contamination issues often encountered in microbe detection. Gold colloids were added to gain additional plasmonic enhancement. The method uses immunomagnetic separation (IMS) beads as bacteria cell concentrators and the only washing steps occur during the pre-enrichment phase. SERS enhancement of different types of gold nanoparticles with Listeria was studied and the colloids with the best enhancement effect were used in combination of R2R nanostructured gold SERS substrates.

3.2.3 Experimental

3.2.3.1 Gold nanoparticle synthesis

Ultrapure nanoparticle fabrication

Hurricane Spectra Physics Ti/sapphire laser operated at 800 nm with pulse duration 110 fs and repetition rate 1000 Hz was used for formation of gold nanoparticles (Au NPs) with a two-step approach (Besner et al., 2006; Maximova et al., 2015). In the first step, a gold target was immersed in 5 ml of deionized water at 10 mm below the water surface. Colloidal solution of Au NPs was produced by ablating the target at 150 mJ per pulse fluence for 30 minutes. The target was moved during the ablation step when material was collected from larger area. In the second step, additional laser fragmentation was performed to narrow the size distribution of Au NPs and to improve their stability. The fragmentation was performed by focussing a laser beam with 85 mJ per pulse fluence in the centre of the liquid volume that was stirred with a permanent magnet for 60 minutes (Besner et al., 2006).

AuNP fabrication for medium and large size particles

Colloidal Au NPs were synthesized by following the Frens-method (Kögler et al., 2016). 100 ml of 0.01 % (wt/vol) $HAuCl_4$ aqueous solution was heated to boil under vigorous and continuous stirring, followed by dropwise addition of 0.6 ml of 1 % (wt/vol) trisodium citrate solution. The solution was kept boiling for approximately 1 h until the color changed to light red. The final AuNP-solution was prepared by centrifugation at 3500 rpm for 5 minutes (Eppendorf model 5430R) and subsequently followed by the removal of the supernatant. The final dark red AuNP-solution with a concentration of about 5500 mg l^{-1} was used and partially diluted in ratio 1:5 in H_2O. Ag NPs with the average size of 40 nm were purchased from Sigma-Aldrich for reference measurements with the commercial time-gated Raman spectrometer (Rojalin et al., 2016).

3.2.3.2 SERS substrate fabrication

The SERS patterns were imprinted on top of a poly(methyl methacrylate – PMMA) polymer sheet with roll-to-roll UV nanoimprint lithography (Oo et al., 2013). The produced polymer webs and die-cut sheets before and after gold deposition are presented in Fig. 18. Reverse gravure technique was used to apply UV-curable lacquer on top of the PMMA web. Embossing reel was used to imprint the SERS patterns and the lacquer was cured through the PMMA web with UV light exposure. After die-cutting SERS substrates from the roll, a 240 nm gold layer was added by evaporating on top of the polymer SERS surface (Oo et al., 2013).
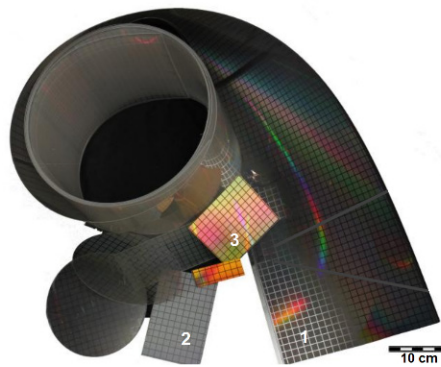
Figure 18 – Photograph of roll-to-roll patterned polymer webs and die-cut sheets before and after gold deposition.

3.2.3.3 PDMS well integration

Sample wells were created into 1 mm thick PDMS sheets (Wacker, Elastosil) by biopsy punches of a diameter of 1–2 mm. These PDMS wells were bonded onto the polymer SERS substrates by physical adsorption. The hydrophobicity of the wells forces the sample to retreat inside the PDMS well and have contact with the gold layered patterned SERS surface.

3.2.3.4 Cultivation of L. innocua and IMS bead separation

L. innocua ATCC 33090 was cultivated in LEE Broth (Labema, Lab M Limited, pH 7.2 ± 0.2) at 35 °C for 20 h without shaking. The concentration was analysed spectrophotometrically (Dynamica HALO DB-20S) and diluted into concentration series (10^3 CFU ml^{-1} to 10^9 CFU ml^{-1}) in LEE broth. IMS was performed using Dynabeads anti-*Listeria* (Life Technologies (Invitrogen) 71006), and a Dynal Magnetic Particle Concentrator DynaMag-2 (Invitrogen Dynal) as follows: 1 ml volumes of bacterial culture was added to each of the microcentrifuge tubes containing a 20 ml volume of Dynabeads anti-Listeria (Dynal) followed by incubation at room temperature for 10 min with continuous mixing by Mix-Mate

(Eppendorf). The beads were concentrated by magnetic field (in the Dynal MPC-M) onto the side of the tube for 3 min, supernatants were carefully aspirated and the samples were washed with the washing buffer (0.15 M NaCl, 0.01 M sodium phosphate buffer, pH 7.4 with 0.05 % Tween 20). After that the beads were concentrated and the supernatant removed. Finally, the bead–bacteria complexes were re-suspended into 100 ml of washing buffer for the SERS detection. For reference a concentration analysis was performed with 50 ml volumes of bead–bacteria complexes streaked onto differential selective agar *Listeria* acc. to Ottaviani and Agosti (ALOA) chromogenic agar (Labema) and incubated at 35 ± 0.5 °C for 24–48 h.

3.2.3.5   *SERS spectral acquisition of Listeria innocua and postprocessing*

Surface-enhanced Raman spectroscopy (SERS) spectra of *L. innocua* with Au NPs were detected from samples pipetted into PDMS wells integrated on top of SERS active substrates. Sample amounts varied from 5 to 10 µl and well diameter varied from 1 to 2 mm. Bacteria samples were pipetted into the wells and the chosen Au NPs were pipetted sequentially. SERS spectra were recorded with an in-house built Raman system coupled into an Olympus microscope with a 785 nm continuous wave (CW) laser. The minimum laser power irradiation used was 10 mW with 40 × magnification to excite the samples. A maximum of 40 mW was used in combination with low magnification (20 ×). The signal collection time was 5 seconds without averaging. Reference spectra for *L. innocua* were recorded with 40 nm sized Ag NPs by a commercial 532 nm picosecond pulsed laser time-gated Raman spectrometer (TimeGate Instruments Oy, Finland) with an average power of 10 mW, as well coupled into Olympus microscope (Rojalin et al., 2016). The signal integration time was set to cover the SERS signal and the fluorescence decay-time from 0.9–1.6 ns. The bacteria sample was pipetted on top of a glass slide prior to the detection. TimeGate measurements where analysed with TimeGate spectral processing tool and the acquired data was baseline corrected with a simple linear algorithm in Matlab (release 2015a, Mathworks Inc., USA) after opening the data with the PLS toolbox, version 2.0 (Eigenvector Research Inc., Manson, WA, USA). Further data handling and figure plotting was executed with Origin Pro (version 9.4, OriginLab corp., USA).

3.2.4 Results and Discussion

3.2.4.1 Methods for the detection of *Listeria innocua*

Typically *Listeria* spp. has been identified by the SERS method from highly concentrated samples, mostly in the range of 10^7 CFU ml^{-1} to 10^{10} CFU ml^{-1}. When the detected concentrations are more realistic and the bacterial cells available for the detection are fewer, then the intensity of the detected Raman peaks diminishes and many of the peaks disappear from the spectrum. Thus it is more difficult to identify the bacteria from other bacterial species and the background with incomplete spectra. In these cases the identification of the bacteria can be handled by pathogen-capture proteins while SERS is used for the detection (Weller et al., 2015), Grow *et al.* have detected *Listeria* on planar SERS substrates by capturing and accumulating bacterial cells near the surface with an antibody layer (Grow et al., 2003). Although they concluded that the use of antibodies was possible and identification of bacteria was successful, the use of antibodies on the surface weakened the signal. This was assumed to be due to the increased separation distance between the surface and the bacterial (Tian et al., 2007). Thus, this approach with planar SERS substrates was not optimal. Another possibility for capturing bacteria is the use of immunomagnetic separation beads which have been used in several *Escherichia coli* studies (Galarreta and Norton, 2011; Huebner et al., 2012) and at least in one *Listeria* growth study (Weidemaier et al., 2015). Usually, the IMS beads are either removed before detection or used as a part of a customised sandwich assay with SERS labels. In order to simplify the detection process we have developed a method to detect *L. innocua* in a label-free manner with IMS beads present during the SERS detection. The bacterial cells were captured by using a commercially available IMS separation kit. The sample was placed into the hydrophobic PDMS well on top of the polymer SERS substrate as is shown in Fig. 19 with the gold nanoparticles. Without IMS beads and PDMS well the bacterial cells in the liquid droplets spread wide apart and typically due to evaporation accumulated randomly to the droplet edges. We found that by using immunomagnetic separation beads during the detection we obtained a more stable SERS signal due to the more constant settling of the heavy IMS beads on to the sensor surface. A close-up transmission electron microscopy (TEM) picture of the IMS beads and a scanning electron microscopy (SEM) picture of IMS beads on top of the patterned SERS substrate can be seen in Fig. 20A and 20B respectively. In order to further enhance the SERS signal and to detect the features of the bacterial cells, gold nanoparticles were added around the bacteria bound to IMS beads.

Figure 19 – Schematic of a PDMS well on top of a patterned SERS substrate with IMS bound *L. innocua* and Au NPs. The integrated hydrophobic PDMS well concentrates the sample inside the well on top of the SERS substrate in a more consistent manner than a free droplet on top of the substrate would. Au NPs are located around the bacteria giving a stronger SERS enhancement. IMS beads bind the bacteria around them and concentrate them inside the excitation laser beam strengthening the SERS signal.

(A)   **(B)**

Figure 20 – (A) TEM image of IMS beads with gold nanoparticles. The scale in the picture is 500 nm. (B) SEM image of the IMS beads (Invitrogen dynabeads) on top of patterned SERS substrate.

3.2.4.2 AuNP characterization

In search for the optimal gold nanoparticles (Au NPs) for bacteria detection with SERS, 3 candidates were selected.
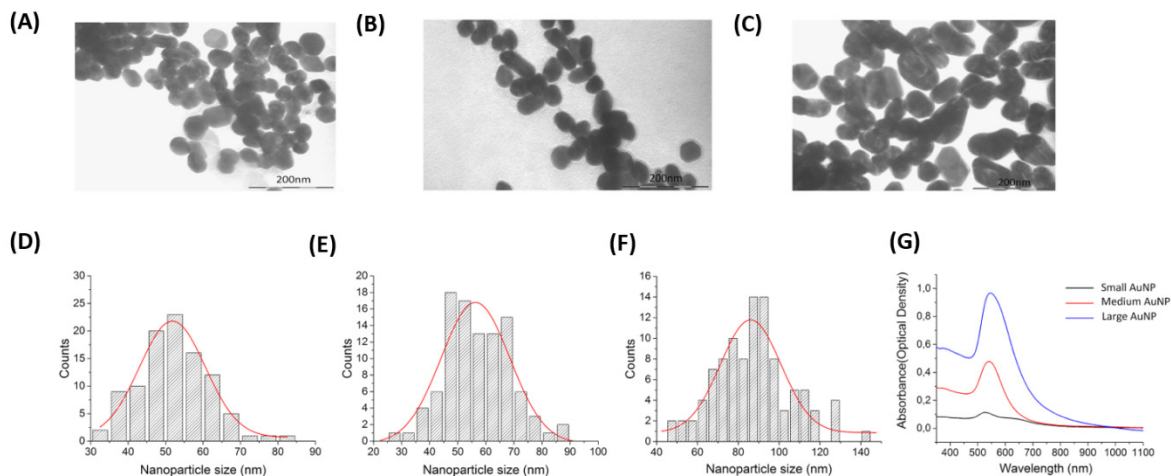
Figure 21 – (A–C) TEM images of the different sized Au NPs: small, medium and large size Au NPs respectively. (D–F) The corresponding size distribution histograms calculated from TEM images of the Au NPs with Gaussian fit: small, medium and large size Au NPs respectively. Each histogram has been calculated from 100 particle sizes with ImageJ software. (G) UV-Vis spectrum for the small, medium and large size Au NPs.

Ultrapure small Au NPs fabricated by femtosecond laser fragmentation were chosen as they could show better biocompatibility with bacteria cells than the synthesized Au NPs (Blandin et al., 2013; Maximova et al., 2015). The physically fabricated Au NPs lack the traces of non-reacted starting reagents, by-products, ions and surfactants, and have an additional advantage of lower background signal. Chemically synthesized medium size Au NPs and larger Au NPs were chosen to compare the signal intensity using differently shaped and sized particles. The NP size has been previously shown to matter in microorganism detection and a rod like shape has seemed beneficial for SERS enhancement (Tamer et al., 2011). The size and morphology of the fabricated Au NPs were retrieved by transmission electron microscopy (TEM) by using a LEO 912 OMEGA (Zeiss, Germany). One droplet of the 10 µl of aqueous nanostructure suspension was deposited onto a carbon-coated copper grid for TEM characterization. Fig. 21 shows the TEM images, the corresponding size distributions of the AuNP with Gaussian fit and the UV-Vis spectra of the AuNP. The maximum size for the different AuNP was estimated with the help of Gaussian fit shown in Fig. 21D–F. For the ultra-pure Au NPs the maximum size was found to be around 50 nm. The medium sized Au NPs showed a maximum of 60 nm with occasional large 90 nm sized particles. The large Au NPs had a maximum of 85 nm and a more rod like shape. From the UV-Vis spectra in Fig. 21G it can be seen how the maximum absorption peak of Au NPs shifts closer to 600 nm

wavelength as the maximum size of the particles grows from 50 nm to 85 nm. The SERS effectiveness of the different sized Au NPs was studied by pipetting 5 µl of bacteria sample and 2 µl of concentrated NP solution into 2 PDMS wells positioned on top of the patterned SERS substrate. The acquired SERS spectra are presented in Fig. 22A. According to the bar plot of the intensity of 737 cm^{-1} peak presented in Fig. 22B, the medium size and the large size particles gave similar intensities for a bacteria concentration of 5×10^5 CFU ml^{-1}.
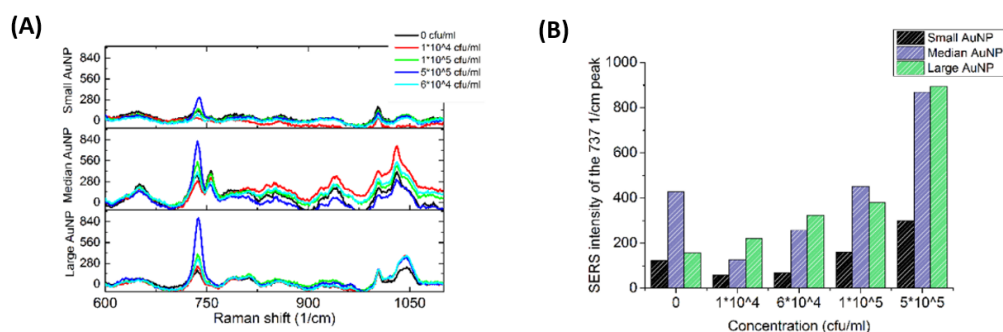
Figure 22 – (A) concentration series of the IMS bound *L. innocua* ATCC 33090 with the Au NPs inside a PDMS well on top of a patterned SERS surface shows how the large Au NPs have the best separation ability between the smallest concentrations and the 0 reference. The results are an average of 18 spectrums. (B) A bar plot of the SERS intensity for the dominant *L. innocua* peak at 737 cm^{-1} for different concentrations with the Au NPs inside a PDMS well on top of patterned SERS surface clarifies the choice of large AuNP as the one to use for further studies for best sensitivity.

However, the large nanoparticles were chosen for further studies because the maximum of their UV-Vis spectra was closest to 785 nm and they provided more consistent spectra compared to the other Au NPs, which originated from the lower amount of background peaks thus giving a better resolution. These results strengthen the hypothesis that larger nanoparticles enhances the signal more than small round ones for microbe detection (Butler et al., 2015). The way the Au NPs were fabricated played a minor role in enhancing the signal. Physical ablation could not benefit the detection in such a manner which would have counterweighted the advantage of the size and the shape of the particles.

3.2.4.3 The development of the detection process

Commercial Dynabeads were used to capture the *L. innocua* cells for the SERS detection. The SERS signal recorded with IMS beads, possibly due to accumulation of more bacterial cells inside the excitation laser spot, was found to be 20 times stronger than the signal recorded without the beads. Fig. 23A shows the results for the comparison of studies with and without IMS beads and Fig. 23B shows the variation between 9 measurements points measured with IMS beads.
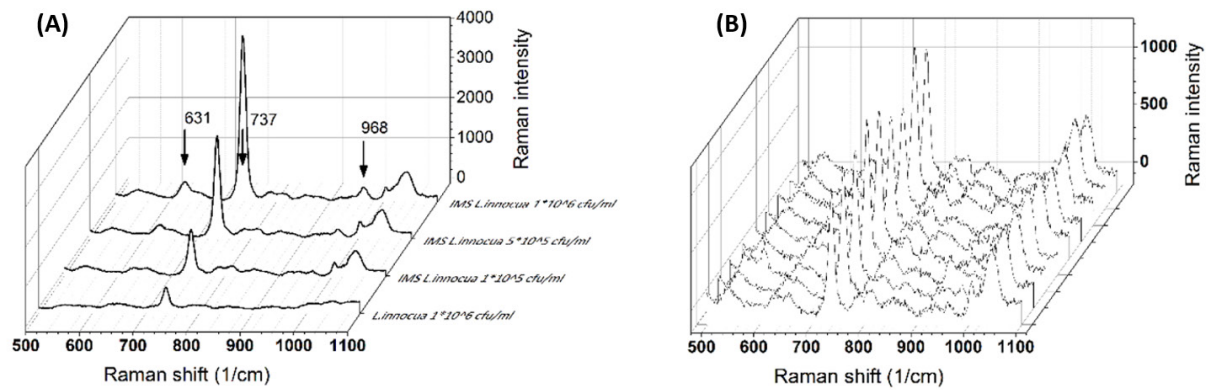
Figure 23 – (A) The effect of IMS concentration to the *L. innocua* ATCC 33090 SERS intensity with the Au NPs inside a PDMS well on top of patterned SERS surface. The cumulative effect of the IMS beads to the bacteria strengthens the SERS signal considerably. The intensity of 1×10^5 CFU ml^{-1} sample with IMS has 2 times stronger 737 cm^{-1} peak than the 1×10^6 CFU ml^{-1} sample without IMS. (B) The variation in SERS spectra of 1×10^5 CFU ml^{-1} *L. innocua* with IMS between 9 measured points.

The detection of *L. innocua* with the IMS beads was further studied on top of the patterned SERS substrate without Au NPs, as well as on top of silicon wafer with Au NPs and on top of patterned SERS substrate with Au NPs to see if there was an advantage in combining the SERS substrate with the Au NPs for bacteria detection. Fig. 24 represents the intensity differences between the measurements and it can be seen that the best intensities for the main dominant peak of 737 cm^{-1} were reached with the combination of the SERS substrate and Au NPs.
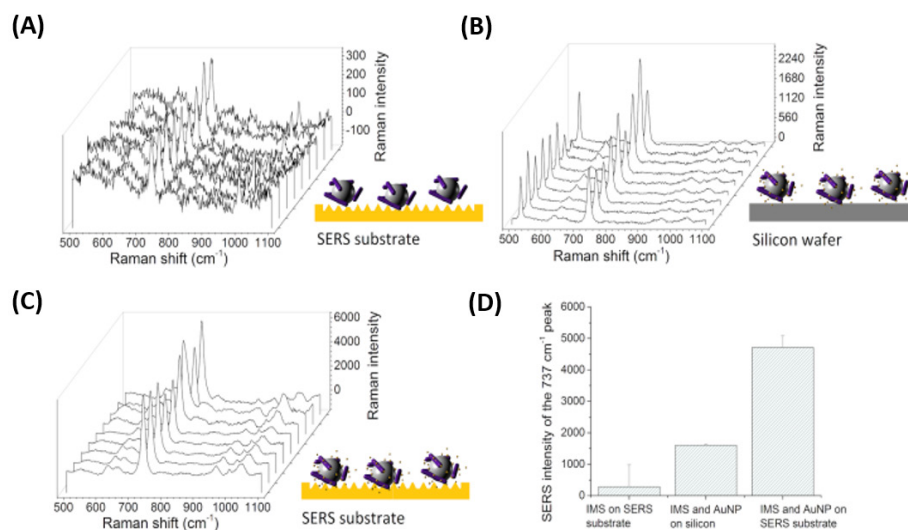
Figure 24 – (A) IMS bound 1×10^7 CFU ml^{-1} *L. innocua* ATCC 33090 inside a PDMS well on top of patterned SERS surface. (B) IMS bound 1×10^7 CFU ml^{-1} 1 *L. innocua* ATCC 33090 with large Au NPs inside a PDMS well on top of a silicon wafer. (C) IMS bound 1×10^7 CFU ml^{-1} *L. innocua* ATCC 33090 with large Au NPs inside a PDMS well on top of a patterned SERS surface. (D) A bar plot of the SERS intensity for the dominant *L. innocua* peak 737 cm^{-1} for the cases presented in (A–C).

3.2.4.4   The detected SERS lines for L. innocua ATCC 33090 and the effect of the traces of culture media and buffers on the SERS spectra

The captured *L. innocua* was first detected inside a PDMS well in a liquid state with a 40 mW laser power and a 20 × magnification. Fig. 25A shows the mean spectra for the *L. innocua* specific Raman bands. It can be noted that when the bacterial amount diminishes some lines stay constant showing the lines created by the traces of culture medium and buffer liquids. Thus, it can be concluded that 9 Raman bands initiating from the bacterial cells were detected. Fig. 25B shows the Raman bands created by the sample matrix and by the original cultivation media of the bacterial cells, i.e., the LEE broth.

Figure 25 – (A) Baseline corrected SERS spectra from *L. innocua* ATCC 33090 with large Au NPs inside a PDMS well on top of patterned SERS surface with IMS beads. Detected with 20 × magnification with a detection limit between 1×10^7 CFU ml^{-1} and 1×10^6 CFU ml^{-1}. The peaks maintaining their height with lower concentrations are caused by cultivation media residuals, Au NPs, IMS beads and other disturbances coming from the sample matrix. (B) Comparison of baseline corrected Raman intensities for the culturing media, i.e., LEE broth, and the 0 CFU ml^{-1} sample. The reason behind the peaks remaining in the *L. innocua* spectrum as the sample concentration is lowered are the peaks originating from the culture broth and the buffer solutions used for IMS bead washing steps.

Most of the background bands seem to originate from traces of the LEE broth. The nine Raman lines detected for *L. innocua* are listed in Table 3 with tentative assignments found in literature references.

Table 3 – Raman bands detected for *L. innocua* ATCC 33090.

Detected lines	Raman shift (cm^{-1})	Tentative assignments	Reference
631	627/620	Phenylalanine (skeletal)	(Luo and Lin, 2008; Maquelin et al., 2002)
737	732	glycosidic ring mode of D-glucoseam-ine (NAG), adenine or CH$_2$ rocking	(L Cui et al., 2015; Luo and Lin, 2008)
968	955	N-C stretching	(Vohnik et al., 1998)
1142	1134/1130	C-N and C-C stretch (carbohydrates)	(Chen et al., 2015; C. Fan et al., 2011)
1271	1230-1295	Amide III	(Liu et al., 2007; Lu et al., 2011a; Maquelin et al., 2002)
1339	1334/1339/1338	Deformation CH/Amide III/ signature of adenosine monophosphate and guanosine monophosphate, aromatic amino ac-ids tyrosine and tryptophan	(Harz et al., 2009; Maquelin et al., 2002; Vohnik et al., 1998)
1374	1371	DNA	(Harz et al., 2009)
1397	1392/1398	Symmetric deformation of CH$_3$ groups	(Al-Qadiri et al., 2008; C. Fan et al., 2011)
1450	1453	CH$_2$ deformation (lipids)	(Li Cui et al., 2015; C. Fan et al., 2011)

The dominant peak at 737 cm^{-1} has been previously suggested to originate from a glycosidic ring, ad-enine or CH$_2$ rocking (Szymborski et al., 2014). Since the presence of adenine on the surface of the bacterial cell is unlikely and since the outer wall structure of Gram-positive bacteria such as Listeria spp. consists of a thick peptidoglycan structure rich in N-acetyl D-glucosamine (NAG), the origin of the peak is more likely caused by a glycosidic ring mode of NAG than adenine (Culha et al., 2012; Luo and Lin, 2008). The three closely aligned lines in the range of 1300–1400 cm^{-1} are interesting since three of them together have not been detected with *L. innocua* or *L. monocytogenes* in previous studies. The line 1339 cm^{-1} has been previously detected with Listeria by Luo et al. (Luo and Lin, 2008) as a shifted line 1331 cm^{-1} which was suggested to originate from CH$_2$ deformation. However, there are closer assignments to the detected 1339 cm^{-1} listed in E. coli studies. Vohník et al. (Vohnik et al., 1998) have suggested that the exact line 1339 cm^{-1} could be originating from amide III and Harz *et al.* suggest that the line is due to the signature of adenosine monophosphate and guanosine monophosphate, aro-matic amino acids tyrosine and tryptophan. Harz *et al*. (Harz et al., 2009) also have a listing very near to the second line 1374 cm^{-1} assigned to DNA. The last line of the group 1397 cm^{-1} is most likely due to the symmetric deformation of CH$_3$ group which has also been detected for the case of *E. coli* (Al-Qadiri et al., 2008; C. Fan et al., 2011). When comparing the Raman bands detected for *L. innocua* with the previous research, it is interesting to note that the SERS spectrum in different studies varies. Liu et

al. among others has stated that this could be due to the differences in the measurement conditions such as the culture broth and temperature that have been used, excitation wavelength of the laser or the SERS enhancer (C. Fan et al., 2011; Liu et al., 2007). To test this hypothesis we recorded the SERS spectra of the same *L. innocua* sample with changed SERS conditions. Fig. 26 shows the peaks detected around the dominant peak 737 cm^{-1} for 3 different SERS conditions. In the first case the combination of Au NPs on top of the patterned SERS substrate with 785 nm CW-excitation was used, while in the second case a SERS spectrum was detected from the same sample on top of a glass slide with Ag NPs and pulsed laser excitation at a different wavelength of 532 nm. The results are consistent. They are also similar to the third case published by Luo *et al*. who used Ag NPs with 785 nm CW-excitation wavelength. Another research group of Kairyte *et al*. (Kairyte et al., 2012) used silver NPs with 1064 nm excitation with a similar outcome.

Figure 26 – Three SERS spectra of *L. innocua* were compared to confirm that the measured spectrum originates from the assumed bacteria. The literature reference has been borrowed from a publication by Luo, B. Steven et al. (2008) with a concentration of 1×10^8 CFU ml^{-1} *L. innocua* measured with CW 785 nm laser excitation with Ag NPs. The 785 nm CW-laser excitation with the in-house built device has been recorded from 1×10^6 CFU ml^{-1} IMS bound *L. innocua* ATCC 33090 with large Au NPs inside a PDMS well on top of a patterned SERS surface with IMS beads, detected with 40 × magnification. The 532 nm Time-gated pulsed laser excitation is a AgNP-enhanced SERS spectra of 1×10^6 CFU ml^{-1} IMS bound *L. innocua* ATCC 33090 placed on top of a glass slide and 40 × magnification (TG-SERS).

Clearly when comparing the results, there is no connection between the variations in spectra and the enhancer used (silver/gold). Additionally the excitation wavelength does not seem to affect the detected spectrum. The detection process was developed further by manually lowering the minimum laser power of the Raman system to 10 mW. This enabled the use of larger magnification with the microscope without burning of the dried specimen during the measurement procedure. The sample density on the SERS substrate was also reduced to prevent the blocking of signal by the media traces of the sample liquids. It was noted that the media was disturbing the SERS signal if an excessive amount

of traces had dried on top of the SERS substrate. Limit of detection and repeatability of the detection process could have been enhanced further with extra washing steps for the IMS beads, but this was avoided in order to not complicate the sample handling. Fig. 27 shows the mean intensity changes of the dominant peak of 737 cm^{-1} as a function of *L. innocua* concentration with 40× magnification and 10 mW laser excitation power for several concentration series. For the concentration series in Fig. 27A and b the Raman intensity was normalised by the background peak at 787 cm^{-1}. The intensity of the dominant 737 cm^{-1} peak is displayed in Fig. 27B as a function of logarithmic *L. innocua* concentration that follows an exponential curve.
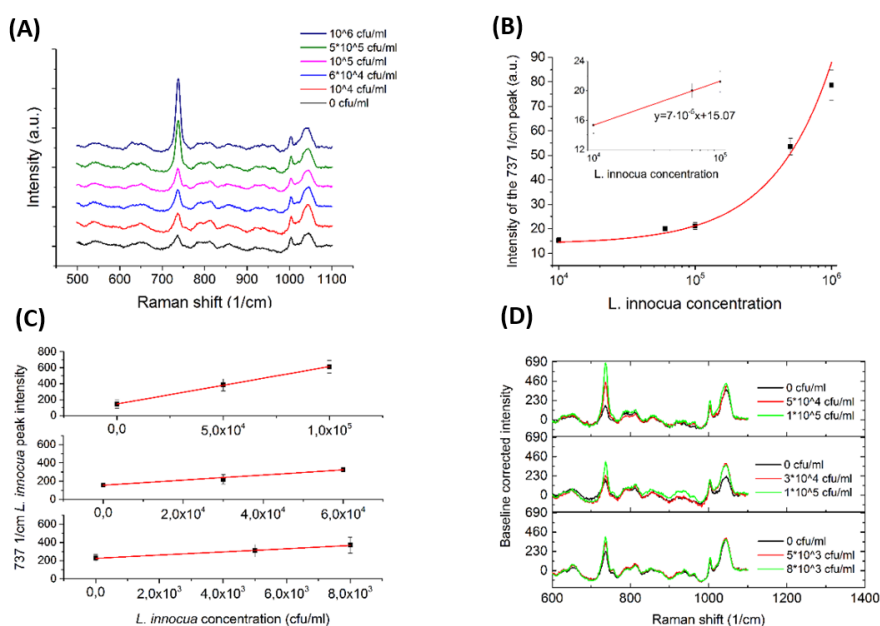
Figure 27 – (A) A normalised concentration series for LOD estimation. (B) An exponential fit for the normalised concentration series in logarithmic scale for the entire series and a linear fit for the small concentrations. (C) Comparison of the 737 cm^{-1} peak intensity for different concentration series with 5–10 ml dried IMS bound *L. innocua* ATCC 33090 samples placed with Au NPs into a 1–1.5 mm PDMS well on top of SERS substrate. (D) Comparison of baseline corrected Raman intensities for three of the concentration series. All figures are a mean of 9 measurement points with mean absolute deviations.

For the concentration range below 10^5 CFU ml^{-1} the relation was found linear. Since the blank 0 CFU ml^{-1} sample exhibits a signal at 737 cm^{-1}, the lowest limit of detection was considered through the deviation of the background signal generated by the sample matrix. According to the international union of pure and applied chemistry, IUPAC, the limit of detection (LOD) can be defined as the smallest concentration detected with reasonable certainty (Long and Winefordner, 1983), and derived from

$$\text{LOD} = k \cdot s_{\text{bi}} \cdot S, \qquad \text{[Eq. 6]}$$

where s_{bi} is the standard deviation of the blank measures, k = 3 is a numerical factor of confidence level approved by IUPAC and S is the slope of the calibration curve. S is defined as

$$S = \Delta c / \Delta I, \qquad\qquad \text{[Eq. 7]}$$

where Δc is the change in concentration and ΔI is the change in Raman intensity (Besse et al., 2005). By using equation (Eq. 7) and determining S from the linear fit shown in Fig. 27B, the LOD was calculated to be 1.4×10^4 CFU ml^{-1}. The concentration series shown in Fig. 27C and 27D confirm the LOD, since the deviation of the concentrations below 10^4 CFU ml^{-1} coincide with the deviations of the mean blank samples. This means that samples with lower concentrations cannot reliably be detected. In case of model *L. innocua* sample, the estimated detection time including pre-culture (Besse et al., 2005), 6 hours for 10^4 CFU ml^{-1} sample concentration, IMS preparation (15 minutes), sample deposition on SERS chip (15 minutes), SERS detection (10 minutes) and data handling (5 minutes), the total microbe analysis is estimated to be 7 hours. The time-saving of the developed method compared to the conventional official ISO 11290-1:1996/amd.1:2004 method in case of the model sample is approximately 41 hours with pre-cultivation. As a summary, we demonstrated in this study the use of disposable polymer SERS platforms and Au NPs with integrated sample wells for fast and simple detection of *L. innocua*. We have shown how the capture and deposit of the IMS bound bacteria cells onto the SERS substrate benefits the detection. In the future, the detection process could be further developed by utilizing the magnetic nature of the IMS beads on the SERS substrate for the removal of matrix traces e.g., by removing the matrix with wicking.

3.2.5 Conclusions

This study analyses the use of different types of Au NPs in addition to a structured polymer SERS substrate for Listeria detection. The polymer based SERS substrate has been produced with roll-to-roll fabrication and thus it is suitable for one time use due to the high volume production and the low cost per substrate. The results of this study provide new insights into *Listeria* diagnostics. We also demonstrate the benefit of using immunomagnetic separation beads as an accumulation assistant of the bacteria for enhanced signal intensity. The use of novel hydrophobic PDMS wells for sample preparation on SERS chips enables controlled sample appliance and reduces mean absolute deviation of SERS signals. The limit of detection in this methodology was determined to be in the range of about 10^4 CFU ml^{-1} shown for the first time with label-free gold enhanced SERS using optimized Au NPs combined with an Au based SERS substrate.

3.3 Bare laser-synthesized Au-based nanoparticles as non-disturbing SERS probes for Bacteria Identification

The Chapter is directly adopted from the correspondent accepted manuscript to the Journal of Biophotonics (Kögler et al. 2017).

Authors: Martin Kögler[a,b](eq.), Yury V. Ryabchikov[c,d](eq.), Sanna Uusitalo[e], Alexey Popov[f,g], Anton Popov[c], Gleb Tselikov[c], Anna-Liisa Välimaa[h], Ahmed Al-Kattan[c], Jussi Hiltunen[e], Riitta Laitinen[i], Peter Neubauer[b], Igor Meglinski[f,g,j], and Andrei V. Kabashin[c,j]*

[a]Drug Research Program, Faculty of Pharmacy, Division of Pharmaceutical Biosciences, University of Helsinki, P.O. Box 56, 00014 Helsinki, Finland

[b]Chair of Bioprocess Engineering, Institute of Biotechnology, Technische Universität Berlin, Ackerstr. 71-76, D-13355 Berlin, Germany

[c]Aix-Marseille University, CNRS, LP3 UMR 7341, Campus de Luminy-Case 917, 13288, Marseille Cedex 9, France

[d]P.N. Lebedev Physical Institute of Russian Academy of Sciences, 53 Leninskii Prospekt, Moscow 199 991, Russia

[e]VTT Technical Research Centre of Finland, Kaitoväylä 1, 90590 Oulu, Finland

[f]Optoelectronics and Measurement Techniques, Faculty of Information Technology and Electrical Engineering, University of Oulu, Erkki Koiso-Kanttilan katu 3, FI-90570 Oulu, Finland

[g]ITMO University, 49 Kronverksky Prospekt, St. Petersburg, 197101 Russia

[h]National Resources Institute Finland (LUKE) Bio-based business and industry, University of Oulu, Paavo Havaksen tie 3, FI-90014 Oulu, Finland

[i]Natural Research Institute Finland (LUKE), Bio-based business and industry, Itäinen pitkäkatu 3,20520 Turku

[j]National Research Nuclear University "MEPhI", Institute of Engineering Physics for Biomedicine (PhysBio), Bio-Nanophotonic Lab., 115409 Moscow, Russia

3.3.1 Abstract

The ability of noble metal-based nanoparticles (Au, Ag) to drastically enhance Raman scattering from molecules placed near metal surface, termed as Surface Enhanced Raman Scattering (SERS), is widely used for identification of trace amounts of biological materials in biomedical, food safety and security applications. However, conventional nanoparticles synthesized by colloidal chemistry are typically contaminated by non-biocompatible by-products (surfactants, anions), which can have negative impacts on many live objects under examination (cells, bacteria) and thus decrease the precision of bioidentification. In this paper, we explore novel ultrapure laser-synthesized Au-based nanomaterials, including Au nanoparticles and AuSi hybrid nanostructures, as mobile SERS probes in tasks of bacteria detection. We show that these Au-based nanomaterials can efficiently enhance Raman signals from model R6G molecules, while the enhancement factor depends on the content of Au in nanoparticle composition. Profiting from the observed enhancement and purity of laser-synthesized nanomaterials, we demonstrate successful identification of two types of bacteria (*Listeria innocua* and *Escherichia coli*). The obtained results promise less disturbing studies of biological systems based on good biocompatibility of contamination-free laser-synthesized nanomaterials.

3.3.2 Introduction

Raman scattering is known to provide a variety of information on the structure and composition of the matter, based on its vibrational fingerprints, and this information can be used for highly precise identification of chemical or biological species (Schmitt and Popp, 2006). Although Raman scattering is a very weak phenomenon, its cross section can be enhanced by many orders of magnitude by using noble metal (Ag, Au) nanostructures (Kneipp et al., 2007; Nie and Emory, 1997). The latter modality, termed as SERS, is based on the property of the metals to support oscillations of free electrons (plasmons) under optical excitation. Such plasmonic oscillations can amplify local electric field near the metal surface and thus drastically enhance Raman signals from target molecules placed near the metal (Kneipp et al., 2007; Nie and Emory, 1997). In particular, Raman spectroscopy (RS) has been adapted for the detection of bacteria species and the analysis of bacteria spores (Harz et al., 2009; Jarvis and Goodacre, 2008). The identification of bacteria is typically based on the detection of some specific organic molecules (bacterial "fingerprints") on the surface of the bacterial membrane via their unique Raman spectra (Harz et al., 2009). In SERS modality of bacteria detection, irregular or patterned metal substrates or metal nanocolloids of different shape and size are normally used for signal enhancement in order to lower the detection limit of this method (Chen et al., 2015; Cowcher et al., 2013; C. Fan et al., 2011; Jarvis et al., 2004; Jarvis and Goodacre, 2008; Knauer et al., 2010; Liu et al., 2007; Prucek et

al., 2012; Ravindranath et al., 2011; Sengupta et al., 2006; Temur et al., 2010; Wilson et al., 2007; Zhou et al., 2015, 2014). Such metal nanostructures adsorb to the surface of bacteria and provide information on molecular structures of the cell wall around the bacteria. It is important that SERS signals are unaffected by water, a significant component of biological cells or bacteria, while the presence of metal can quench auto-fluorescence, which is always present as a background in biological systems (Harz et al., 2009; Jarvis and Goodacre, 2008).

However, conventional Au or Ag nanoparticles (NPs) synthesized by chemical methods, such as the reduction of a gold precursor in the presence of a capping ligand (Brust et al., 1994; Frens, 1973), have some limitations for studies of live objects such as cells and bacteria. The problem is that nanomaterials prepared by chemical methods are typically contaminated by non-reacted starting reagents, by-products, anions and surfactants, as well as often covered by stabilizing ligands (Balasubramanian et al., 2010; Mukherjee et al., 2001). As shown in many studies (see, e.g., (Alkilany and Murphy, 2010; Chatterjee et al., 2011; Cui et al., 2013; El-zahry et al., 2015)), the use of such nanomaterials can be accompanied by a drastic aggravation of proliferation and viability of bacteria and cells under study. In other words, chemically-synthesized NPs are often disturbing for live bacterial or cell cultures under examination that decreases the precision of SERS based identification. In addition, SERS signals can be strongly affected by parasitic noise signals from the contaminants of NPs-stabilizing ligands, which complicates biomolecular identifications under ultra-low concentrations of target material.

Pulsed Laser Ablation in Liquids (PLAL) has recently emerged as a physical alternative to conventional synthesis (Fojtik et al., 1993; Kabashin and Meunier, 2007, 2003; Mafune et al., 2001; Sibbald et al., 1996), which promises a solution of the contamination problem of chemically-synthesized nanomaterials. This method is based on laser radiative removal (ablation) of material from a solid target in a liquid ambience, leading to a natural production of nanoclusters and their subsequent coalescence to form colloidal NPs solutions (Kabashin et al., 2010; Zhang et al., 2017). As a huge advantage of this method, laser ablation can be performed in ultrapure environment (e.g., in deionized water), which excludes any toxic contaminant on the surface of synthesized nanomaterials (Kabashin et al., 2010). Furthermore, using methods of ultrashort laser ablation (Mafune et al., 2001; Sibbald et al., 1996) or fragmentation (Besner et al., 2006; Maximova et al., 2015), one can prepare extremely stable aqueous solutions of "bare" (ligand-free) Au NPs having unique surface chemistry (Sylvestre et al., 2004) and different reactivity (Hebie et al., 2015; Wagener et al., 2012) compared to conventional colloidal nanomaterials. The absence of ligands and contaminants on the surface of such Au-based NPs gives a promise for their successful use as mobile probes for SERS applications and their efficiency in such tasks was recently

confirmed in our studies (Uusitalo et al., 2017a, 2016). Moreover, despite the absence of any biopolymer coating such "bare" Au NPs were found to have relatively low toxicity and a good cell uptake, which promises their successful use in live systems (Correard et al., 2014).

It should be noted that the versatility of laser-ablative technique makes possible an easy synthesis of a variety of alternative materials and composite structures, including nanomaterials having excellent compatibility with biological systems. Crystalline silicon (Si) is a prominent example of such material, which is one of essential elements in live organisms and is present in many biological tissues in the form of orthosilicate (SiO_4^{4-}) (He and Su, 2014). We recently showed that contamination-free laser-synthesized Si NPs are not only well compatible with biological systems in vitro and in vivo (Al-kattan et al., 2016; Tamarov et al., 2014), but are also biodegradable as they decay in aqueous environment into orthosilicic acid $Si(OH)_4$ and excrete from biological systems without any harmful effects (Baati et al., 2016). We envision that the incorporation of Si fraction into the composition of SERS probes could improve the compatibility of these probes with biological systems and bring novel functionalities. We recently showed the possibility for synthesizing such hybrid Au-Si nanostructures with controlled content of Si in NPs composition (Ryabchikov et al., 2016). In this paper, we employ bare (ligand-free) Au-based nanomaterials, including pure Au and AuSi NPs, synthesized by methods of laser ablation in deionized water, as SERS probes and access their efficiency in tasks of bacteria identification.

3.3.3 Materials and Methods

3.3.3.1 Laser fabrication of Au-based nanomaterials for SERS

The synthesis of pure Au NPs and Au-Si composite structures was described in detail in our previous studies (Mafune et al., 2001; Ryabchikov et al., 2016; Sibbald et al., 1996). Briefly, for the fabrication of pure Au NPs, radiation from a Ti:Sapphire laser (Hurricane Spectra Physics Laser, USA, 110 fs pulse duration, 800 nm wavelength, 1 kHz repetition rate) was focused by a 50 mm focal distance lens onto a gold target (99.99 %) immersed in 10 mL solution of deionized water (18 MΩ) and placed 20 mm below the liquid surface level. A platform containing the target in a liquid vessel was constantly moved in order to avoid ablation from the same area on the target surface. A solution of bare Au NPs was typically obtained after 20 min of irradiation onset and this process was accompanied by its deep red coloration. As follows from transmission electron microscopy (TEM) analysis (Fig. 28A), the mean size of Au NPs prepared by this method was about 25 nm. To prepare solutions of Au-Si hybrid structures with controllable Au content, we first prepared a solution of bare Si NPs in deionized water. Here, a Si wafer ((100), N-doped, 1–10 Ω cm) was ablated by the Ti:Sapphire laser similarly to how it was done in the case of gold. After several minutes of the ablation experiment, a solution of bare Si NPs with

concentration of 150 µg ml^{-1} was obtained. Then, the gold target was placed into so prepared solutions of Si NPs (preliminarily diluted to concentrations of 45 µg ml^{-1} and 25 µg ml^{-1}, respectively) and ablated similarly to how it was done in case of pure water ambience. As we previously showed (Ryabchikov et al., 2016), such ablation of Au in Si NPs solutions leads to the formation of Au-Si hybrid NPs and the size of these structures depends on initial concentration of Si NPs. As shown in Fig. 28B and C, composite Au-Si NPs prepared under 25 µg ml^{-1} and 45 µg ml^{-1} concentrations of initial Si colloids had the mean size of 14 nm and 9 nm, respectively. The decrease of the mean NPs size under the increase of initial Si NPs concentration was explained in our previous paper (Ryabchikov et al., 2016) by the existence of a strong interaction of laser-ablated Au nanoclusters with already formed water-dispersed Si NPs, similarly to how it happens in the case of biopolymers and other molecules (Correard et al., 2014; Sylvestre et al., 2004). Here, higher concentration of Si NPs causes the finalization of Au nanocluster growth at earlier stages, leading to a smaller mean size of hybrid NPs (Ryabchikov et al., 2016). As we also showed from EDX data (Ryabchikov et al., 2016), the content of Au in NPs composition appears to be inversely proportional to initial concentration of Si NPs. Therefore, smallest Au-Si NPs prepared at higher concentrations of Si NPs typically have a lower content of Au in their composition. For our experiments, we used 3 types of NPs with different content of Si in their composition: pure Au-100 % NPs (100 % Au); Au-60 % (60 %Au/40 % Si) and Au-30 % (30 %Au /70 % Si). Parameters of these three types of NPs are summarized in Table 4.

Table 4 – Characteristics of Au-based NPs prepared by laser ablation of the gold target in deionized water or Si NPs colloidal solutions.

Samples	Initial Si concentration (µg/ml)	Size, nm	Au/Si atomic ratio
Au-100 %	0	25 nm	100 % Au
Au-60 %	25	14 nm	60 %Au/40 % Si
Au-30 %	45	9 nm	30 %Au/70 % Si

3.3.3.2 Structural and optical characterization of laser-synthesized nanomaterials

A high-resolution transmission electron microscope (HR-TEM) JEOL 3010 (Japan) operating at 300 kV was used for investigation of the shape and the size of the fabricated Au-based NPs. For this purpose, a drop of freshly prepared colloidal solution was deposited on a carbon-coated copper grid, dried at room temperature and then examined by TEM. The size distribution of Au-based NPs was calculated by ImageJ software using 1000 particles. Chemical composition of laser-synthesized NPs was examined by EDX spectroscopy.

Raman Spectroscopy investigation of freshly prepared NPs was carried out using a confocal Raman system (Ntegra Spectra, NT-MDT Corp., Russia). An inverted optical scheme implying the excitation and collection of signals from the bottom side of the system was used for sample analysis. An oil immersion objective (100 x, 1.3 NA, Olympus, Japan) was used for focusing 532 nm CW laser radiation on the samples. Laser radiation was set to low power values (20 µW) to avoid heating effects during the measurements. The samples were prepared by dropping NPs solution on 150 µm thick borosilicate glass substrate and their subsequent drying at ambient conditions.

3.3.3.3 Rhodamine 6G sample preparation and SERS detection

Rhodamine 6G (R6G) was mixed with deionized water and diluted into concentration series (1 mM – 1 µM). 2 µl of R6G samples were dried into 1.5 mm polydimethylsiloxane (PDMS) wells placed on top of a silicon wafer or gold-coated polymer-based SERS substrates. 2 µl of Au–based NPs were added on top of the samples. The prepared samples were measured with an in-house built Raman system integrated with a microscope (Olympus, Japan) using 785 nm continuous-wave laser excitation. The used integration time was set to 2 s with a 40 x objective and 10.5 mW power at the sample. For the sensitivity testing with 1 µM – 500 µM R6G concentration range, 5–30 s integration times were used with a 50 x objective and 7.5 mW laser power at the sample.

3.3.3.4 Immuno-magnetic beads bound L. innocua sample preparations and SERS detection

The model bacteria (*L. innocua* ATCC 33090) were grown in LEE Broth, pH 7.2 ± 0.2 (Labema, Finland) at 35 °C for 20 h. A spectrophotometer HALO DB-20S (Dynamica, UK) was used for measuring the concentration. The samples were diluted to achieve bacteria concentrations of 10^5–10^6 cfu/ml in LEE Broth. The bacteria were captured with anti-*Listeria* Dynabeads (Life Technologies 71006, Thermo Fisher Scientific, USA) and a magnetic particle concentrator DynaMag-2 (Thermo Fisher Scientific, USA) was used for the capture as follows: 1 ml of bacterial culture was incubated with 20 µl volume of anti-*Listeria* Dynabeads for 10 min at room temperature under continuous mixing. The beads were pelleted by a magnet (Dynal MPC-M) onto the side of Eppendorf tubes, supernatants were removed and the samples were rinsed with a washing buffer. The beads were concentrated, the supernatant was removed and the captured bacteria with beads were resuspended into 100 ml of washing buffer for the SERS detection. The blank Raman spectrum of IMS beads in LEE Broth can be found in our earlier studies (Uusitalo et al., 2017a, 2016). Bacteria spectra were detected with 785 nm laser excitation, 60 s integration time, 50 x objective and 7.5 mW power. The average SERS spectra were calculated from 30 points measured for each concentration.

3.3.3.5 E. coli sample preparation and SERS detection

The model bacteria samples *E. coli* W3110 (wild-type strain) were grown in standard 250 ml shaking flasks by using a shaker/incubator device (LT-X series, Kuhner, Switzerland), at approximately 220 rpm and at a temperature of 37 °C. The amount of 100 ml Yeast Tryptone Phosphate Glucose (2xYTPG) growth medium with 10 ml of *E. coli* W3110 culture was used for the cultivation in two shaking flasks, one for the reference and one for the actual sample. The optical density respective to the biomass increase at different time spots was measured with a spectrophotometer at 600 nm (OD600). *E. coli* W3110 cells were harvested after 6 h of cultivation. The final *E. coli* W3110 biomass had an OD600 of 5.2. The sample was stored at + 4 °C, three times washed in deionized water and centrifuged prior the experiment to remove media traces. Approximately 25 µL sample volume was pipetted into a stainless steel cup used for the measurements. Au-based NPs were pipetted on top of the *E. coli* W3110 sample. The measurement was performed with a commercial time-gated Raman spectrometer (Timegate Instruments Oy, Finland) using pulsed laser excitation at a wavelength of 532 nm. The Raman device was connected to a standard laboratory Raman BWTek RPB 532 probe (B&W-Tek, USA) and approximately 25 mW was used at the sample spot. The signal collection time was set to cover the SERS signal and the fluorescence decay time 1.3–1.8 ns.

3.3.3.6 Post processing of the SERS spectral data

The *L. innocua* ATCC 33090 data was transferred into Matlab 2015a (Mathworks, USA) with PLS toolbox 2.0 (Eigenvector Research, USA) for linear baseline correction. The *E. coli* W3110 data was analyzed with a spectral processing tool (Timegate Instruments Oy, Finland) prior the Matlab plotting. Further data handling and plotting of the figures were performed with Origin Pro 9.4 (OriginLab, USA).

3.3.4 Results and discussion

In our experiments, we used 3 types of NPs with decreasing content of Au in their composition, as shown in Table 1: pure Au-100 % NPs (100 % Au); Au-60 % (60 % Au/ 40 % Si) and Au-30 % (30 % Au/70 % Si). As shown in Fig. 28, Au-based NPs were perfectly spherical in all three cases, while the mean size of NPs progressively decreased under the increase of Si content in NPs composition: 25 nm (Au-100 %); 14 nm (Au-60 %) and 9 nm (Au-30 %).
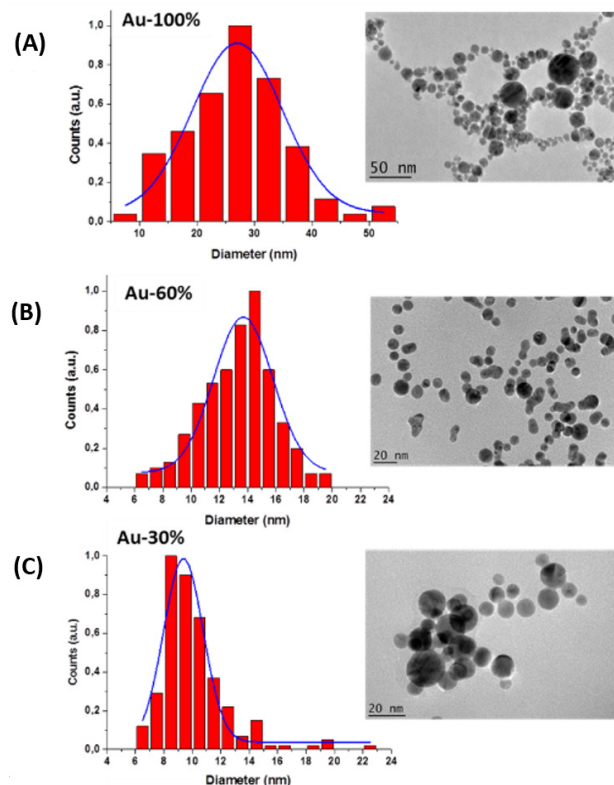
Figure 28 – HR-TEM images of Au-100 % (100 % Au) (A), Au-60 % (60 % Au/40 % Si) (B), and Au-30 % (30 % Au/70 % Si) (C) prepared by methods of femtosecond laser ablation in water, with corresponding size distribution.

As shown in Fig. 29A, extinction spectra from laser-synthesized Au-based NPs exhibited a characteristic peak around 520 nm, which is normally attributed to free electron oscillations (surface plasmons) over Au nanoparticles. Here, despite a significant content of Si in the composition of Au-60 % and especially Au-30 % NPs in the NPs shell, they still exhibited pronounced peaks associated with the excitations of plasmons over their gold fraction. This experimental fact is very important as it evidences the possibility of plasmon-related field enhancement even over composite Au-Si structures having a reduced content of plasmonic metal (Au) in their composition. It should be noted that in all three cases the plasmonic extinction peak was close to 520 nm, while for Au-60 % and Au-30 % it was red-shifted (by 1 nm and 3 nm, respectively), which could be explained by high refractive index of Si fraction compared to that of the aqueous environment (3.5 RIU over 1.33 RIU) (Jain et al., 2006).

Figure 29B shows Raman Scattering spectra from samples of dried Au-100 %, Au-60 %, and Au-30 % NPs deposited on glass substrates and measured by a highly sensitive Ntegra Spectra Raman confocal microscopy system.
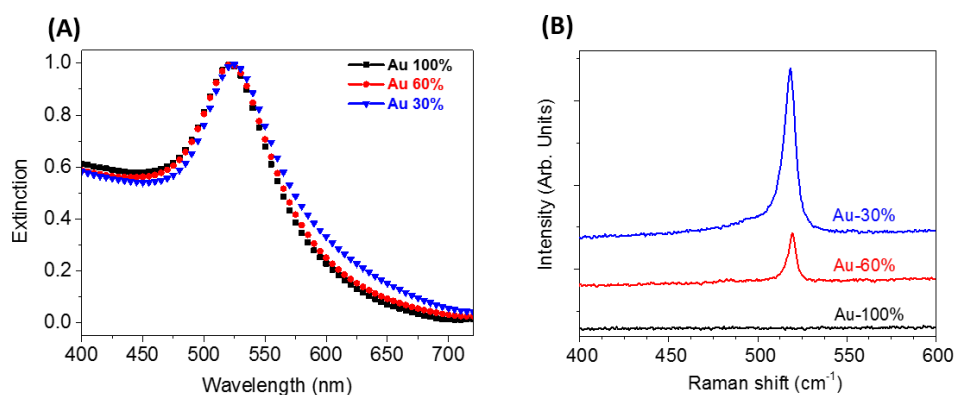
Figure 29 – Normalized extinction (absorption + scattering) (A) and Raman (B) spectra from laser-synthesized Au-based NPs with different content of Au in their composition: Au-100 % (black), Au-60 % (red) and Au-30 % (blue).

It is visible that Au-100 % NPs did not show any Raman features, which is normal for pure gold NPs samples. However, samples Au-60 % and Au-30 % exhibited a strong Raman peak at 520 cm^{-1}, which is generally attributed to crystalline Si, while the intensity of this peak increased under the increase of Si content reaching its maximal value for Au-30 % samples. Thus, in contrast to pure Au NPs, hybrid Au-Si structures exhibited a distinct Si-based Raman line as a new functionality. We believe that this functionality can be employed in biomedical studies, e.g., to track the localization of such SERS probes in biological objects (cells) or tissues. Furthermore, it can be used as internal Au-Si NP quality standard. In our work, the capability of ultrapure laser-synthesized Au and Au-Si NPs was assessed by studying the enhancement of R6G, which was earlier used as a standard test Raman active molecule (Zhang et al., 2005). Figure 30 shows SERS spectra (785 nm excitation) of R6G detected with Au-100 %, Au-60 % and Au-30 % NPs placed in a PDMS well on top of a silicon wafer. One can see that all types of NPs could provide a considerable enhancement of signals from R6G and the recorded enhanced spectra were relatively stable and reproducible for different measurements. The enhancement factor depended on the content of Au in NPs composition, with the largest enhancement factor for pure Au nanoparticles (Au-100 %), followed by Au-60 % and Au-30 % NPs, respectively.

Figure 30 – Normalized SERS spectra (upon 785 nm CW excitation) of 100 µM Rhodamine 6G (R6G) detected with different Au-Si compositions (Au-100 %, Au-60 % and Au-30 %) on top of a silicon wafer. The average SERS spectra were calculated from 18 points measured for each concentration.

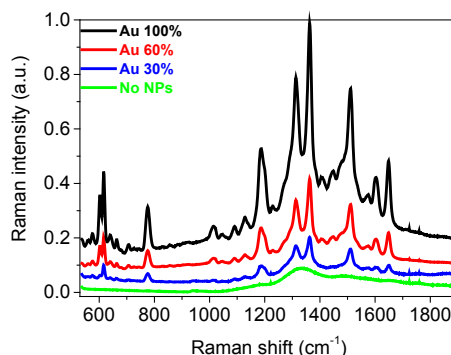Here, even NPs having a dominating content of Si (Au-30 %) were able to enhance Raman signals from R6G. The enhancement of pure Au-100 % NPs was 2–5 times and 10–15 times larger than in the case of Au-60 % or Au-30 % NPs, respectively, but the superiority of enhancement for these NPs can be partially explained by a much larger mean size (25 nm compared to 14 nm and 9 nm, respectively). However, it is critically important that all three types of NPs provided nearly identical enhanced spectral features of R6G. Therefore, the presence of Si content in NPs composition could somewhat decrease the enhancement factor, but it did not cause any distortion of Raman "fingerprint" and provided true spectra. This experimental fact gives a promise for the employment of hybrid Au-Si NPs as SERS probes for tasks of biomolecular identification.

In general, our results unambiguously evidence that laser-synthesized Au-based NPs do generate plasmon enhancement by their own, even if the content of Au in their composition is relatively low. It should be noted that all enhancement factors were achieved by using 785 nm wavelength excitation, which is far from the optimal absorption band for the used NPs (520-525 nm, as follows from Fig. 29A). To further maximize the enhancement factor for 785 nm excitation, we explored the use of these NPs in combination with structured SERS substrates, which had been introduced and described in our previous studies (Uusitalo et al., 2015). Such substrates are produced by imprinting of specially profiled patterns on top of a poly(methyl methacrylate) (PMMA) polymer sheet by roll-to-roll UV nanoimprint lithography, followed by evaporation-based coating of the patterns by a thin layer of gold, and the integration of the structures into hydrophobic PDMS wells (Oo et al., 2013). Fig. 31A shows SERS spectra of dried 100 µM R6G molecules enhanced by Au-60 % and Au-30 % NPs. It is visible that the substrate itself provided a relatively weak signal, while the addition of Au-based NPs led to its drastic enhancement with slightly larger enhancement factors for Au-60 % NPs compared to Au-30 % NPs. On the other hand, our data show that the involvement of the substrate led to nearly 10-fold increase of

intensity of SERS signals from 100 µM R6G using Au-60 % and Au-30 % NPs as Raman probes. Thus, the combination of laser-synthesized Au-based NPs and structured SERS substrate provides a much improved signal enhancement and thus offers an attractive and versatile SERS-based platform for biological identification. Fig. 31B shows the dependence of SERS signal on concentration of R6G using this platform (data are given for Au-60 % NPs).
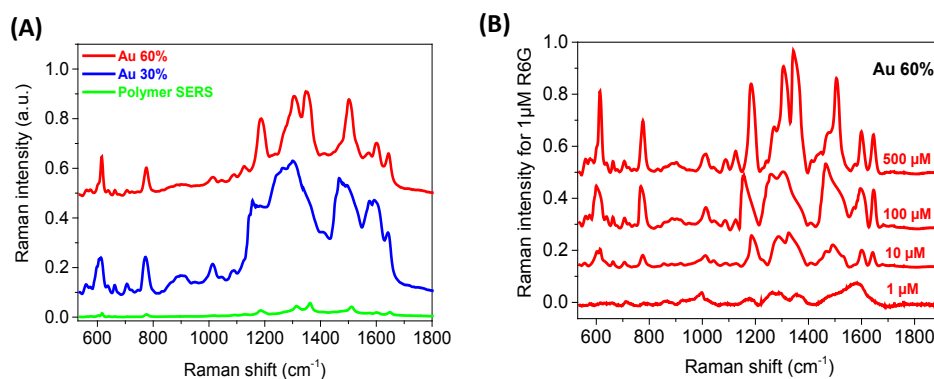
Figure 31 – A) SERS spectra of 2 µl of dried 100 µM Rhodamine 6G (R6G) detected with different Au-Si composition in a 1.5 mm diameter PDMS well on top of a polymer-based Au coated SERS substrate. The average SERS spectra were calculated from 18 points measured for each concentration. B) Normalized with integration time SERS spectra of a concentration series of R6G detected using Au-60 % NPs and a polymer-based Au-coated SERS substrate. The average SERS spectra were calculated from 9 points measured for each concentration using 785 nm CW excitation.

As follows from the spectra, SERS signal amplitude is proportional to the concentration, while the minimal detectable concentration of R6G was lower than 10^{-5} M (under 3 s integration time) that is good enough for biological cell sensing. The applicability of the Au-based NPs for biosensing was studied with various bacteria species. In order to reduce the effect of auto-fluorescence of the biological cells, we used infrared (785 nm) wavelength excitation from a continuous wave (CW) laser, which is out of the auto-fluorescence range of most biological species. Since plasmonic absorption peak does not match 785 nm wavelength, Au-based NPs were used in combination with a patterned gold-coated substrate to enhance SERS signals. In addition, we used 532 nm wavelength excitation from a pulsed laser, which fits well the plasmon absorption peak, but appears to be in the range of increased auto-fluorescence from biological species (bacterial cells). To solve the auto-fluorescence problem, we used time-gated detection making possible the suppression of most auto-fluorescence noises due to picosecond time-gated registration of signals (Kostamovaara et al., 2013).

L. innocua ATCC 33090 was the first bacteria of our interest. Bacterial cells were bound to immunomagnetic beads to separate them from the growth broth in order to minimize the effect of the broth on the SERS signal and concentrate the cells. The use of IMS beads typically improves the detection

sensitivity by 10-fold. Our measurements were carried out under 785 nm excitation using long integration time (60 s). Figure 32 shows Raman spectra of *L. innocua* ATCC 33090 using the patterned SERS substrate combined with Au-60 % NPs, and the substrate alone.
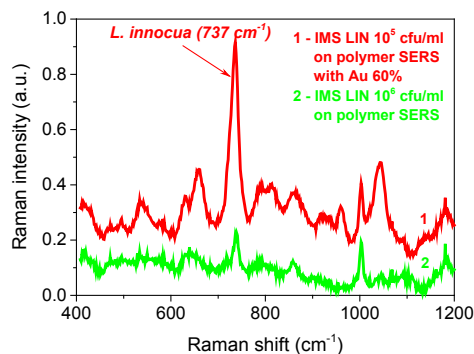
Figure 32 – Normalized SERS spectra of IMS bead captured *L. innocua* (IMS LIN) detected using a polymer-based SERS substrate (green) and a combination of the substrate and Au-60 % NPs (red) using 785 nm CW excitation.

One can find that in both cases we registered similar Raman peaks, including a peak at 737 cm^{-1}, which is characteristic for *L. innocua* according to the literature (Kairyte et al., 2012; Luo and Lin, 2008). However, the intensity of the 737 cm^{-1} Raman peak for the combined detection (SERS substrate plus Au-based NPs) was 4.4 times higher than in the case of SERS substrate alone. Thus, laser-synthesized Au-60 % NPs provided a considerable enhancement of characteristic peak for *L. innocua* ATCC 33090 even for the excitation wavelength out of their optimal absorption range. It should be noted that even without any special optimization of the measurement procedure using combined SERS substrate – mobile NPs probe platform and non-optimal excitation wavelength, we were able to achieve the detection limit lower than 10^5 cfu ml^{-1}.

E. coli W3110 was another example of bacteria used in our analysis. In this case, we explored time-gated Raman detection at a wavelength of 532 nm. *E. coli* bacteria were taken straight from a growth broth after reaching the stationary phase of the cultivation without a need for IMS beads or the use of an additional SERS substrate. Figure 33 shows SERS spectra of *E. coli* W3110 measured with 532 nm wavelength excitation.
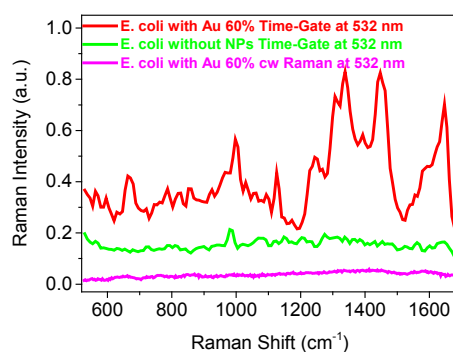
Figure 33 – SERS spectra of *E. coli* W3110 measured with time-gated Raman using 532 nm wavelength picosecond pulsed excitation with the use of Au-60 % NPs as Raman probes (red) and without them (green). For comparison we show Raman spectra without time gating (pink).

As follows from pink spectrum, without time-gating we could not identify any SERS signal from bacteria due to too high level of auto-fluorescence noises. However, as shown in the Figure 33, the use of time-gating offered an elegant solution of the auto-fluorescence problem. Green and red spectra show spectra from *E. coli* alone and *E. coli* decorated by Au-60% NPs, respectively. One can see that the employment of NPs led to more than one order of magnitude amplification of SERS signal and thus reveal a variety of novel Raman lines. Among these lines, one can clearly identify the features commonly attributed to *E. coli*: nucleic acids (666 cm^{-1}), proteins (830 cm^{-1}), vibration bands of Amide III (1200–1300 cm^{-1}) and Amide I (1650 cm^{-1}) (Notingher, 2007; Yang et al., 2016). The peaks around 1650 cm^{-1} corresponding to the protein C=O stretching mode are characteristic for their shape and are often used for calibration in FTIR-measurements (Vonhoff et al., 2010). The *E. coli* W3110 wild-type stain also shows characteristic amino acid spectral lines, such as phenylalanine (around 1000 cm^{-1}) and lipids (1447 cm^{-1}). Thus, the laser-synthesized Au-based NPs appear to be efficient SERS probes to detect *E. coli* at ultra-low quantities with the detection limit lower than 10^5 cfu ml^{-1}. We believe that the employment of "bare" laser-synthesized Au-based NPs as SERS probes for biomolecular identification can be promising for least two reasons. First, these NPs are exempt of ligands or contaminants, which enables one to avoid undesirable Raman signals presenting background noise. Second, phenomena related to quenching of auto-fluorescence in a studied system due to the direct contact of target biomolecules with metal (Dong et al., 2011; Dulkeith et al., 2005), can profit from a high purity of bare laser-synthesized nanomaterials. The advantages of bare nanomaterials were clearly visible during our recent comparative tests involving laser-synthesized NPs and different chemical counterparts, including citrate-coated NPs and gold nanostars, as SERS probes for the identification of beverage spoilage yeasts (Uusitalo et al., 2017a). As follows from this study, bare laser-synthesized NPs did not provide the strongest enhancement (while the enhancement factor was among the best ones), but they much

outperformed all counterparts in terms of signal-to-noise ratio, which is an ultimate parameter describing the performance of SERS probes. As an example, 16 nm bare NPs were more efficient in terms of this parameter than 10, 80, 150, and 200 nm citrate-coated NPs, as well as 80 nm nanostars. Notice that after incubation in real biological environment the NPs can be covered by protein corona, which can also provide auto-fluorescence noise. However, in the case of bare NPs the impact of the protein corona should not be as critical as in the case of ligand-protected counterparts, as the close contact of metal with this corona promises efficient quenching of auto-fluorescence channel. It should be also noted that the detection limit for bacterial detection in our experiments (10^5 cfu ml^{-1}) was not the lowest compared to the literature. As an example, some references reported the level of detection of the order of 10^3 cfu ml^{-1} (see, e.g. (Chen et al., 2015)). However, to the best of our knowledge, this level was observed with Ag NPs, which are known to be the champions in plasmonic enhancement, but cannot be used for in situ control of biological object of interest due to low biocompatibility (Ag NPs are known to be very harmful (AshaRani et al., 2008; Bar-Ilan et al., 2009)). In contrast, the presented bare Au-based nanoformulations are supposed to provide this low-disturbing option. In addition, we believe that after a proper optimization of the measurement system (laser wavelength, substrate-based or substrate-free geometry, composition, size and architectures of used nanoformulations) laser-synthesized NPs could provide much improved detection limit, as it was demonstrated in our recent paper (Uusitalo et al., 2017a).

The efficient enhancement of electric field and demonstration of SERS effect for AuSi composites is another important result. As we explained above, Si and its compounds are among the best inorganic materials from the point of view of non-disturbing character of interaction with biological systems. As an example, some previous studies used designed SERS probes based on silica (SiO_2)-coated plasmonic structures, including gold nanorods and nanostars (Fales et al., 2013; Rodríguez-Fernández et al. 2015; Lai et al., 2017), to improve the biocompatibility and efficiency of SERS probes. The inclusion of non-oxidized crystalline silicon (Si) fraction into composition of SERS probes is expected to further improve the biocompatibility of these probes, as Si is one of essential materials in biological systems, which does not provoke any toxic effects even under massive injection in vitro or in vivo (Al-Kattan et al., 2016; Tamarov et al., 2014; Baati et al., 2016). In addition, in contrast to silica, silicon can provide a distinct Raman scattering peak around 520 cm^{-1}, which was clearly visible in our tests (Fig. 29B). This distinct Raman feature of Au-Si NPs promises a new attractive functionality in SERS studies related to the possibility of their tracking in biological objects (cells) or tissues, e.g., to clarify the distribution of the probes in different living cell compartments.

3.3.5 Conclusions

We explored the employment of ultrapure ligand-free Au-based nanomaterials, including pure Au NPs (Au-100 %) and Au-Si hybrid NPs (Au-60 % and Au-30 %), synthesized by methods of laser ablation in deionized water, as SERS probes for bacteria detection. We first characterized and examined these NPs using standard Raman active molecules (R6G). Our experiments showed that the enhancement factor depends on the content of Au in NPs composition, being the largest for pure Au nanoparticles (Au-100%), followed by Au-60% and Au-30% NPs, respectively. On the other hand, the presence of Si in the NPs composition of hybrid NPs gives a promise for tracking them by following a characteristic Raman line of crystalline Si around 520 cm^{-1}, which can be used for their tracking. We finally used the NPs for the detection of bacteria, *L. innocua* ATCC 33090 and *E. coli* W3110, with a detection limit below 10^5 cfu ml^{-1}. We suppose that the employment of ultrapure (contamination-free), ligand-free Au-based NPs, having much improved biocompatibility compared to chemically-synthesized counterparts, can open up opportunities for non-disturbing studies of live biological systems such as bacterial and cell cultures.

3.4 Comparison of time-gated surface-enhanced Raman spectroscopy (TG-SERS) and classical SERS based monitoring of *Escherichia coli* cultivation samples

The Chapter is directly adopted from the correspondent submitted manuscript to analytical chemistry journal (Kögler et al. 2017).

Authors: Martin Kögler[a,c], Andrea Paul[b], Emmanuel Anane[a], Mario Birkholz[a,d], Alex Bunker[c], Tapani Viitala[c], Michael Maiwald[b], Stefan Junne[a] and Peter Neubauer[a]

[a]Chair of Bioprocess Engineering, Department of Biotechnology, Technische Universität Berlin, Acker-str. 76 ACK24, D-13355 Berlin, Germany

[b]Bundesanstalt für Materialforschung und -prüfung (BAM), Richard-Willstätter-Straße 11, 12489 Berlin, Germany

[c]Drug Research Program, Division of Pharmaceutical Biosciences, Centre for Drug Research, University of Helsinki, P.O. Box 56, 00014 Helsinki, Finland

[d]IHP, Im Technologiepark 25, 15236 Frankfurt (Oder), Germany

3.4.1 Abstract

The use of Raman spectroscopy as an in-situ monitoring technique for bioprocesses is severely limited by a large background signal originating from fluorescing compounds in the culture media. Here we compare time-gated Raman (TG-Raman), continuous wave NIR-process Raman (NIR-Raman) and continuous wave micro-Raman (micro-Raman) approaches in combination with surface enhanced Raman spectroscopy (SERS) for their potential to overcome this limit. For that purpose, we monitored metabolite concentrations of Escherichia coli bioreactor cultivations in cell-free supernatant samples. We investigated concentration transients of metabolites glucose, acetate, AMP and cAMP at different substrate availability, from deficiency to excess. Raman and SERS signals were compared to off-line metabolite analysis of carbohydrates, carboxylic acids and nucleotides. Results demonstrate that SERS, in almost all cases, led to a higher number of identifiable signals and better resolved spectra. Spectra derived from the TG-Raman were comparable to those of micro-Raman resulting in well-discernable Raman peaks, which allowed for the identification of a higher number of compounds. In contrast, NIR-Raman provided a superior performance for the quantitative evaluation of analytes, both with and without SERS nanoparticles when using multivariate data analysis.

3.4.2 Introduction

Raman spectroscopy is a versatile technique for simultaneous concentration monitoring of various target compounds in the liquid phase of biotechnological processes. However, the broad application of Raman spectroscopy for the detection of compounds in the liquid phase upstream of microbial processes is mainly restricted to research purposes so far, although, in comparison to IR spectroscopic approaches, Raman bands of most analytes exhibit little interference with vibrations from water molecules (Classen et al., 2016; Lee et al., 2004; Smith and Dent, 2005).

This is due to the basic drawback of Raman spectroscopy, i.e. a high fluorescence background that causes high threshold values for most analytes in biological samples (Butler et al., 2015; Rojalin et al., 2016), and thus a low sensitivity (Petry et al., 2003). In addition the fluorescence background often dominates the Raman spectrum even when using common near-infrared (NIR) laser excitation sources (Mogilevsky et al., 2012; Wei et al., 2015).

Several approaches have been developed to overcome impacts of fluorescence background, e.g., shifted-excitation Raman difference spectroscopy (SERDS), coherent anti-Stokes Raman spectroscopy (CARS), resonance Raman spectroscopy (RR), surface-enhanced Raman spectroscopy (SERS) and time-gated (TG) Raman. SERDS is based on the difference spectrum of two identically recorded spectra which are separated, typically by the full-width-at-half-maximum (FWHM). When applying this, Raman

bands are shifted by the FWHM whereas the broad fluorescence remains unchanged. Fluorescence background is supressed by the difference Raman spectrum which is obtained by subtraction of the two recorded spectra (De Luca et al., 2010; Sowoidnich and Kronfeldt, 2012). CARS involves the measurement of anti-Stokes shifted Raman and requires two pulsed laser excitation sources. It provides a nonlinear stimulated Raman emission at a shorter wavelength than the excitation laser wavelength. This wavelength has a larger distance from the maximum sample induced fluorescence (Rodriguez et al., 2006; Song et al., 1976). RR combined with a picosecond (ps) short-pulsed infra-red excitation laser source is capable of separating the Raman signal from fluorescence (Smith et al., 2011). SERDS, CARS and RR have good prospects but are currently more academic approaches and have thus not yet been widely applied. In contrary to these approaches, SERS and TG-Raman have become mature techniques and are in the focus of this work.

SERS uses the enhancement of the Raman signal by a factor of $10^4 - 10^{10}$ near metallic roughened surfaces, electrodes or on colloidal metal nanoparticles. The effect is related to the excitation of localized surface plasmons and enables a single-molecule (Kneipp et al., 1999, 1997). In addition, the strong enhancement of the Raman signal with SERS quenches the fluorescence background, which was confirmed earlier with the Gersten-Nitzan model and the Mie scattering theory (Cardinal et al., 2017; Petry et al., 2003; Wei et al., 2015; Geddes et al., 2017). Despite the high potential of SERS for signal enhancement, the practical implementation is still a challenge. Recently, the focus lies on the improvement of reproducibility of real-time measurements under process conditions as shows within the first study in 3.1 (Strehle et al., 2007). While SERS reduces the fluorescence background by enhancing the Raman signal, time-gating "gates out" not only the fluorescence, but also other disturbing signals like cosmic rays or even room light (McNay et al., 2011; Rojalin et al., 2016). The TG-Raman approach has reached the stage of a commercially available solution enabling routine process measurements. The set-up utilizes the synchronization of a pulsed laser excitation in a 100 ps-time regime with a complementary metal–oxide–semiconductor (CMOS) single-photon avalanche diode (SPAD)-detector, as opposed to the more common charge-coupled device (CCD) detectors (Kostamovaara et al., 2013; Rojalin et al., 2016).

We therefore decided to utilize TG-Raman and two continuous wave (CW) Raman approaches with and without SERS and compare their potential to analyse cell-free supernatant samples of an an *Escherichia coli* cultivation. The conventional approaches comprise a CW laser Raman process spectrometer with NIR excitation at 785 nm and a confocal CW-microscopic set-up at 633 nm, which is considered to be the most precise instrument regarding spectral resolution with high spatial accuracy as a stand-

ard to perform SERS as a reference (cf., Chapter 3.4.3.3). For SERS measurements, we used commercially available inexpensive silver nanoparticles (Ag NPs) which are known to be stable over extended time with good signal enhancement and uniformity in particle size.

We aimed at the quantification of glucose as main carbon source, acetate as main side metabolite, and selected amino acid and nucleotide concentrations with all three set-ups. The spectra were evaluated by both univariate and multivariate data analysis (MVDA). Enzymatic analysis and high-performance liquid chromatography (HPLC) were used as reference data for calibration and validation of the chemometric approaches. The following topics were addressed: (i) which experimental set-up is best suited for a comprehensive analysis of the analytes of interest, (ii) to what extent does SERS offer benefits over conventional Raman, and (iii) which specifications have to be provided for efficient bioprocess monitoring by Raman spectroscopy?

3.4.3 Experimental section

3.4.3.1 Chemicals

Commercial silver nanoparticles (Ag NPs) of a size of 40 nm (TEM), in a suspension of 0.02 mg mL^{-1} in aqueous buffer, containing sodium citrate as stabilizers (Sigma-Aldrich, St. Louis, MO) were applied for SERS to avoid eventual fast aggregation. Prior to measurements, the stock solution was centrifuged (CT15RE from VWR, Radnor, PA) at 4,000 rpm / 1610 g for 4 min, subsequently followed by removing the supernatant to reach a final concentration of about 2800 mg L^{-1}. The effect of different size, shape and enhancement material was tested in our earlier studies (cf., Chapter 3.2 and Uusitalo et al., 2017b), in which these Ag NPs showed good performance at different wavelengths with different spectroscopic set-ups. The nanotoxicity of Ag NPs on *E. coli* cells was described elsewhere (Cui et al., 2013), however, it shouldn't be relevant, as the assay was used exclusively for the time of the SERS measurement.

3.4.3.2 Microbial cultivation

A stirred-tank bioreactor batch and subsequent fed-batch cultivation of *E. coli* with varying, pulse-based feeding was applied to achieve different concentrations of metabolites, including those typical appearing effects under metabolic overflow conditions. The culture was grown in mineral salt medium (Neubauer et al., 1995). The temperature was maintained at 37 °C, the pH-value was controlled at 7.0, and the dissolved oxygen concentration was kept above 20 % of saturation to avoid oxygen limitation. Cell-free supernatant samples were taken through a membrane filter (pore-size of 0.22 μm), with which the supernatant was directly separated from cells during sampling. The samples were frozen

and stored at -80 °C prior to further analysis. All reference measurements were conducted within a close time span to the Raman spectroscopy measurements.

3.4.3.3   Raman spectroscopy

Raman microscope (micro-Raman)

A confocal Raman microscope (InVia from Renishaw, Wotton-under-Edge, UK) (Renishaw, 2017), CCD-detector, which was temperature-controlled at − 70 °C during measurements, and a CW He-Ne laser with an excitation at λ_{exc} = 633 nm, a laser power of 10 mW at lens (N Plan EPI from Leica, Wetzlar, Germany) with a magnification factor of 20x and numerical aperture (NA) of 0.4. The spectral acquisition time was set to 10 s. An average of 5 captures was considered without automated cosmic ray removal, which was performed afterwards manually. The spectral resolution of the InVia Raman microscope was 0.3 cm^{-1} full-width-at-half-maximum (FWHM).

NIR Raman spectrometer (NIR-Raman)

A commercially available process Raman spectrometer RXN1 (Kaiser Optical Systems, Ann Arbor, MI) (Kaiser Optical Systems, 2015), was used that was equipped with a temperature-controlled CCD detector at − 40°C and a CW-laser excitation at λ_{exc} = 785 nm at a laser power of 135 mW at a non-immersion Raman MR process probe (NA = 0.29). The spectral acquisition with CW-Raman was performed with an integration time of 20 s. An average of 5 captures was considered, which reduced cosmic ray disturbances. The spectral resolution of the RXN1 spectrometer amounted to 4 cm^{-1} (FWHM).

Time-gated Raman (TG)

For this study, a prototype system set-up of a time-gated Raman process-spectrometer TGM1 (TimeGate Instruments, Oulu, Finland) equipped with a state of the art non-cooled CMOS SPAD-detector with a 100 ps pulsed Nd:YVO$_4$ laser at λ_{exc} = 532 nm was used. A standard laboratory Raman probe BWTek RPB 532 (B&W Tek,Newark, DE) with an approximate average laser power of 30 mW and NA of 0.22 at the sample focal point was applied. No cosmic ray removal was necessary due to the fast gating duty cycle of the measurement principle. The time-gating principle was described elsewhere (Kostamovaara et al., 2013; Rojalin et al., 2016; Wei et al., 2015). SERS was conducted with the same spectral range, laser power, repetitions and temporal settings. Even though a single measurement at the temporal position of high intensity of a Raman or SERS signal was recorded in about 1.5 seconds, repetitions in temporal direction were necessary (15 minutes total collection time) to achieve a well-resolved overall spectrum for one sample (cf., Fig. S2). However, for practical reasons, each Timegate-spectrometer is

equipped with individually adjustable delay-settings, which results in a temporal off-set from $t = 0$ (launch of a laser pulse), as shown in the results of the raw data (cf., Fig. S1). The temporal window used in this study has been set to cover the Raman and SERS signal captures between $t = 1.2 - 2.1$ ns. The spectral resolution of the TGM1 system was 10 cm^{-1} (FWHM).

Prior to analyses, a wavelength calibration was performed for all three Raman spectrometers. Laser and detectors were temperature-stabilized.

3.4.3.4 Sample preparation & measurement procedure

Prior to the analyses, a wavelength calibration was performed for all three Raman spectrometers. Laser and detectors were temperature-stabilized. Measurements were performed with an in-house developed anodized aluminum microwell plate with a cavity volume of 20 µL. At first, 3 µL of samples were filled into the wells. Subsequently Raman spectra were recorded. In a next step, 3 µL of concentrated Ag NPs solution was added without mixing into the sample. Subsequent SERS measurements were performed after focussing beneath the liquid surface of each sample, while adjusting to the maximum Raman/SERS intensity at each spectrometer set-up (cf., Fig. 34 and Fig. 35).

All spectra were taken immediately after pipetting the supernatant samples into the wells. Repeated SERS measurements were performed sequentially right after each Raman measurement by adding Ag NPs on top of the sample. Fig. 34 shows the settings used for the different measurements.

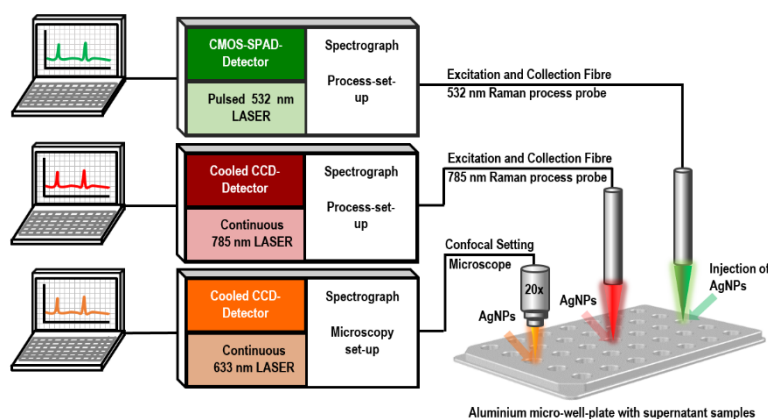**Figure 34** – Different spectroscopic set-ups: TG-Raman (TGM1) with pulsed green λ_{exc} = 532 nm laser, NIR-Raman (RXN1) with red λ_{exc} = 785 nm laser and confocal setting of CW-microscope (InVia) with orange λ_{exc} = 633 nm laser used in this work; each measurement without and with injection of Ag NPs into each microwell.

3.4.3.5 Reference analysis

Glucose concentration was enzymatically determined with the glucose hexokinase FS kit (DiaSys Diagnostics, Holzheim, Germany) following the supplier's instructions. Carbohydrates, short chain carboxylic acids and ethanol were quantified with a refractive index detector on a HPLC-system (1200 series system, Agilent, Waldbronn, Germany), amino acids were quantified with a fluorescence detector on a HPLC (1260 series system, Agilent) with pre-column derivatization with o-Phthal-dialdehyde (Junne et al., 2011). Nucleotides were quantified with a diode-array detector (1200 series system, Agilent). For separation, a Supelcosil TM LC-18T column (150 mm × 4.6 mm I.D., 3 µm particle size) connected to a guard column cartridge (particle size of 5 µm) was applied (both Supelco, Bellefonte, PA). Chromatographic conditions were set as described elsewhere with a flow rate of 1.0 mL min^{-1} (Ryll and Wagner, 1991). Repeated Raman and SERS reference measurements for most media compounds were performed with a concentration range from close to the limit of detection up to the highest available concentration (cf., Fig. S3, S4 and S5).

3.4.3.6 Spectral data processing

In order to achieve time-gated Raman spectra, a post-processing was performed using the instruments' post-processing software (Timegate Instruments Oy, 2015). The TG-Raman raw measurement data provides a three dimensional data cube, i.e., intensity versus Raman signal wavenumbers versus time delay information. The latter exhibits the Raman signal as function of the time delay in several nanoseconds. The time region with a typical time span of 0.5 – 5.5 ns, in which the Raman signals arises shortly before the fluorescence signal, is of great importance. Typical 3D raw-data cubes are depicted in the supplementary information under Figure S1. Further analysis was performed with OriginPro (V. 2016, OriginLab, Northampton, MA). MVDA of Raman and SERS in general started with principal component analysis (PCA) for initial data inspection followed by partial least squares regression (PLSR) of mean-centered data with the software The Unscrambler X (V.10.4. CAMO Software, Oslo, Norway). The off-line derived data for optical density (OD), acetate, glucose, amino acid and nucleotide, i.e., adenosine monophosphate (AMP) and cyclic AMP (cAMP) concentrations were included as response variables for calibration and validation of the PLSR models. Prior to regression analysis, TG spectra were baseline-corrected and normalized, whereas micro-Raman and NIR-Raman spectra were treated following a first derivative transformation and second order polynomial smoothing using a Savitzky-Golay (S-G) filter (21 columns) before nomalization. In general, the so-called fingerprint region of each spectroscopic data set was evaluated using unweighted spectral data. Final steps in PLSR models included the selection of significant spectral variables based on a t-test and the regression coefficients of sub-models in cross-validation as implemented in the software.

83

3.4.4 Results and discussion

The aim of this study was to compare the potential of different Raman and SERS approaches for both, the spectral identification and quantification of relevant compounds in cell-free supernatants, namely NIR-Raman at 785 nm with continuous excitation and TG-Raman at 532 nm with pulsed excitation. The micro-Raman at a continuous excitation of 633 nm was used as reference. Measurements were performed with supernatant samples of an *E. coli* cultivation with mineral salt medium. These cultivation samples are characterized by a changing matrix composition in the course of the cultivation progress by the accumulation of analytes and side products, and also by an increasing fluorescence background (Wilén et al., 2008). To achieve best conditions for monitoring, all measurements were conducted in aluminum microwells. Fig. 35A represents a sketch of the measurement set-up, the suggested distribution of the Raman signal inside the aluminum microwells, when the focus beam is adjusted just below the fluid surface. The highest Raman scattering intensity is achieved by focussing just beneath the liquid sample surface (Cooney et al., 1996). Fig. 35B illustrates the signal enhancement achieved through SERS. Backscattering of the Raman and SERS signal depends on the turbidity of the sample, following the Lambert-Beer law (Gordon 1989). The walls and the bottom of the aluminum microwell are acting as a diffuse reflector for the excited laser emission, as shown in Fig. 35.
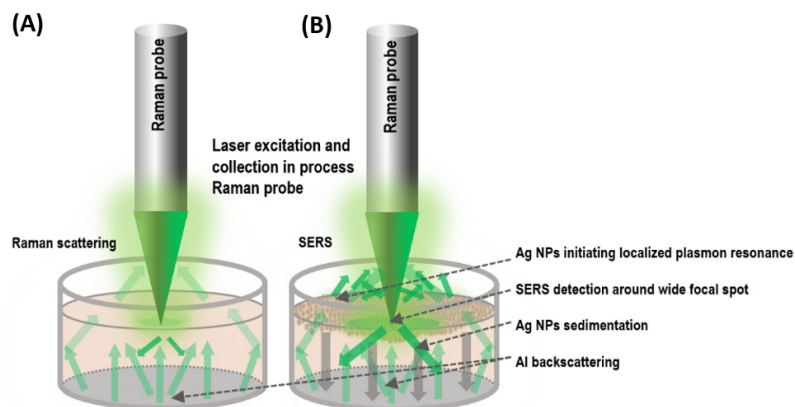
Figure 35 – Microwell with supernatant sample - symbolical representation of (A) Raman and (B) SERS measurement set-up in a single aluminium well.

The aluminum oxide film that is naturally formed on every Al surface did not affect the measurement. According to Zhang et. al., anodized aluminum oxide films exhibit weak SERS bands at wavelengths of 1600 cm^{-1}, which are outside the spectral range evaluated in this study. Bands would occur only if the measurement was tightly focused directly on the Al surface (Zhang et al., 2007). In common plastic like

polystyrene and polyethylenterephthalat microwell plates, however, significant interference of a strong Raman band at around 1000 cm^{-1} can occur when using small sampling volume. Al in contrast, if used as material and metallic sample holder, may even act as signal enhancer due to back-reflection (Ryder et al., 2010; Cui et al., 2016). Thus, Al seems to be a suitable sample enclosure for a disturbance-reduced Raman and SERS analysis (Knight et al., 2014; Ryder et al., 2010).

Since the highly concentrated Ag NPs remain stable at the surface during the short measurement process in the microwell (as depicted in Fig. 35B), repeated SERS measurements can be conducted reliably (Strehle et al., 2007) in the same way for each microwell within the given measurement time of the respective Raman techniques used here (cf., Fig. S8). Fig. 36 summarizes the Raman spectra from both non-SERS measurements (top-row) and SERS-measurements (bottom-row) of the cell-free supernatant samples. As the spectra are presented for the region of interest and offset separated, the impact of fluorescence on NIR- and micro-Raman is not obvious. The highest fluorescence backgrounds are observed with micro-Raman (Fig. 36C and Fig. S8B), which is due to the excitation at 633 nm close to the maximum fluorescence of biological samples. For easier comparison of individual spectra, only a selection is represented. All non-SERS Raman spectra (at the top-row of Fig. 36) show similar Raman bands, but with varying relative intensities with best resolution for TG-Raman.
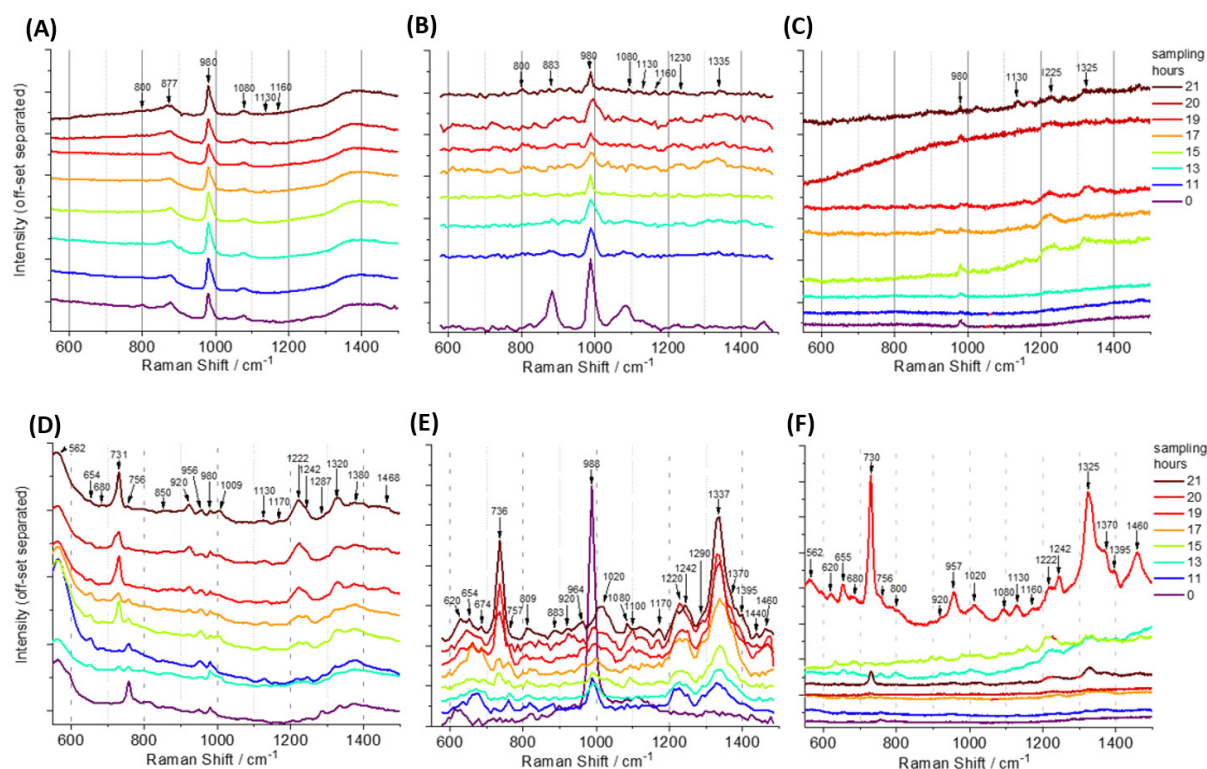
Figure 36 – Normal Raman results with CW-Raman (RXN1), TG-Raman and CW-microscope (A-C) and with SERS measurement mode (D-F).

Although TG-Raman excites samples even at the fluorescence maximum of many biological compounds, it seems that the fluorescent background is sufficiently reduced and the spectra are clearly distinguishable from the noise (cf., Fig. 36B and 36E) (Rojalin et al., 2016). Generally, all non-SERS measurements of the three spectroscopic set-ups demonstrate similar results. They appear significantly different from the respective SERS measurements of the supernatant samples (Fig. 36 bottom row).

The detection of analytes with the addition of SERS reveals rather different spectra for the respective Raman technique. The most severe difference between enhanced and non-enhanced measurements are observable from the micro-Raman spectra, with strong variations of the background, spectral peaks and the signal intensity. Overall, the application of SERS using Ag NPs to each sample right before the measurements clearly leads to a better separation of signals from the background noise in the supernatant samples with all Raman techniques (bottom row of Fig. 36D–F). Addition of Ag NPs reveals spectral structures originating from the substrate and product, specifically oligonucleotides (678, 730, 925, 1104, and 1330 cm^{-1}) like adenosine derivatives (cAMP and AMP), whereas without Ag NPs,

mainly compounds of the media substrate such as magnesium sulfate (at 980 cm^{-1}), trace elements and carbohydrates (877–883 cm^{-1} and 1130 cm^{-1}) dominate the Raman spectra (Efeoglu and Culha, 2013).

Table 5 shows the observed Raman and SERS peaks related to literature references, and a comparison of detection with the three different techniques.

It is feasible to recognize most changes of substrate and product compounds in the mineral salt medium with all spectroscopic set-ups, but it appears that SERS in general provides better resolved spectra (Fig. 36D and 36E). A high effort for adjustment is needed in the case of the microscope set-up (Fig. 3F), yet no distinct peak around 980 cm^{-1} is detectable throughout the course of the cultivation. One reason for this effect may be the smaller focal spot in the sample liquid. Nanoparticles for SERS need to be captured within this tiny spot. The focal spot with the probes used for NIR- and TG-Raman is 10-20 fold larger, which likely reduces thresholds, and further results in increased reproducibility of the SERS measurements (Lewis and Griffiths, 1996).

Table 5 – Tentative Raman/SERS band assignments with different spectroscopic settings (- not detectable; + detectable; ND out of spectral range).

Detected Bands Peak/ cm^{-1}	Tentative band assignment	Origin/category	Raman CW-Raman (RXN1)	Raman CW-Microscope	Raman Pulsed TG-Raman (TGM1)	SERS CW-Raman (RXN1)	SERS CW-Microscope	SERS Pulsed TG-Raman (TGM1)	Reference
562–580	Ring and CH-deformation	Carbohydrate in medium	-	-	-	+	+	ND	(Makino et al., 2003)
655	Ring breathing of Guanine (oligo G)	DNA	-	-	-	+	+	+	(L Cui et al., 2015)
674–680	Ring breathing of Guanine (oligo G)	DNA	-	-	-	+	+	+	(Green et al., 2006)
732–736	Glycosidic ring mode of D-glucosamine (NAG), Adenine, CH_2 or cAMP	DNA, Nucleotide	-	-	-	+	+	+	(Kubryk et al., 2016; Premasiri et al., 2016)
756	Thiamine	Substrate from medium	-	-	-	+	+	+	(Leopold et al., 2005)
800–810	Acetate (weak peak TG-Raman w. SERS)	Product	+	-	-	-	+	+	own observation
877–891	Acetate (weak peak in CW-Raman)	Product	+	+	+	-	-	-	own observation
920	C-C stretch of proline ring-glucose or lactic acid	Product	-	-	-	+	+	+	(Efeoglu and Culha, 2013; Lee et al., 2004; Uusitalo et al., 2017a)
957–964	C=C deformation, guanine	DNA	-	-	-	+	+	+	(Witkowska et al., 2017)
1025	C–H bending	Lipid	-	-	-	-	+	+	(Cui et al., 2017)
1080	Potassium di-hydrogen phosphate	Phosphates in medium	+	+	+	-	+	+	(Narayanan, 1951)
1130	C–N and C–C stretch	Carbohydrate in medium	-	-	-	+	+	+	(C. Fan et al., 2011)
1160	C–O–C or P=O stretch	Phosphates in medium	+	-	+	-	-	-	(Hampton and Demoin, 2010; Moody et al., 2017)
1170	Tryptophan (Trp) or phenylalanine (Phe)	Aromatic amino acids	-	-	-	+	+	+	(David, 2012)
1320–1340	Adenine (AMP)	Nucleotide	-	-	-	+	+	+	(Premasiri et al., 2016)

Fig. 37 shows the development of the concentrations of glucose, acetate, cAMP and AMP over the course of the cultivation measured with the corresponding SERS respectively Raman bands (normalized peak intensities) in comparison to concentrations determined by HPLC.
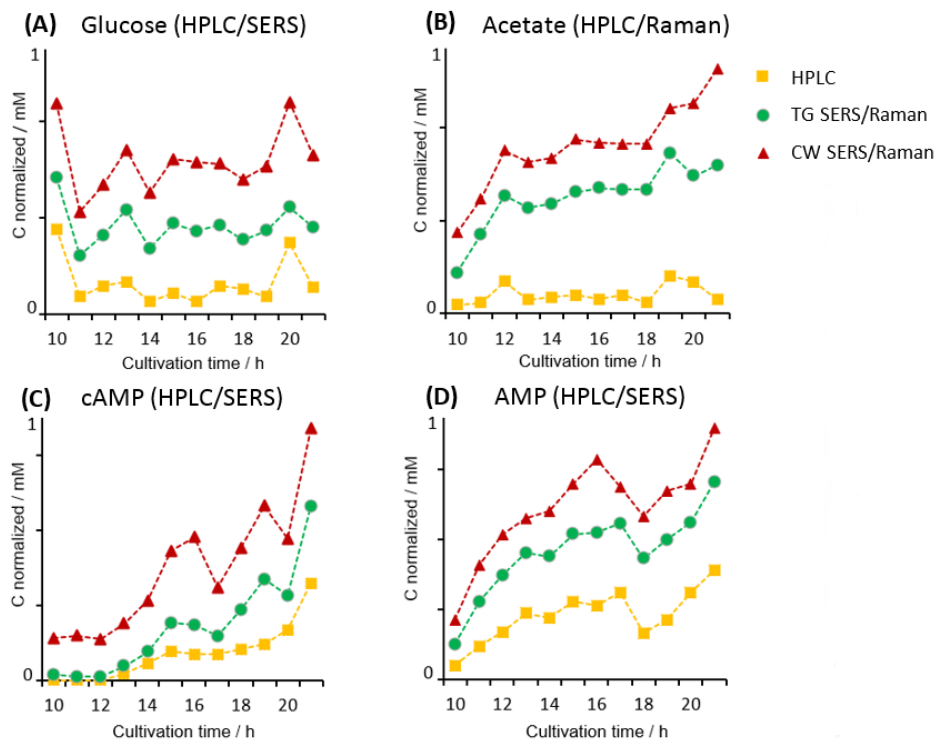
Figure 37 – Normalized (0-1) concentrations of A) glucose (1130 cm⁻¹), B) acetate (877–891 cm⁻¹), C) cAMP (731–736 cm⁻¹), and D) AMP (1320–1340 cm⁻¹), corresponding max. peak height measured by NIR-Raman (red triangles) and TG-Raman (green dots) in SERS mode except for acetate (Raman max. peaks). The yellow curve with squares refers to the actual HPLC concentration in mM per sample during the cultivation.

In all cases, a similar development is observed; values of the corresponding quantitative regression analysis are shown in Table 6.

Table 6 – Prediction of analyte concentrations based on Raman and SERS measurements.

Raman technique	CW-microscope (Renishaw inVia)				CW-process Raman (RXN1)			TG-Raman (TGM1)***	
Data pre-treatment for PLSR	1st derivative, S–G smoothing, 2nd order polynomial, 21 wavenumbers, unit vector normalization				1st derivative, S–G smoothing, 2nd order polynomial, 31 wavenumbers, unit vector normalization			Baseline correction, unit vector normalization	
Analyte / conc. Range	**Sample**	**RMSEC**	**RMSECV**	**RMSEP****	**RMSEC**	**RMSECV**	**RMSEP***	**RMSEC**	**RMSECV**
Glucose / g L^{-1}	Raman	0.69	0.78	1.03	**0.32**	**0.51**	**0.39**	0.75	1.42
Range: 0.065 – 5.00	SERS	0.57	0.68	0.57	0.54	0.61	0.91	0.70	1.01
Acetate / g L^{-1}	Raman	0.07	0.09	n.d.	**0.07**	**0.09**	**0.08**	n.d.	n.d.
Range: 0– 0.56	SERS	0.06	0.08	0.14	n.d.	n.d.	n.d.	0.03	0.19
AMP / mM	Raman	n.d.	n.d.	n.d.	0.005	0.01	0.02	n.d.	n.d.
Range: 0– 0.19	SERS	n.d.	n.d.	n.d.	**0.003**	**0.01**	**0.01**	n.d.	n.d.
cAMP / mM	Raman	0.02	0.05	0.06	**0.01**	**0.02**	**0.05**	n.d.	n.d.
Range: 0– 0.51	SERS	0.04	0.06	0.07	0.04	0.05	0.07	n.d.	n.d.

Best results for each analyte are indicated in bold,

*PLSR = full CV (leave one out), external CV: independent measurement of samples of one cultivation,

**RMSEP = root mean square error of prediction,

*** Only one dataset, no external validation, with TG-spectra, RMSE provided are back-transformed for comparison.

As pulses were applied after a certain time under nutrient-limited fed-batch cultivation conditions, glucose and the concentration of overflow metabolites like acetate varies. This dynamic course is well-captured for glucose and AMP, and at most time points also for cAMP. In case of acetate, which was only analyzed at samples of non-SERS measurements with NIR-Raman and TG-Raman, general trends were also reflected well, however, with reduced conformity.

For the quantitative evaluation of Raman and SERS spectra (*X* variables), we applied PLSR using the reference data as response variables (*Y* variables, cf., section 3.4.3.5). The resulting root mean square errors of calibration (RMSEC) and validation (RMSECV) can be compared among various Raman measurements for the same analyte. The validation was performed as internal (full) cross validation, and pseudo-external validation (RMSEP), using repeated measurements of samples. This procedure allows for a comparison among different models and compounds w/o the issue of biological variation, if samples of different batch cultivations would have been compared. Nevertheless, it provides no measure for the estimation of uncertainties for true "unknown" samples as it would be the case with an external validation using samples that were obtained from another cultivation under the same condition. Depending on the quality of the spectral data, which were obtained from the three Raman techniques and SERS, different pre-treatments were applied to obtain PLSR models, which appear plausible with respect to the explained *Y* variance of calibration and validation, scores, loadings and regression coefficients.

The spectra obtained from micro-Raman exhibited a high spectral resolution over a wide spectral range, but strong variations of intensities and background, especially for the SERS measurements (cf., Fig. 36C–F), whereas those obtained from NIR-Raman were less resolved with varying offset. In contrast, TG spectra had only traces of offset, well discernable peaks, but a stronger signal to noise ratio. Furthermore, the spectral region was limited to 1000 cm^{-1} in maximum with a poor spectral resolution of the prototype system set-up used here.

Consequently, both micro- and NIR-Raman data needed a combined derivative and S-G transformation to reduce background signals. TG spectra were evaluated after linear baseline correction. A unit vector transformation allows for a quantitative comparison of data retrieved partly at different experimental periods and thus was applied as a final step for all spectral data. In Table 6, a summary of the resulting RMSE for the analytes glucose, acetate, cAMP and AMP is provided for both SERS and non-SERS Raman spectra. The "best" results for each analyte are highlighted in bold, meaning the approach with the smallest RMSE and the least variation among RMSEC-RMSECV and/or RMSEP.

In case of glucose, acetate and cAMP concentrations, indeed non-SERS Raman spectra obtained from the NIR-Raman yielded to lowest RMSE. However, for AMP, SERS spectra were slightly superior to Raman spectra obtained with the NIR-Raman. To our surprise, for no particular analyte, the well-resolved microscopic spectra yielded to superior results in quantitative evaluation, but for one analyte, i.e. AMP, quantification even failed. Although nominal low RMSE were obtained for SERS measurements of acetate by micro-Raman, the model performs poorly otherwise (cf., supplementary data, Fig. S7A and B) and has the highest error of 14% based on the RMSEP occurred at acetate (Table 6). The plot in Fig. S7A reveals no ideal model for acetate from NIR-Raman spectra as well with a clear nonlinear trend observed at higher acetate concentrations, however, the grouping of scores seemed reasonable. At least 76% of variance was explained in cross validation. In contrast with the explained variance of the PLSR model for the Raman spectra of the microscope, only 13 % was reached with cross validation (cf., Fig. S7B). We therefore concluded that acetate was not suited for quantitation in the samples used here yielding to high uncertainties for all approaches.

In comparison, for glucose, AMP, and cAMP concentrations, relative uncertainties of 8, 5, and 10 % were achieved (cf., Fig. S6A-B). From a physiological point of view, the cAMP concentration in *E. coli* increases under limited substrate supply (Lin et al., 2004; Notley-McRobb et al., 2006). cAMP is an important molecule to indicate the energetic state of a culture and the degree of starvation under typically applied fed-batch conditions, in which the main nutrient is limiting (Junne et al., 2011). Due to the oscillating feed rate and different phases of starvation, its concentration increased during the cultivation. The highest peak of cAMP is reached when the ratio of the glucose fed to the residual biomass is at its minimum at 21 h, which is in agreement to observations of Notley-McRobb et al. 2006 (Notley-McRobb et al., 2006). While TG-Raman can follow the development of cAMP, NIR-Raman was performing best regarding quantitative analysis of cAMP (cf., Fig. 37 and Table 6). Although the reproducibility of SERS results remains challenging, the direct measurements after injection of Ag NPs into the Al microwells yielded to results, which agree very well with the reference analytics. Dominant substrate bands like thiamine (756 cm^{-1}), phosphates (1160 cm^{-1}) and carbohydrates (1130 cm^{-1}) were reduced, while product bands such as lactate (920 cm^{-1}), proteins (around 1220 cm^{-1}), and lipids (1460 cm^{-1}) appear enhanced (cf., table 5). These results suggest to consider surface-enhanced Raman spectroscopy a reliable approach for the monitoring of metabolites in bioprocesses and make it a promising approach for the refined detection of low-concentrated analytes such as AMP.

3.4.5 Conclusions

The motivation for this study was a comparison of different Raman spectroscopic techniques regarding their suitability for the analysis of essential compounds in cell culture media, namely glucose, acetate, cAMP, and AMP as an indicator of the process status. The comparison was performed with respect to parallel and/or online measurement combined with high sensitivity and robustness. Furthermore, the benefit of a combined SERS approach with each technique was assessed.

In general, SERS and non-SERS spectra of the three set-ups closely resembled each other. Addition of SERS particles led to an increase of information of Raman active species, at the same time reducing intensities and identifiability of other compounds present in the non-SERS measurements.

Surprisingly, the spectra derived from the most precise instrument, a high-resolution Raman microscope, yielded to no superior results for quantitative analysis of any of the observed analytes. Even though producing the best-resolved spectra regarding the number of analytes, SERS added no further benefit for quantitative analysis in this particular study. In contrast, best results in quantitative analysis were obtained from the instrument operating with CW-NIR excitation at 785 nm. Although the signal-to-noise ratio of the Raman peaks seemed poor due to a high fluorescence background, good results were obtained in combination with suitable data transformation and chemometric (PLSR) evaluation. It should be noted that for the quantitative evaluation of the NIR-Raman data MVDA is essential (Kämmer et al., 2015). In case of cAMP, addition of SERS particles further improved the prediction results from PLSR, however, for glucose, acetate and AMP, no comparable effect was observed with SERS although the spectra exhibited more spectral lines and details (Kostamovaara et al., 2013). Remarkably, the application of complex media, as applied in many industrial processes, might lead to different conclusions about the benefits of SERS pre-treatment and Raman spectroscopy evaluation.

Spectra derived from the TG-Raman resulted in well-discernable spectral peaks, which allow the identification of a much higher number of peaks compared to NIR-Raman. Especially this feature makes TG-Raman spectroscopy an important tool for the screening of complex mixtures as they occur in bioprocesses.

Supplements   Comparison of time-gated surface-enhanced Raman spectroscopy (TG-SERS) and classical SERS based monitoring of Escherichia coli cultivation samples

Figure S1 - Normalized extinction (absorption + scattering) UV-Vis spectrum of Ag-based NPs used for SERS detection

Figure S2 - Time-Gate (TG) raw-data as data cubes including SERS/Raman (x-axis), intensity (y-axis) and temporal signal as decay time (z-axis) of supernatant sample at beginning of the cultivation S0 (0h) and the end S21 (21h), SERS results (A, C, E) and Raman results (B, D, F). (A) – TG with SERS S0, (C) TG with SERS S21 resulting in 5-6 x higher raw-signal with clearly identifiable peaks compared to (B) TG without SERS which shows low fluorescence background for S0 and clearly increased fluorescence background for (D) at S21. The decay time in nanoseconds is set to cover the same range for all measurements up to 2 ns. (E) Overlay of SERS results and (F) overlay of Raman results.

(A)

Regression coefficient for AMP integrated over spectral range

(B)

Regression coefficient for cAMP integrated over spectral range

Figure S3 - Integration of the regression coefficients for (A) AMP and (B) cAMP over the spectral range respectively with SERS on NIR-Raman.

(A)

(B)

Figure S4 - Trace elements of MSM-medium: (A) with SERS and without including repetition measurements; (B) Pure glucose 400 g/L without SERS, MSM-medium with glucose and salts.

(A) MgSO4 with an without AgNPs

(B) Thiamine

(C) MSM-Medium with all components mixed

Figure S5 - (A) MgSO4 with SERS (red/black) and without (green/blue) including repetition measurements; (B) Thiamine with SERS (red/black) and without (green/blue) including repetition measurements; (C) Mineral salt medium (MSM) as stock-solution with nutrition components as mix before usage at cultivation – difference of SERS bands (red/black) and without SERS (violet), yellow and cyan spectra are the SERS measurements with decreased peaks after more than 1h after injection of the Ag NPs into the microwells.

Figure S6 - PLSR results including weighted regression coefficients (upper row) and predicted vs. reference plots (lower row) for (A) cAMP using the micro-Raman (RMSEC/RMSEC = 0.042/0.056), (B) cAMP using the NIR-Raman spectrometer (RMSEC/RMSEC = 0.0098/0.0187). Black-colored regression coefficients are considered significant, blue-colored not. Blue colors refer to calibration data and red colors to full cross validation in the regression plots.

Figure S7 – PLSR results for acetate from (A) NIR-Raman and (B) micro-Raman spectra using cross validation. Upper left: scores plot, upper right: weighted regression coefficients, lower left: explained variance and lower right: vs. reference plots (lower lane). Black-colored regression coefficients are considered significant, blue-colored not. Blue colors refer to calibration data and red colors to full cross validation in the regression plots.

Figure S8 - Exemplarily presentation of fluorescence background influence of sample S21 (21h of cultivation) with SERS and without – (A) TG-SERS (green/dark-green), NIR-Raman-SERS (red/dark-red) and micro-Raman-SERS-microscope (orange/pink) with repeated measurement; (B) TG-Raman (green/dark-green), NIR-Raman (red/dark-red) and micro-Raman (orange/pink) with repeated measurement. The sharp peaks at around (A) 1200 and 1300 cm^{-1} and (B) 1170 cm^{-1} in the micro-Raman spectra denote interfering's of the SERS/Raman detection by cosmic rays.

4. Results

4.1 Summary of the key findings

Various aspects were investigated: (**i** – **Real-time Raman based approach for identification of biofouling**) the creation of an SERS online sensor platform – from gold nanoparticles (Au NPs) immobilized onto the top layer of different kinds of membranes for membrane filtration purpose, enabling a long-term detection of biofilms such as small biomolecules in very low concentrations at initial adhesion phase up to contiguous biofouling areas in a real filtration process; (**ii** – **Detection of *Listeria innocua* on roll-to-roll produced SERS substrates with gold nanoparticles**) the demonstration of bacteria detection with even improved LOD using SERS nanoparticles (Au NPs) and SERS UV-nano-imprinted roll-to-roll produced structures (a special VTT designed Au-patterned-structure) in combination, enabling low-cost dual-SERS sensors; (**iii** – **Bare laser-synthesized Au-based nanoparticles as non-disturbing SERS probes for Bacteria Identification**) bare-laser synthesised Au NPs open up non-disturbing studies of biological systems due to excellent biocompatibility which was tested on model bacteria (*Listeria innocua* and *Escherichia coli*); (**iv** – **Comparison of time-gated surface enhanced Raman spectroscopy (TG-SERS) and classical SERS based monitoring of *Escherichia coli* cultivation samples**) the investigation of temporal changes of *Escherichia coli* cell-culture media at different cultivation phases from bioreactors with SERS and without SERS using classical Raman and Time-Gate Raman technologies following critical process parameters such as glucose, acetate, cAMP and AMP.

4.2 Own original findings per section

(**i** – **Real-time Raman based approach for identification of biofouling**) A specialized flow-cell set-up was realized which enables biofouling detection in real-time under industrial filtration condition. To enable this, a special suction technique was developed which was applied for the first time. It immobilizes the Au NPs onto the top-layer of the filtration membrane by applying a certain constant pressure from the opposite side of the membrane during the preparation of the SERS sensing area. A detection of early-stage biofouling in continuous liquid-flow with gold nanoparticles (Au NPs) was thus realized. This assay quenches the disturbing narrow cellulose Raman peaks arising from most industrial filtration-membranes almost completely. Strong vibrations caused by process-pumps, a high water-flux and system pressure do not interfere a stable SERS based detection of early-stage biofouling. The focus of the optical Raman probe onto the Au-based SERS sensing area will remain steady and unchanged for an extended time when measuring in a specifically for the process adapted flow-cell. Rod-shaped col-

loidal gold nanoparticles with a dimension of approximately 120 nm have an excellent SERS performance at 785 nm excitation wavelength, demonstrated in **(ii)** as well, and are generally well suited for biological applications such as the identification of bacteria. Furthermore, for Au NPs at larger diameters >100 nm, the resonance linewidth and the specificity is increased (Butler et al., 2016). The application demonstrated here is not exclusively limited to membrane drinking water filtration. NIR-spectroscopic flow-cell set-ups with filtration membranes are for instance applied in bioprocess downstream execution of industrial enzyme production (Klimkiewicz et al., 2014). The performance of such SERS sensing area is depended on both, the nanoparticle concentration immobilized on the membrane surface and the three dimensional distribution profile on the membrane substrate, thus it is difficult to reliably immobilize it equally well and reliably for long-term observations on all different membrane surfaces (Guo et al., 2012; Virtanen et al., 2017). Paper-based SERS substrates have shown practical advantages for quick trace identification, where silver or gold NPs in high concentration are submerged with the cellulose fibre-structure of the paper and do not exhibit fluorescence from the substrate (Guo et al., 2012; S. Lee et al., 2011; Yu and White, 2012). However, they cannot be used in wet processes of industrial filtration where high cross-flow and fluid stresses exist. A limitation of the applied proof-of-concept solution is that a small area of the filtration membrane is occupied by the SERS sensing area, for the proof-of-concept it was in the range of several millimetres, which has an effect on the permeability. It blocks the pores of the membrane (Virtanen et al., 2017). This can be further optimized since the diameter of the focal spot, which is needed for a reliable bacteria identification with SERS, can be in sub-millimetre range, to leave a security margin in case heavy vibrations appearing within the process.

(ii – **Detection of *Listeria innocua* on roll-to-roll produced SERS substrates with gold nanoparticles**) Mass production of low-cost SERS substrates are highly desired to 1) enable a fast and reproducible screening option and 2) in order to bring down the costs for measurements and replicate measurements necessary with SERS substrates, which is a prerequisite for the industrial potential of this technique to be realized (Buckley and Ryder, 2017). Roll-to-Roll produced UV- nanoimprint lithography structures have shown good enhancement properties and provide reproducible measurement results (cf., Table 1). When combining a set-up of Au NPs (different size distribution, uniformity, shape was tested) of a specific size and a surface Au-based SERS patterned structure, an increased localized surface plasmon resonance can be achieved. It turned out that the largest and rod-shaped Au NPs, the ones which have been produced the same way as in **(i)** showed the most consistent, reproducible SERS spectra with the highest enhancement compared to the other NPs. This is due to the fact that the UV-Vis spectrum of these larger Au NP is more red shifted which is beneficial for the 785 nm excitation

wavelength. Both Raman set-ups, a process CW-Raman including SERS and time-gated Raman including SERS were tested as confocal microscope coupled systems. For the TG-Raman commercial Ag NPs of 40 nm size where used because these NPs are more beneficial than larger Au NPs in visible 532 nm green laser excitation. The 40 nm sized Ag NPs appeared to be ideal as SERS enhancers and have been chosen for the cell-culture media study in **(iv)**. The commercial time-gated Raman was tested for the first time in combination with SERS, creating the term TG-SERS and demonstrating the feasibility to detect low concentrations of the model-bacteria. Additionally, to ensure a constant and stable SERS signal, immunomagnetic separation (IMS) beads were used and showed improved signals with regards of the reproducibility of the measurements. In a follow-up study (Uusitalo et al., 2017b), a further stability optimized signal of the same microorganism with a neodymium magnet underneath the developed SERS chip was confirmed. As a result, the Au NPs colloids in combination with the magnetic IMS beads and the *Listeria innocua* model bacteria settled more rapidly onto the roll-to-roll patterned SERS structure which improved the spatial and temporal stability of SERS signal significantly.

Speculations of the origin of the band around 730 cm^{-1} which typically is the most prominent peak may have been misjudged. Most likely it is the marker for cyclic adenosine monophosphate (cAMP), according to newer studies (Kubryk et al., 2016; Premasiri et al., 2016), which was discussed in detail in **(iv)**, and cannot be exclusively assigned to glycosidic ring mode of D-glucosamine (NAG) from cell walls of *Listeria innocua*. However, this SERS peak is an ideal maker for the quality of reproducible SERS spectra of cell-culture media with and without bacteria which the extensive performance test on different spectroscopic options and excitation wavelengths of the temporal change of the SERS signal from mineral salt medium of E. coli further reveals. The peak was used to identify the level of LOD.

Concluding the results of the Listeria study on R2R-produced SERS structures with different Au NPs, the hypothesis that disagreements within the literature regarding bacterial spectra results from conditions present during the detection process has not been supported. Another key-finding was that the effect of the SERS enhancing metal itself, whether Au or Ag, and the excitation wavelength (532 nm with pulsed laser excitation or 785 nm with CW laser excitation) on the detected spectra was neglectable. The sensitivity of our SERS detection was improved through optimization of the concentration of the sample inside the hydrophobic polydimethylsiloxane (PDMS) wells. Immunomagnetic separation (IMS) beads were used to assist the accumulation of bacteria into the path of the beam of the excitation laser. With this combination we have detected *Listeria* with gold enhanced SERS in a label free manner from such low sample concentrations as 10^4 CFU ml^{-1}.

(**iii** – **Bare laser-synthesized Au-based nanoparticles as non-disturbing SERS probes for Bacteria Identification**) This study is a continuation of bacteria identification (*Listeria innocua* and *Escherichia coli*) study of **(ii)**, showing the advantages of physically laser ablated Au NPs, a methodological novelty.

These nanoparticles offer a much improved biocompatibility compared to chemically-synthesized NPs with the option to track the efficiency to the SERS signal in bacterial and cell cultures. Such unique nano-formulations were produced by non-chemical methods of laser ablation in deionized water. These ultra-pure Au NPs have several advantages. The major advantage is that in the supernatant of the NPs are no chemical residuals from the synthesis process, i.e., there are no starting reactants such as ions or surfactants which could harm the microorganism during inspection, thus they exclude any toxic surface contaminants. Another advantage is the possibility for the synthesis of a variety of alternative materials and composite structures such as orthosilicate (SiO_4^{4-}) or crystalline silicon found in biological tissues, and that there is a low background signal originating from the NPs itself.

Tracking of SERS efficiency was possible due to the presence of the 520 cm^{-1} band (main silicon contribution) as an interesting feature, since employed in biomedical studies, e.g., to track the localization of such SERS probes in biological objects onto cells or tissues. This can be used as internal standard because the silicon band around 520 cm^{-1} is often used to calibrate a Raman spectrometer. Common chemically synthesised Au NPs consist of non-biocompatible by-products such as surfactants and anions which are generated during the synthesis. As already shown in **(i)**, the SERS signal of biofouling from pure adenine was accompanied by the presence of a band from the synthesis process of the chemically synthesised Au NPs, namely the strong band around 980 cm^{-1}. Therefore, this is a first assessment of novel ligand-free (bare) hybrid Au-Si nanoparticles with controlled content of Au in their composition (30-100%) as mobile SERS probes in tasks of bacteria detection which was demonstrated. Even in the case of minor fraction of Au, the nanoparticles support plasmonic oscillations and provide considerable SERS effect, which is confirmed in experiments using standard 6RG Raman model. Profiting from the observed enhancement and purity of laser-synthesized nanomaterials, a successful identification of two types of bacteria (*Listeria innocua* and *Escherichia coli*) was demonstrated.

(iv – Comparison of time-gated surface enhanced Raman spectroscopy (TG-SERS) and classical SERS based monitoring of *Escherichia coli* cultivation samples) Cell-culture media is changing during the course of the cultivation which effects the product yield and finally the (Rowland-Jones et al., 2017). The same group suggests for the analysis of the development of cell culture media to use Raman spectroscopy over NIR and 2D-fluorescence based on their results of MVDA. Significant metabolic changes can be determined using classical Raman without SERS enhancement but an interference from fluorescent compounds is covering the signal which makes analysis difficult. This is not the case at all stages of the cultivation but occasionally fluorescing compounds may overlap Raman signals completely (Rowland-jones et al., 2017). For the study in **(iv)** cell-free supernatant samples of *Escherichia coli* with a range of substrate levels, from deficiency to excess, using a pulsed-feed strategy in mineral salt media

were investigated. Motivation for this study was to see whether there are significant differences in in terms of qualification and quantification of Raman and SERS signals from different spectroscopic set-ups with different measurement principles and excitation wavelengths. To have equal measurement conditions, Raman measurements and the SERS application were applied for all three set-ups in the same way using an anodized aluminium microwell plate, resulting in stable and repeatable results.

The pure Raman signal without SERS shows mainly compounds from substrates of the mineral salt medium, such as sulphates, trace elements and carbohydrates. In this respect the three spectroscopic set-ups shows similar results. The CW-microscope setup close to fluorescence maximum at 633 nm showed slightly more interference from fluorescence than TG-Raman at the fluorescence maximum (here is the fluorescence suppression is effectively working) and the CW-Raman at 785 nm far away from fluorescence maximum (cf., Fig. 36 and Fig. 5). In contrast classical Raman combined with SERS and time-gated Raman with SERS (TG-SERS) show additionally bands from amino acids, proteins and DNA without much disturbance of fluorescence which are currently not possible to detect with other techniques in such short measurement period non-destructive, without contact and sample preparation. The same Ag NPs have been used in **(iv)** for the three different spectroscopic set-ups as already tested with TG-Raman in **(ii)**. SERS based CW-Raman, CW-microscope and TG-SERS methods cover the detection of the whole range of all analytes present in the cell-culture media whereas chromatographic- based methods demand the measurement of different kind of analytes with different set-ups. The challenge here was whether it would be possible to build a multivariate data model (different pre-treatments were applied to obtain PLSR-models) to observe Raman and SERS data quantitatively and compare them with chromatographic reference data. The results show that SERS spectral peaks are more clearly identifiable when using process Raman spectrometer set-ups (CW-Raman at 785 nm and pulsed TG-Raman at 532 nm excitation) and were proven to be repeatable (several repeat measurements were performed, cf., supporting material). The comparison of HPLC-data with the SERS data showed identical trends throughout the cultivation process for glucose, acetate, cAMP and AMP. The analysis with MVDA revealed that CW-Raman at 785 nm, due to sufficient enough spectral resolution, was most suitable for the quantitative analysis than the other set-ups but TG-Raman (currently limited by poor spectral resolution) was more suited for the qualitative analysis throughout the course of the cultivation. Remarkably, the spectral results from the most precise high-resolution CW-microscope showed no superior quantifiable results. This is due to the tiny focal sport compared the other set-ups which creates especially with SERS a higher variance in the spectral results. Furthermore, the integration of the regression coefficient of cAMP and AMP shows a pattern which is an indication of a relation between spectral peaks of both compounds (cf., Fig. S2). They seem to develop in the same pace throughout the cultivation. SERS results of CW-Raman and TG-Raman also clearly show the temporal

behaviour of the usage of the substrate peaks with respect to the increase of certain peaks such as cAMP, identifying this relationship. In fact, this is the first time that a performance test with and without SERS was applied to follow critical bioprocess parameters such as glucose, acetate, cAMP and AMP of one cultivation using three different spectroscopic set-ups.

5. Discussion and Outlook

Chromatographic techniques have been dominating analytical tools in bioprocess based production since several decades. In fact they are the common analytical tool in the biopharmaceutical industry. They require sampling, excessive sample preparation, dilution and the measurement process itself is slow. These requirements become a bottleneck when many samples are needed to be analysed. Additionally, different chromatographic separation-columns and detector set-ups are required when analysing different compounds of the same sample, resulting in unnecessary repeated measurements and the need of a large analytic laboratory. Frequently the aging of a separation-column can also lead to shifts of the retention time of peaks in the chromatogram. Highly skilled personal is required and the overall operation costs of the laboratory are relatively high. However, chromatographic techniques are the analytic standard par excellence in bioprocess and biopharmaceutics, thus they are an ideal reference to new methodological approaches (Bourget et al., 2014; Buckley and Ryder, 2017). To overcome the problems, a detection technique is required which is faster, non-destructive- and invasive, does not require sample preparation and dilution, allows for in-situ process measurements, is able to handle fluid stresses with respect to the substrates and to some extend can be automatable for bioprocesses. It seem that optical techniques are the future, especially when analytic handling and specifically chemometrics can be automated.

While this thesis has highlighted the many benefits of the optical techniques, in particular Raman spectroscopy, there are several remaining limitations that need to be addressed. The main reason why Raman is not yet accepted in bioproduction, is the disturbing fluorescence background which makes the measurements often difficult or impossible to analyse. Within this thesis two solutions, namely SERS and TG-Raman are examined which as standalone or in combination overcome this limitation. The weakness of the low intensity Raman signal can be overcome by SERS which enhances the cross section by many orders of magnitude using noble metal (Ag, Au) colloids, nanostructures or the combination of both. In contrary to NIR, Raman and SERS bands of cells and cell culture media are typically narrow and unaffected by water signals, allowing an easy assignment if the bands are not totally overlapping. Since SERS is a distance dependent effect, in some cases the plasmonic oscillations are not strong enough to create a local electric field, i.e., a too large gap between the molecules of interest and the enhancing metal structure, under which SERS is not efficiently working to counterweight the disturbing influence of fluorescence (cf. Fig. 7). SERS has been also found to be a fluorescence quencher but it requires metallic nanoparticles or patterned structures to function well. Time-gating on the other hand

makes use of the principle that fluorescence is with all compounds exhibited at a delayed temporal stage than the instantly exhibited Raman signal.

There are other techniques which can be used to minimize the fluorescence impact such as differential techniques. However, they include the fluorescence background and other signals being measured without the ability to discriminate them from each other, e.g., detector noise and cosmic rays, which therefore makes time-gating an interesting technique, as it is capable to "gate out " almost all the noise as exemplified in Fig. 8 and equation [Eq. 5.] Raman spectroscopy for measuring cells and cell-culture media with high molecular specificity and without major background disturbances from fluorescence, in addition the option to measure even low concentrations, the applications of SERS and TG, have good prospects in bioprocess and biopharmaceutical production. The limitations to overcome from this point are that SERS still needs the optimization between reproducibility and enhancement, more efficient substrates, and a solution for mass-production of non-aggregating colloids to lower the costs. The lithographically roll-to-roll produced UV-nano-imprinted structured SERS surfaces used in two studies within this thesis are a good example to be highlighted.

Time-gate Raman detection has become commercially available as compact and portable solution for a process spectrometer. One of the current limitation of the time-gated approach was the poor spectral resolution which would have otherwise showed better results. An improved resolution and increased overall measurement time is desirable and under way which may include micro lens-arrays as already mentioned in the introduction part 1.5.2.

Promising alternative advanced Raman techniques with also high prospect for bioprocess monitoring are for instance coherent anti-Stokes Raman spectroscopy (CARS) with surface-enhancement functionality (SE-CARS) and tip-enhanced Raman spectroscopy (TERS) (Namboodiri et al., 2011; Schmid et al., 2008). Both techniques employ the here presented principles of SERS in a different manner. They would require a confocal microscope, and in case of TERS a metallic cantilever (similar as in atomic force microscopy, AFM) which acts as Raman enhancer, but it may need to be arranged and embedded into e.g. a flow-cell set-up to achieve a viable bioprocess monitoring setting.

Furthermore, the use of a process Raman spectrometer e.g., TG-Raman in confocal microscopy set-up, as shown in Fig. 1. would bring several advantages. Typically with a common CW-Raman system connected to the microscope the user is limited in the image observation and simultaneous measurement of e.g., cells in media. The reason is that a tightly focused laser beam near a cell or cell assembly will also, depending on the used laser power, physically push the cell away from the focal point due to the

heat generated at the spot and it is a "blind spot" in common Raman microscopy. This becomes even more difficult with colloidal SERS nanoparticles in close proximity. Having the option to live-view or image the situation of the Raman/SERS measurements is highly desired. With common CW-Raman microscopes it is not possible to measure the Raman/SERS signal and simultaneously observe what happens, while the short measurement, in terms of the laser beam pushing the liquid out of focus. When applying TG principle in such confocal microscope set-up, the observing live-camera can be left on with light illumination to the sample, through the lens because of the picosecond short TG-Raman measurement duty-cycle no interfering will occur, as explained in the introduction part of TG-Raman in Chapter 1.5. This would enable real-time observation of the sample assay.

The future of advanced bioprocess analytics may be in the combination as "sensor fusion" of different optical measurement techniques such as digital holographic microscopy, particle analysis (quantification and shape-scan with time-of-flight (TOF) technology), electro-optically polarizability and Raman/SERS in flow-cell or microfluidic set-ups with machine-vision support, respectively machine learning algorithms. In fact these techniques share common optoelectronic properties for that it might be straight forward to merge them together into a single measurement device. Particularly the particle analysis with TOF technology is based on the same measurement principle as TG-Raman and only one detector a SPAD would be needed for both measurement principles. This example alone merges two important and for bioprocess analytics relevant techniques. Combining these techniques reliably will allow for (i) the correct snapshot of the measurement under real-time condition, (ii) faster and automated detection and (iii) delivering of robust information for sequential or even parallel multivariate statistical data analysis. As an example, the initially discussed chromatographic based techniques have been merged in flow-cell set-ups with parallel Raman based detection while the sample is been pushed through the separation-column (Geissler et al., 2017; Kennedy et al., 1997). Raman/SERS and HPLC can have a shared common future as bioprocess analytical tools not just as reference or completely separate techniques.

Finally, combining the results presented and discussed here, the findings hold high potentials to be refined advanced for future application since both methods, SERS and time-gated Raman are constantly been developed further for a manifold range of applications.

References

Abu-absi, N.R., Kenty, B.M., Cuellar, M.E., Borys, M.C., Sakhamuri, S., Strachan, D.J., Hausladen, M.C., Li, Z.J., 2011. Real Time Monitoring of Multiple Parameters in Mammalian Cell Culture Bioreactors Using an In-Line Raman Spectroscopy Probe. Biotechnol. Bioeng. 108, 1215–1221. doi:10.1002/bit.23023

Afseth, N.K., Kohler, A., 2012. Extended multiplicative signal correction in vibrational spectroscopy, a tutorial. Chemom. Intell. Lab. Syst. 117, 92–99. doi:10.1016/j.chemolab.2012.03.004

Albrecht, M. G., Creighton, J. A., 1977. Anomalously intense Raman spectra of pyridine at a silver electrode. Journal of the american chemical society. 99, 15, 5215-5217.

Al-Kattan, A., Ryabchikov, Y. V, Baati, T., Chirvony, V., Sa, J.F., Sentis, M., Braguer, D., Timoshenko, V.Y., Estève, M.-A., Kabashin, A. V, 2016. variable oxidation states for biomedical applications. J. Mater. Chem. B 4, 7852–7858. doi:10.1039/C6TB02623K

Al-Qadiri, H.M., Lin, M., Al-Holy, M.A., Gavinato, A.G., Rasco, B.., 2008. Detection of Sublethal Thermal Injury in Salmonella enterica Serotype Typhimurium and Listeria monocytogenes Using Fourier Transform Infrared (FT-IR) Spectroscopy (4000 to 600 cm – 1) Introduction. J. Food Sci. 73, 54–61. doi:10.1111/j.1750-3841.2007.00640.x

Alkilany, A.M., Murphy, C.J., 2010. Toxicity and cellular uptake of gold nanoparticles: What we have learned so far? J. Nanoparticle Res. 12, 2313–2333. doi:10.1007/s11051-010-9911-8

Anker, J.N., Hall, W.P., Lyandres, O., Shah, N.C., Zhao, J., Duyne, R.P. Van, 2008. Biosensing with plasmonic nanosensors. Nat. Mater. 7, 8–10.

AshaRani, P. V., Low Kah Mun, G., Hande, M. P., & Valiyaveettil, S., 2008. Cytotoxicity and genotoxicity of silver nanoparticles in human cells. ACS nano. 3, 2, 279-290. doi:10.1021/nn800596w

Baati, T., Al-kattan, A., Esteve, M., Njim, L., Ryabchikov, Y., Chaspoul, F., Hammami, M., Sentis, M., Kabashin, A. V, Braguer, D., 2016. Ultrapure laser-synthesized Si- based nanomaterials for biomedical applications : in vivo assessment of safety and biodistribution. Sci. Rep. 6, 1–13. doi:10.1038/srep25400

Baia, M., Astilean, S., Iliescu, T., 2008. Fundamentals of Infrared and Raman Spectroscopy, SERS, and Theoretical Simulations, in: Raman and SERS Investigations of Pharmaceuticals. Springer-Verlag Berlin Heidelberg, Heidelberg, pp. 9–29. doi:10.1007/978-3-540-78283-4

Balasubramanian, S.K., Yang, L., Yung, L.L., Ong, C., Ong, W., Yu, L., 2010. Characterization, purification, and stability of gold nanoparticles Suresh. Biomaterials 31, 9023–9030. doi:10.1016/j.biomaterials.2010.08.012

Bantz, K.C., Meyer, A.F., Wittenberg, N.J., Im, H., Kurtulus, O., Lee, S.H., Lindquist, N.C., Oh, S.-H., Haynes, C.L., 2011. Recent progress in SERS biosensing. Phys. Chem. 13. doi:10.1039/c0cp01841d

Baranska, M., 2014. Optical Spectroscopy and Computational Methods in Biology and Medicine. Springer Dordrecht Heidelberg New York London. doi:10.1007/978-94-007-7832-0

Bar-Ilan, O., Albrecht, R. M., Fako, V. E., & Furgeson, D. Y. (2009). Toxicity assessments of multisized gold and silver nanoparticles in zebrafish embryos. Small. 5, 16, 1897-1910. doi:10.1002/smll.200801716

Belfort, G.; Pimbley, J. M.; Grainer, A.; Chung, K.Y., 1993. Diagnosis of membrane fouling using a rotating annular filter. 1. Cell culture media. J. Membr. Sci. Sci 77, 1–22.

Bell, S.E.J., Sirimuthu, N.M.S., 2006. Surface-Enhanced Raman Spectroscopy (SERS) for Sub-Micromolar Detection of DNA / RNA Mononucleotides. J. Am. Chem. Soc. 128, 15580–15581.

Besner, S., Kabashin, A. V, Meunier, M., 2006. Fragmentation of colloidal nanoparticles by femtosecond laser-induced supercontinuum generation Fragmentation of colloidal nanoparticles by femtosecond laser-induced supercontinuum generation. Appl. Phys. Lett. 233122, 1–3. doi:10.1063/1.2402944

Besse, G.N., Audinet, N., Kerouanton, A., Colin, P., Kalmokoff, M., 2005. Evolution of Listeria populations in food samples undergoing enrichment culturing. Int. J. Food Microbiol. 104, 123–134. doi:10.1016/j.ijfoodmicro.2005.01.012

Bibikova, O., Bykov, A., Bogatyrev, V., Tuchin, V., 2015. Optical properties of plasmon- resonant bare and silica-coated nanostars used for cell imaging. J. Biomed. Opt. 7, 11. doi:10.1117/1.JBO.20.7.076017

Blacksberg, J., Alerstam, E., Maruyama, Y., Cochrane, C.J., Rossman, G.R., 2016. Miniaturized time-resolved Raman spectrometer for planetary science based on a fast single photon avalanche diode detector array. Appl. Opt. 55, 739–748. doi:10.1364/AO.55.000739

Blandin, P., Maximova, K.A., Gongalsky, M.B., Sanchez-Royo, J.F., Chirvony, V.S., Sentis, M., Timoshenko, Y., Kabashin, A. V, 2013. Femtosecond laser fragmentation from water-dispersed microcolloids : toward fast controllable growth of ultrapure Si-based nanomaterials for biological applications. J. Mater. Chem. B 1, 2489–2495. doi:10.1039/c3tb20285b

Boccaccio, T., Bottino, A., Capannelli, G., Piaggio, P., 2002. Characterization of PVDF membranes by vibrational spectroscopy 210, 315–329.

Bocklitz, T., Walter, A., Hartmann, K., Rösch, P., Popp, J., 2011. How to pre-process Raman spectra for reliable and stable models? Anal. Chim. Acta 704, 47–56. doi:10.1016/j.aca.2011.06.043

Bourget, P., Amin, A., Vidal, F., Merlette, C., Lagarce, F., 2014. Comparison of Raman spectroscopy vs . high performance liquid chromatography for quality control of complex therapeutic objects: Model of elastomeric portable pumps filled with a fluorouracil solution. J. Pharm. Biomed. Anal. 91, 176–184. doi:10.1016/j.jpba.2013.12.030

Boyaci, I.H., Temiz, T.H., Genis, H.E., Soykut, E.A., Yazgan, N.N., Guven, B., Uysal, R.S., Bozkurt, A.G., Ilaslan, K., Toruna, O., Seker, F.C.D., 2015. Dispersive and FT-Raman spectroscopic methods in food analysis. RCS Adv. 5, 56606–56624. doi:10.1039/C4RA12463D

Brognaux, A., Bugge, J., Schwartz, F.H., Thonart, P., Telek, S., Delvigne, F., 2013. Real-time monitoring of cell viability and cell density on the basis of a three dimensional optical reflectance method (3D-ORM): Investigation of the effect of sub-lethal and lethal injuries. J. Ind. Microbiol. Biotechnol. 40, 679–686. doi:10.1007/s10295-013-1271-9

Brown, R.J.C., Milton, M.J.T., 2008. Nanostructures and nanostructured substrates for surface-enhanced Raman scattering (SERS). J. Raman Spectrosc. 39, 1313–1326. doi:10.1002/jrs.2030

Brust, M., Walker, M., Bethell, D., Schiffrin, D.J., Whyman, R., 1994. Synthesis of Thiol-derivatised Gold Nanoparticles in. J. Chem. Soc. 801–802.

Buckley, K., Ryder, A.G., 2017. Applications of Raman Spectroscopy in Biopharmaceutical Manufacturing: A Short Review. Appl. Spectrosc. 71, 1085–1116. doi:10.1177/0003702817703270

Butler, H.J., Ashton, L., Bird, B., Cinque, G., Curtis, K., Dorney, J., Esmonde-white, K., Fullwood, N.J., Gardner, B., Martin-Hirsch, P.L., Walsh, M.J., Mcainsh, M.R., Stone, N., Martin, F.L., 2016. Using Raman spectroscopy to characterise biological materials. Nat. Protoc. 11, 664–687. doi:10.1038/nprot.2016.036

Butler, H.J., Fogarty, S.W., Kerns, J.G., Martin-Hirsch, P.L., Fullwood, N.J., Martin, F.L., 2015. Gold nanoparticles as a substrate in bio-analytical near-infrared surface-enhanced Raman spectroscopy. Analyst 140, 3090–7. doi:10.1039/c4an01899k

Böttger, U., Maiwald, M., Hanke, F., Braune, M., Pavlov, S.G., Schröder, S., Weber, I., Busemann, H., Sumpf, B., Tränkle, G., Hübers, H.-W., 2017. Shifted Excitation Raman Difference Spectroscopy applied to extraterrestrial particles returned from the asteroid Itokawa. Planet. Space Sci. 144, 106–111. doi:10.1016/j.pss.2017.05.004

Cabrera, F.C., Aoki, P.H.B., Aroca, R.F., Constantino, C.J.L., Santos, D.S., Job, A.E., 2012. Portable smart films for ultrasensitive detection and chemical analysis using SERS and SERRS. J. Raman Spectrosc. 2010–2013. doi:10.1002/jrs.3074

Calvet, A., Ryder, A.G., 2014. Monitoring cell culture media degradation using surface enhanced Raman scattering (SERS) spectroscopy. Anal. Chim. Acta 840, 58–67. doi:10.1016/j.aca.2014.06.021

Camesano, T.A., 2014. Nanotechnology to Aid Chemical and Biological Defense. Springer-Verlag Berlin Heidelberg. doi:10.1007/978-94-017-7218-1

Cardinal, M.F., Vander Ende, E., Hackler, R.A., McAnally, M.O., Stair, P.C., Schatz, G.C., Van Duyne, R.P., 2017. Expanding applications of SERS through versatile nanomaterials engineering. Chem. Soc. Rev. 46, 3886–3903. doi:10.1039/C7CS00207F

Chalmers, J.M., Edwards, H.G.M., Hargreaves, M.D., 2012. Infrared and Raman Spectroscopy in Forensic Science. John Wiley & Sons, Ltd. doi:10.1002/9781119962328

Chase, B., Parkinson, B., 1991. A Study of the Wavelength and Potential Dependence of Surface-Enhanced Raman Scatterm on Cu, Ag, and Au Electrodes. J. Phys. Chem 95, 7810–7813.

Chatterjee, S., Bandyopadhyay, A., Sarkar, K., 2011. Effect of iron oxide and gold nanoparticles on bacterial growth leading towards biological application. J. Nanobiotechnology 9, 1–7.

Chen, J., Shen, B., Qin, G., Hu, X., Qian, L., Wang, Z., Li, S., Ren, Y., Zuo, L., 2012. Fabrication of Large-Area, High-Enhancement SERS Substrates with Tunable Interparticle Spacing and Application in Identifying Microorganisms at the Single Cell Level. J. Phys. Chem. C 116, 3320–3318. doi:10.1021/jp210147c

Chen, L., Mungroo, N., Daikuara, L., Neethirajan, S., 2015. Label-free NIR-SERS discrimination and detection of foodborne bacteria by in situ synthesis of Ag colloids. J. Nanobiotechnology 13, 45. doi:10.1186/s12951-015-0106-4

Chen, P., Cui, L., Zhang, K., 2014. Surface-enhanced Raman spectroscopy monitoring the development of dual-species biofouling on membrane surfaces. J. Memb. Sci. 473, 36–44. doi:10.1016/j.memsci.2014.09.007

Chen, T., Wang, H., Chen, G., Wang, Y., Feng, Y., Teo, W.S., Wu, T., Chen, H., 2010. Hotspot-induced transformation of surface-enhanced Raman scattering fingerprints. ACS Nano 4, 3087–3094. doi:10.1021/nn100269v

Chung, A.J., Huhab, Y.S., Erickson, D., 2011. Nanoscale Large area flexible SERS active substrates using engineered nanostructures. Nanoscale 3, 2903–2908. doi:10.1039/c1nr10265f

Cialla, D., März, A., Böhme, R., Theil, F., Weber, K., Schmitt, M., Popp, J., 2012. Surface-enhanced Raman spectroscopy (SERS): Progress and trends. Anal. Bioanal. Chem. 403, 27–54. doi:10.1007/s00216-011-5631-x

Clarke, S.J., Littleford, R.E., Smith, W.E., Goodacre, R., 2005. Rapid monitoring of antibiotics using Raman and surface enhanced Raman spectroscopy. Analyst 130, 1019–1026. doi:10.1039/b502540k

Classen, J., Aupert, F., Reardon, K.F., Solle, D., Scheper, T., 2016. Spectroscopic sensors for in-line bioprocess monitoring in research and pharmaceutical industrial application. Anal. Bioanal. Chem. 1–16. doi:10.1007/s00216-016-0068-x

Clementschitsch, F., Jürgen, K., Florentina, P., Karl, B., 2005. Sensor combination and chemometric modelling for improved process monitoring in recombinant E. coli fed-batch cultivations. J. Biotechnol. 120, 183–196. doi:10.1016/j.jbiotec.2005.05.030

Coles, R., Chiang, J., Cinabro, D., Haupt, J., Kotov, I., Neal, H., Nomerotski, A., Takacs, P., 2017. An automated system to measure the quantum efficiency of CCDs for astronomy. Planet. Space Sci. 4014, 1–2. doi:10.1088/1748-0221/12/04/C04014

Cooney, T.F., Skinner, H.T., Angel, S.M., 1996. Comparative study of some fiber-optic remote Raman probe designs. Part I: Model for liquids and transparent solids. Appl. Spectrosc. 50, 836–848. doi:10.1366/0003702963905592

Correard, F., Maximova, K., Estève, M.-A., Villard, C., Roy, M., Al-kattan, A., Sentis, M., Gingras, M., Kabashin, A. V, Braguer, D., 2014. Gold nanoparticles prepared by laser ablation in aqueous biocompatible solutions : assessment of safety and biological identity for nanomedicine applications. Int. J. Nanomedicine 9, 5415–5430.

Cowcher, D.P., Xu, Y., Goodacre, R., 2013. Portable, Quantitative Detection of Bacillus Bacterial Spores Using Surface-Enhanced Raman Scattering. Anal. Chem. 85, 3297–3302. doi:10.1021/ac303657k

Cui, L., Chen, P., Chen, S., Yuan, Z., Yu, C., Ren, B., Zhang, K., 2013. In Situ Study of the Antibacterial Activity and Mechanism of Action of Silver Nanoparticles by Surface-Enhanced Raman Spectroscopy. Anal. Chem. 85, 5436–5443. doi:dx.doi.org/10.1021/ac400245j

Cui, L., Chen, P., Zhang, B., Zhang, D., Li, J., 2015. Interrogating chemical variation via layer-by-layer SERS during biofouling and cleaning of nanofiltration membranes with further investigations into cleaning efficiency. Water Res.

Cui, L., Chen, P., Zhang, B., Zhang, D., Li, J., Martin, F.L., Zhang, K., 2015. Interrogating chemical variation via layer-by-layer SERS during biofouling and cleaning of nano fi ltration membranes with further investigations into cleaning ef fi ciency. Water Res. 87, 282–291. doi:10.1016/j.watres.2015.09.037

Cui, L., Butler, H. J., Martin-Hirsch, P. L., Martin, F. L. 2016. Aluminium foil as a potential substrate for ATR-FTIR, transflection FTIR or Raman spectrochemical analysis of biological specimens. Analytical Methods. 8, 3, 481-487. doi:10.1039/C5AY02638E

Cui, L., Yang, K., Zhou, G., Huang, W.E., Zhu, Y., 2017. Surface-Enhanced Raman Spectroscopy Combined with Stable Isotope Probing to Monitor Nitrogen Assimilation at Both Bulk and Single-Cell Level. Anal. Chem. doi:10.1021/acs.analchem.6b04913

Cui, L., Yao, M., Ren, B., Zhang, K.-S., 2011. Sensitive and Versatile Detection of the Fouling Process and Fouling Propensity of Proteins on Polyvinylidene Fluoride Membranes via Surface-Enhanced Raman Spectroscopy. Anal. Chem. 1709–1716. doi:10.1021/ac102891g

Culha, M., Cullum, B., Lavrik, N., Klutse, C.K., 2012. Surface-Enhanced Raman Scattering as an Emerging Characterization and Detection Technique. J. Nanotechnol. 2012, 1–15. doi:10.1155/2012/971380

David, C., 2012. Raman Spectroscopy for proteins [WWW Document]. Raman Spectrosc. URL http://www.horiba.com/fileadmin/uploads/Scientific/Documents/Raman/HORIBA_webinar_proteins.pdf (accessed 7.13.17).

De Luca, A.C., Mazilu, M., Riches, A., Herrington, C.S., Dholakia, K., 2010. Online Fluorescence Suppression in Modulated Raman Spectroscopy. Anal. Chem. 82, 738–745. doi:10.1021/ac9026737

Demtröder, W., 2007. Laserspektroskopie Grundlagen und Techniken. Springer-Verlag Berlin Heidelberg New York. doi:10.1063/1.1144861

Dong, L., Ye, F., Hu, J., Popov, S., Friberg, A. T., Muhammed, M., 2011. Photostability of lasing process from water solution of Rhodamine 6G with gold nanoparticles. J. Eur. Opt. Soc., 6, 11019. doi:10.1364/OL.37.000034

Dulkeith, E., Ringler, M., Klar, T.A., Feldmann, J., Javier, A.M., Parak, W.J., 2005. Gold nanoparticles quench fluorescence by phase induced radiative rate suppression. Nano Lett. 5, 585–589. doi:10.1021/nl0480969

Dyar, T.F., Boucher, S., Giguere, C.M., Hoff, L.B., Breitenfeld, M., Parente, T.J., Tague, J., Wang, P., Mahadevan, S., 2015. Baseline Removal in Raman spectroscopy: optimization techniques. 46th Lunar Planet. Sci. Conf. 2464.

Edsall, J.T., 1937. Raman Spectra of Amino Acids and Related Compounds. IV. Ionization of Di- and Tricarboxylic Acids. J. Chem. Phys. 5, 508–517. doi:10.1021/ja01548a004

Efeoglu, E., Culha, M., 2013. In situ-monitoring of biofilm formation by using surface-enhanced raman scattering. Appl. Spectrosc. 67, 498–505. doi:10.1366/12-06896

Efrima, S., Zeiri, L., 2009. Understanding SERS of bacteria. J. Raman Spectrosc. 40, 277–288. doi:10.1002/jrs.2121

El-zahry, M.R., Mahmoud, A., Refaat, I.H., Mohamed, H.A., Bohlmann, H., Lendl, B., 2015. Antibacterial effect of various shapes of silver nanoparticles monitored by SERS. Talanta 138, 183–189. doi:10.1016/j.talanta.2015.02.022

Fales, A. M., Yuan, H., & Vo-Dinh, T. (2013). Cell-penetrating peptide enhanced intracellular Raman imaging and photodynamic therapy. Molecular pharmaceutics. 10, 6, 2291-2298. doi:10.1021/mp300634b

Fan, C., Hu, Z., Mustapha, A., Lin, M., 2011. Rapid detection of food- and waterborne bacteria using surface-enhanced Raman spectroscopy coupled with silver nanosubstrates. Appl. Microbiol. Biotechnol. 92, 1053–1061. doi:10.1007/s00253-011-3634-3

Fan, M., Andrade, G.F.S., Brolo, A.G., 2011. A review on the fabrication of substrates for surface enhanced Raman spectroscopy and their applications in analytical chemistry. Anal. Chim. Acta 693, 7–25. doi:10.1016/j.aca.2011.03.002

Fane, A.G., Fell, C.J.D., 1987. A review of fouling and fouling control in ultrafiltration. Desalination 62, 117–136. doi:10.1016/0011-9164(87)87013-3

Fleischmann, M., Hendra, P.J., McQuillan, A.J., 1974. Raman spectra of pyridine adsorbed at a silver electrode. Chem. Phys. Lett. 26, 163–166. doi:10.1016/0009-2614(74)85388-1

Flemming, H.C., Neu, T.R., Wozniak, D.J., 2007. The EPS matrix: The "House of Biofilm Cells." J. Bacteriol. 189, 7945–7947. doi:10.1128/JB.00858-07

Flemming, H.C., Schaule, G., Griebe, T., Schmitt, J., Tamachkiarowa, a, 1997. Biofouling - the Achilles heel of membrane processes. Desalination 113, 215–225. doi:10.1016/S0011-9164(97)00132-X

Fojtik, A., Giersig, M., Henglein, A., 1993. Formation of Nanometer-Size Silicon Particles in a Laser Induced Plasma in SiH4. Berichte der Bunsengesellschaft für Phys. Chemie 97, 1493–1496. doi:10.1002/bbpc.19930971112

Fossum, E.R., 1993. Active Pixel Sensors: Are CCD's Dinosaurs? Eric R. Fossum Jet Propulsion Laboratory, California Institute of Technology 4800 Oak Grove Drive, Pasadena, California 91109 USA. Sensors (Peterborough, NH) 1900, 1–13.

Frens, G., 1973. Controlled Nucleation for the Regulation of the Particle Size in Monodisperse Gold Suspensions. Nat. Phys. Sci. 241, 20–22.

Galarreta, B.C., Norton, P.R., 2011. SERS Detection of Streptavidin / Biotin Monolayer Assemblies. Langmuir 27, 1494–1498. doi:10.1021/la1047497

Gandhi, M., Chikindas, M.L., 2007. Listeria: A foodborne pathogen that knows how to survive. Int. J. Food Microbiol. 113, 1–15. doi:10.1016/j.ijfoodmicro.2006.07.008

Gasanov, U., Hughes, D., Hansbro, P.M., 2005. Methods for the isolation and identification of *Listeria* spp. and *Listeria monocytogenes* : a review. FEMS Microbiol. Rev. 29, 851–875. doi:10.1016/j.femsre.2004.12.002

Geddes, C.D., 2017. Surface Plasmon Enhanced, Coupled and Controlled Fluorescence, first edit. ed. John Wiley & Sons.

Geissler, D., Heiland, J.J., Lotter, C., Belder, D., 2017. Microchip HPLC separations monitored simultaneously by coherent anti-Stokes Raman scattering and fluorescence detection. Microchim. Acta 184, 315–321. doi:10.1007/s00604-016-2012-3

Gil, G.A., 2005. Online Raman Spectroscopy for Bioprocess Monitoring. Massachusetts Institute of Technology.

Golcuk, K., Mandair, G.S., Callender, A.F., Sahar, N., Kohn, D.H., Morris, M.D., 2006. Is photobleaching necessary for Raman imaging of bone tissue using a green laser? Biochim. Biophys. Acta 1758, 868–873. doi:10.1016/j.bbamem.2006.02.022

Gordon, H.R., 1989. Can the Lambert-Beer law be applied to the diffuse attenuation coefficient of ocean water? Limnol. Oceanogr. 34, 1389–1409. doi:10.4319/lo.1989.34.8.1389

Graham, D., Moskovits, M., Tian, Z.-Q., 2017. SERS – facts, figures and the future. Chem. Soc. Rev. 46, 3864–3865. doi:10.1039/C7CS90060K

Green, G.C., Chan, A.D.C., Goubran, R.A., Luo, B.S., Lin, M., 2008. A Rapid and Reliable Method of Discriminating between Listeria Species Based on Raman Spectroscopy, in: Instrumentation and Measurement Technology Conference Proceedings (IMTC '08). Victoria, pp. 513–517.

Green, M., Liu, F.M., Cohen, L., Kollensperger, P., Cass, T., 2006. SERS platforms for high density DNA arrays. Faraday Discuss 132, 269–319. doi:10.1039/B506636K

Grow, A.E., Wood, L.L., Claycomb, J.L., Thompson, P. a., 2003. New biochip technology for label-free detection of pathogens and their toxins. J. Microbiol. Methods 53, 221–233. doi:10.1016/S0167-7012(03)00026-5

Guo, W., Ngo, H., Li, J., 2012. Bioresource Technology A mini-review on membrane fouling. Bioresour. Technol. 122, 27–34. doi:10.1016/j.biortech.2012.04.089

Habouti, S., Solterbeck, C.-H., Es-Souni, M., 2010. Synthesis of silver nano-fir-twigs and application to single molecules detection. J. Mater. Chem. 20, 5215. doi:10.1039/c0jm00564a

Hain, R., Kähler, C.J., Tropea, C., 2007. Comparison of CCD, CMOS and intensified cameras. Exp. Fluids 42, 403–411. doi:10.1007/s00348-006-0247-1

Hallman, L.W., 2015. Single Photon Detection Based Devices and Techniques for Pulsed Time-of-Flight Applications. University of Oulu.

Hallman, L.W., Haring, K., Toikkanen, L., Leinonen, T., Ryvkin, B.S., Kostamovaara, J.T., 2012. 3 nJ, 100 ps laser pulses generated with an asymmetric waveguide laser diode for a single-photon avalanche diode time-of-flight (SPAD TOF) rangefinder application. Meas. Sci. Technol. 23, 025202–025210. doi:10.1088/0957-0233/23/2/025202

Hampton, C., Demoin, D., 2010. Tutorial: Sulfur and phosphorus. Vib. Spectrosc.

Harz, M., Rösch, P., Popp, J., 2009. Vibrational spectroscopy—A powerful tool for the rapid identification of microbial cells at the single-cell level. Cytom. Part A.

Haynes, C.L., McFarland, A.D., Duyne, R.P. Van, 2005. Raman Spectroscopy. Anal. Chem. 338–346. doi:10.1002/9780470689592.ch7

He, S., Zhang, W., Liu, L., Huang, Y., He, J., Xie, W., Wu, P., Du, C., 2014. Baseline correction for Raman spectra using an improved asymmetric least squares method. Anal. Methods 6, 4402–4407. doi:10.1039/c4ay00068d

He, Y., Su, Y., 2014. Silicon Nano- biotechnology. Springer Heidelberg New York Dordrecht London. doi:10.1007/978-3-642-54668-6

Hebie, S., Holade, Y., Maximova, K., Sentis, M., Delaporte, P., Kokoh, K.B., Napporn, T.W., Kabashin, A. V, 2015. Advanced Electrocatalysts on the Basis of Bare Au Nanomaterials for Biofuel Cell Applications. ACS Catal. 5, 6489–6496. doi:10.1021/acscatal.5b01478

Himmelsbach, D.S., Barfon, F.E., McClung, A.M., Champagne, E.T., 2001. Prediction of protein and amylose contents of rice flour by NIR-FT Raman spectroscopy. Abstr. Pap. Am. Chem. Soc. 219, 83–AGFD.

Holma, J., Nissinen, I., Nissinen, J., Kostamovaara, J., Member, S., 2017. Characterization of the Timing Homogeneity in a CMOS SPAD Array Designed for Time-Gated Raman Spectroscopy. IEEE Trans. Instrum. Meas. 66, 1837–1844.

Hong, S., Li, X., 2013. Optimal Size of Gold Nanoparticles for Surface-Enhanced Raman Spectroscopy under Different Conditions 2013.

Hoppmann, E.P., Yu, W.W., White, I.M., 2014. Inkjet-Printed Fluidic Paper Devices for Chemical and Biological Analytics Using Surface Enhanced Raman spectroscopy. IEEE J. Sel. Top. quantum Electron. 20, 195–204.

Huebner, U., Weber, K., Cialla, D., Haehle, R., Schneidewind, H., Zeisberger, M., Mattheis, R., Meyer, H., Popp, J., 2012. Microelectronic Engineering Microfabricated polymer-substrates for SERS. Microelectron. Eng. 98, 444–447. doi:10.1016/j.mee.2012.05.036

Ivleva, N.P., Wagner, M., Szkola, A., Horn, H., Niessner, R., Haisch, C., 2010. Label-free in situ SERS imaging of biofilms. J. Phys. Chem. B 114, 10184–10194. doi:10.1021/jp102466c

Jain, P.K., Lee, K.S., El-sayed, I.H., El-sayed, M.A., 2006. Calculated Absorption and Scattering Properties of Gold Nanoparticles of Different Size, Shape, and Composition: Applications in Biological Imaging and Biomedicine. J. Phys. Chem. B 110, 7238–7248.

Janknecht, P., Melo, L.F., 2004. Online biofilm monitoring. Rev. Environ. Sci. Bio/Technology 2, 269–283.

Jarvis, R.M., Brooker, A., Goodacre, R., Raman, S., 2004. Surface-Enhanced Raman Spectroscopy for Bacterial Discrimination Utilizing a Scanning Electron Microscope with a Raman Spectroscopy Interface Surface-Enhanced Raman Spectroscopy for Bacterial Discrimination Utilizing a Scanning Electron Microscope with a 76, 5198–5202. doi:10.1021/ac049663f

Jarvis, R.M., Goodacre, R., 2008. Characterisation and identification of bacteria using SERS. Chem. Soc. Rev. 37, 931–936. doi:10.1039/b705973f

Jeanmaire, D. L., Van Duyne, R. P., 1977. Surface Raman spectroelectrochemistry: Part I. Heterocyclic, aromatic, and aliphatic amines adsorbed on the anodized silver electrode. Journal of electroanalytical chemistry and interfacial electrochemistry. 84, 1, 1-20.

Jestel, N.L., 2010. Process Raman Spectroscopy, in: Bakeev, K.A. (Ed.), Process Analytical Technology. John Wiley and Sons, Chichester, pp. 133–169. doi:10.1002/9780470988459.ch5

Jun, B.-H., Kim, G., Noh, M.S., Kang, H., Kim, Y.-K., Cho, M.-H., Jeong, D.H., Lee, Y.-S., 2011. Surface-enhanced Raman scattering-active nanostructures and strategies for bioassays. Nanomedicine 6, 1463–1480. doi:10.2217/nnm.11.123

Junne, S., Klingner, A., Kabisch, J., Schweder, T., Neubauer, P., 2011. A two-compartment bioreactor system made of commercial parts for bioprocess scale-down studies: Impact of oscillations on Bacillus subtilis fed-batch cultivations. Biotechnol. J. 6, 1009–1017. doi:10.1002/biot.201100293

Kabashin, A. V, Meunier, M., 2007. Femtosecond laser ablation in aqueous solutions : a novel method to synthesize non-toxic metal colloids with controllable size, in: Journal of Physics: Conference Series 59, Eighth International Conference on Laser Ablation. pp. 354–359. doi:10.1088/1742-6596/59/1/074

Kabashin, A. V, Meunier, M., 2003. Synthesis of colloidal nanoparticles during femtosecond laser ablation of gold in water Synthesis of colloidal nanoparticles during femtosecond laser ablation of gold in water. J. Appl. Phys. 94, 7941–7943. doi:10.1063/1.1626793

Kabashin, A. V, Pereira, A., Grojo, D., Torres, R., Sentis, M., 2010. Nanofabrication with Pulsed Lasers. Nanoscale Res. Lett. 5, 454–463. doi:10.1007/s11671-010-9543-z

Kairyte, K., Luksiene, Z., Sablinskas, V., 2012. Identification of different Listeria monocytogenes strains by surface enhanced FT Raman spectroscopy. Chem. Technol. 3, 46–49. doi:http://dx.doi.org/10.5755/j01.ct.61.3.2712

Kaiser Optical Systems, I., 2015. RXN1 instrument specifications [WWW Document]. URL http://www.kosi.com/na_en/products/Raman spectroscopy /raman-analyzers/raman-rxn1-analyzer.php (accessed 8.10.17).

Kallioinen, M., Huuhilo, T., Reinikainen, S.P., Nuortila-Jokinen, J., Mänttäri, M., 2006. Examination of membrane performance with multivariate methods: A case study within a pulp and paper mill filtration application. Chemom. Intell. Lab. Syst. 84, 98–105. doi:10.1016/j.chemolab.2006.04.015

Kämmer, E., Olschewski, K., Stöckel, S., Rösch, P., Weber, K., Cialla-May, D., Bocklitz, T., Popp, J. 2015. Quantitative SERS studies by combining LOC-SERS with the standard addition method. Analytical and bioanalytical chemistry. 407, 29, 8925-8929. doi:10.1007/s00216-015-9045-z.

Kennedy, B.J., Milofsky, R., Carron, K.T., 1997. Development of a Cascade Flow Cell for Dynamic Aqueous Phase Detection Using Modified SERS Substrates. Anal. Chem. 69, 4708–4715.

Kennedy, B.J., Spaeth, S., Dickey, M., Carron, K.T., 1999. Substrates Based on Self-Assembled Monolayers Formed Using Alkanethiols. J. Phys. Chem. B 103, 3640–3646. doi:10.1021/jp984454i

Kessler, R.W., 2013. Perspectives in process analysis. J. Chemom. 27, 369–378. doi:10.1002/cem.2549

Kessler, W., 2007. Multivariate Datenanalyse: für die Pharma-, Bio- und Prozessanalytik, Multivariate Datenanalyse. Wiley-VCH. doi:10.1002/9783527610037

Khulbe, K.C., Matsuura, T., 2000. Characterization of synthetic membranes by Raman spectroscopy , electron spin resonance , and atomic force microscopy ; a review. Polymer (Guildf). 41, 1917–1935.

Klimkiewicz, A., Mortensen, P.P., Zachariassen, C.B., Berg, F.W.J. Van Den, 2014. Monitoring an enzyme purification process using online and in-line NIR measurements. Chemom. Intell. Lab. Syst. 132, 30–38.

Knauer, M., Ivleva, N.P., Niessner, R., Haisch, C., 2012. A flow-through microarray cell for the online SERS detection of antibody-captured E. coli bacteria. Anal. Bioanal. Chem. 402, 2663–2667. doi:10.1007/s00216-011-5398-0

Knauer, M., Ivleva, N.P., Niessner, R., Haisch, C., 2010. Optimized surface-enhanced Raman scattering (SERS) colloids for the characterization of microorganisms. Anal. Sci. 26, 761–766. doi:10.2116/analsci.26.761

Kneipp, J., Kneipp, H., Wittig, B., Kneipp, K., 2007. One- and Two-Photon Excited Optical pH Probing for Cells Using Surface-Enhanced Raman and Hyper-Raman Nanosensors. Nano Lett. 7, 2819–2823. doi:10.1021/nl071418z

Kneipp, K., Kneipp, H., Itzkan, I., Dasari, R.R., Feld, M.S., 1999. Surface-enhanced nonlinear Raman scattering at the single-molecule level. Chem. Phys. 247, 155–162. doi:10.1016/S0301-0104(99)00165-2

Kneipp, K., Wang, Y., Kneipp, H., Perelman, L.T., Itzkan, I., 1997. Single molecule detection using surface-enhanced Raman scattering (SERS). Phys. Rev. Lett. 78, 9, 1667–1670. doi:10.1103/PhysRevLett.78.1667

Knight, M.W., King, N.S., Liu, L., Everitt, H.O., Nordlander, P., Halas, N.J., 2014. Aluminum for plasmonics. ACS Nano 8, 834–840. doi:10.1021/nn405495q

Kostamovaara, J., Tenhunen, J., Kögler, M., Nissinen, I., Nissinen, J., Keränen, P., 2013. Fluorescence suppression in Raman spectroscopy using a time-gated CMOS SPAD. Opt. Express. doi:10.1364/OE.21.031632

Krause, M., Ro, P., Radt, B., 2008. Localizing and Identifying Living Bacteria in an Abiotic Environment by a Combination of Raman and Fluorescence Microscopy. Anal. Chem. 80, 8568–8575. doi:10.1021/ac8014559

Krishnan, R.S., Shankar, R.K., 1981. Raman effect: History of the discovery. J. Raman Spectrosc. 10, 1–8. doi:10.1002/jrs.1250100103

Kubryk, P., Niessner, R., Ivleva, N.P., 2016. The origin of the band at around 730 cm−1 in the SERS spectra of bacteria: a stable isotope approach. Analyst 141, 2874–2878. doi:10.1039/c6an00306k

Kögler, M., Zhang, B., Cui, L., Shi, Y., Yliperttula, M., Laaksonen, T., Viitala, T., Zhang, K., 2016. Real-time Raman based approach for identification of biofouling. Sensors Actuators, B Chem. 230, 411–421. doi:10.1016/j.snb.2016.02.079

Lai, S., Centi, S., Borri, C., Ratto, F., Cavigli, L., Micheletti, F., ... & Rossi, F. (2017). A multifunctional organosilica cross-linker for the bio-conjugation of gold nanorods. Colloids and Surfaces B: Biointerfaces, 157, 174-181.

Lamsal, R., Harroun, S.G., Brosseau, C.L., Gagnon, G.A., 2012. Use of surface enhanced Raman spectroscopy for studying fouling on nanofiltration membrane. Sep. Purif. Technol. 96, 7–11. doi:DOI 10.1016/j.seppur.2012.05.019

Law, J.W., Mutalib, N.A., Chan, K., Lee, L., 2015. Rapid methods for the detection of foodborne bacterial pathogens : principles , applications , advantages and limitations. Front. Microbiolo 5, 1–19. doi:10.3389/fmicb.2014.00770

Lee, C.H., Hankus, M.E., Tian, L., Pellegrino, P.M., Singamaneni, S., 2011. Highly Sensitive Surface Enhanced Raman Scattering Substrates. Anal. Chem. 83, 8953–8958. doi:10.1021/ac2016882

Lee, H.L.T., Boccazzi, P., Gorret, N., Ram, R.J., Sinskey, A.J., 2004. In situ bioprocess monitoring of Escherichia coli bioreactions using Raman spectroscopy. Vib. Spectrosc. 35, 131–137. doi:10.1016/j.vibspec.2003.12.015

Lee, S., Yoon, J.H., Yoon, S., 2011. Adsorption patterns of gold nanoparticles on methyl-terminated self-assembled monolayers. J. Phys. Chem. C 115, 12501–12507. doi:10.1021/jp202013j

Leopold, N., Cîntă-Pînzaru, S., Baia, M., Antonescu, E., Cozar, O., Kiefer, W., Popp, J., 2005. Raman and surface-enhanced Raman study of thiamine at different pH values. Vib. Spectrosc. 39, 169–176. doi:10.1016/j.vibspec.2005.02.019

Lewis, I.R., Griffiths, P.R., 1996. Raman spectrometry with fiber-optic sampling. Appl. Spectrosc. 50. doi:10.1366/0003702963904908

Li, H., Fane, A.G., Coster, H.G.L., Vigneswaran, S., 2003. Observation of deposition and removal behaviour of submicron bacteria on the membrane surface during crossflow microfiltration. J. Memb. Sci. 217, 29–41. doi:10.1016/S0376-7388(03)00066-8

Li, J., Fang, Y., 2007. An investigation of the surface enhanced Raman scattering (SERS) from a new substrate of silver-modified silver electrode by magnetron sputtering. Spectrochim. Acta Part A 66, 994–1000. doi:10.1016/j.saa.2006.05.012

Li, J.F., Zhang, Y.J., Ding, S.Y., Panneerselvam, R., Tian, Z.Q., 2017. Core-shell nanoparticle-enhanced raman spectroscopy. Chem. Rev. 117, 5002–5069. doi:10.1021/acs.chemrev.6b00596

Li, Z., Xu, H., 2016. Nanoantenna effect of surface-enhanced Raman scattering: managing light with plasmons at the nanometer scale. Adv. Phys. X 1, 492–521. doi:10.1080/23746149.2016.1220263

Lin, H., Hoffmann, F., Rozkov, A., Enfors, S.O., Rinas, U., Neubauer, P., 2004. Change of extracellular cAMP concentration is a sensitive reporter for bacterial fitness in high-cell-density cultures of Escherichia coli. Biotechnol. Bioeng. 87, 602–613. doi:10.1002/bit.20152

Lin, M., Xu, B., Yao, H., Shen, A., Hu, J., 2016. An in vivo quantitative Raman-pH sensor of arterial blood based on laser trapping of erythrocytes. Analyst 141, 3027–3032. doi:10.1039/C5AN02315G

Liu, Y., Chao, K., Nou, X., Chen, Y.R., 2009. Feasibility of colloidal silver SERS for rapid bacterial screening. Sens. Instrum. Food Qual. Saf. 3, 100–107. doi:10.1007/s11694-008-9064-y

Liu, Y., Chen, Y.-R., Nou, X., Chao, K., 2007. Potential of surface-enhanced Raman spectroscopy for the rapid identification of Escherichia coli and Listeria monocytogenes cultures on silver colloidal nanoparticles. Appl. Spectrosc. 61, 824–31. doi:10.1366/000370207781540060

Lombardi, J.R.J.R., Birke, R.L.R.L., 2008. A Unified Approach to Surface-Enhanced Raman Spectroscopy. J. Phys. Chem. C 112, 5605–5617. doi:10.1021/jp800167v

Long, G., Winefordner, J., 1983. Limit of Detection - A Closer Look at the IUPAC Definition. Anal. Chem. 55, 712–724.

Lu, X., Al-Qadiri, H.M., Lin, M., Rasco, B.A., 2011a. Application of Mid-infrared and Raman Spectroscopy to the Study of Bacteria. Food Bioprocess Technol. 4, 919–935. doi:10.1007/s11947-011-0516-8

Lu, X., Rasco, B. a., Kang, D.H., Jabal, J.M.F., Aston, D.E., Konkel, M.E., 2011b. Infrared and Raman spectroscopic studies of the antimicrobial effects of garlic concentrates and diallyl constituents on foodborne pathogens. Anal. Chem. 83, 4137–4146. doi:10.1021/ac2001498

Luo, B.S., Lin, M., 2008. A portable Raman system for the identification of foodborne pathogenic bacteria. J. Rapid Methods Autom. Microbiol. 16, 238–255. doi:10.1111/j.1745-4581.2008.00131.x

Mafune, F., Kohno, J., Takeda, Y., Kondow, T., 2001. Formation of Gold Nanoparticles by Laser Ablation in Aqueous Solution of Surfactant. J. Phys. Chem. B 105, 5114–5120.

Makino, R., Obayashi, E., Homma, N., Shiro, Y., Hori, H., 2003. YC-1 facilitates release of the proximal his residue in the NO and CO complexes of soluble guanylate cyclase. J. Biol. Chem. 278, 11130–11137. doi:10.1074/jbc.M209026200

Maquelin, K., Kirschner, C., Choo-smith, L., Braak, N. Van Den, Endtz, H.P., 2002. Identification of medically relevant microorganisms by vibrational spectroscopy. J. Microbiol. Methods 51, 255–271.

Martyshkin, D. V., Ahuja, R.C., Kudriavtsev, A., Mirov, S.B., 2004. Effective suppression of fluorescence light in Raman measurements using ultrafast time gated charge coupled device camera. Rev. Sci. Instrum. 75, 630–635. doi:10.1063/1.1646743

Matousek, P., Parker, A.W., 2007. Non-invasive probing of pharmaceutical capsules using transmission Raman spectroscopy. J. Raman Spectrosc. 38, 563–567. doi:10.1002/jrs.1688

Matousek, P., Towrie, M., Parker, A.W., Facility, C.L., Rutherford, C., Ma, C., Kwok, W.M., Phillips, D., 2001. Fluorescence Suppression in Raman Spectroscopy using a High Performance Picosecond Kerr Gate. J. Raman Spectrosc. 32, 983–988.

Maximova, K., Aristov, A., Sentis, M., Kabashin, A. V, 2015. Size-controllable synthesis of bare gold nanoparticles by femtosecond laser fragmentation in water. Nanotechnology 26, 1–8. doi:10.1088/0957-4484/26/6/065601

Mayilo, S., Kloster, M. a, Wunderlich, M., Lutich, a, 2009. Long-range fluorescence quenching gold nanoparticles in a sandwich immunoassayfor cardiac troponin T. Nano Lett. 9, 4558–4563.

McNay, G., Eustace, D., Smith, W.E., Faulds, K., Graham, D., 2011. Surface-enhanced Raman scattering (SERS) and surface-enhanced resonance raman scattering (SERRS): A review of applications. Appl. Spectrosc. 65, 825–837. doi:10.1366/11-06365

Mehdizadeh, H., Lauri, D., Karry, K.M., Moshgbar, M., Procopio-Melino, R., Drapeau, D., 2015. Generic Raman-based calibration models enabling real-time monitoring of cell culture bioreactors. Biotechnol. Prog. 31, 1004–1013. doi:10.1002/btpr.2079

Mendonça, M., Conrad, N.L., Conceição, F.R., Moreira, A.N., da Silva, W.P., Aleixo, J.A., Bhunia, A.K., 2012. Highly specific fiber optic immunosensor coupled with immunomagnetic separation for detection of low levels of Listeria monocytogenes and L. ivanovii. BMC Microbiol. 12, 275. doi:10.1186/1471-2180-12-275

Mogilevsky, G., Borland, L., Brickhouse, M., Fountain III, A.W., 2012. Raman Spectroscopy for Homeland Security Applications. Int. J. Spectrosc. 2012, 1–12. doi:10.1155/2012/808079

Moody, A.S., Baghernejad, P.C., Webb, K.R., Sharma, B., 2017. Surface Enhanced Spatially Offset Raman Spectroscopy Detection of Neurochemicals Through the Skull. Anal. Chem. acs.analchem.7b00985. doi:10.1021/acs.analchem.7b00985

Mukherjee, P., Ahmad, A., Mandal, D., Senapati, S., Sainkar, S.R., Khan, M.I., Parishcha, R., Ajaykumar, P. V, Alam, M., Kumar, R., Sastry, M., 2001. Fungus-Mediated Synthesis of Silver Nanoparticles and Their Immobilization in the Mycelial Matrix : A Novel Biological Approach to Nanoparticle Synthesis. Nano Lett. 1, 515–519. doi:10.1021/nl0155274

Mungroo, N.A., Oliveira, G., Neethirajan, S., 2015. SERS based point-of-care detection of food-borne pathogens. Microchim. Acta. doi:10.1007/s00604-015-1698-y

Mänttäri, M., Nyström, M., 2000. Critical flux in NF of high molar mass polysaccharides and effluents from the paper industry. J. Memb. Sci. 170, 257–273. doi:10.1016/S0376-7388(99)00373-7

Namboodiri, V., Namboodiri, M., Diaz, G.I.C., Oppermann, M., Flachenecker, G., Materny, A., 2011. Vibrational Spectroscopy Surface-enhanced femtosecond CARS spectroscopy (SE-CARS) on pyridine. Vib. Spectrosc. 56, 9–12. doi:10.1016/j.vibspec.2010.08.005

Narayanan, P.S., 1951. Raman spectrum of potassium di-hydrogen phosphate. Proc. Indian Acad. Sci. - Sect. A 33, 240–244. doi:10.1007/BF03039052

Neubauer, P., Haggström, L., Enfors, S. -O., 1995. Influence of Substrate Oscillations on Acetate Formation and Growth Yield in Escherichia co/i Glucose Limited Fed-Batch Cultivations. Biotechnol. Bioeng. 47, 139–146.

Nguyen, T., Roddick, F.A., Fan, L., 2012. Biofouling of Water Treatment Membranes: A Review of the Underlying Causes, Monitoring Techniques and Control Measures. Membranes (Basel). 2, 804– 840. doi:10.3390/membranes2040804

Nie, S., Emory, S.R., 1997. Probing Single Molecules and Single Nanoparticles by Surface-Enhanced Raman Scattering. Science (80-.). 275, 1102–1106.

Nissinen, I., Nissinen, J., Keränen, P., Kostamovaara, J., 2017. On the effects of the time gate position and width on the signal-to-noise ratio for detection of Raman spectrum in a time-gated CMOS single-photon avalanche diode based sensor. Sensors Actuators, B Chem. 241, 1145–1152. doi:10.1016/j.snb.2016.10.021

Nissinen, I., Nissinen, J., Länsman, A.K., Hallman, L., Kilpelä, A., Kostamovaara, J., Kögler, M., Aikio, M., Tenhunen, J., 2011. A sub-ns time-gated CMOS single photon avalanche diode detector for Raman spectroscopy, in: European Solid-State Device Research Conference. doi:10.1109/ESSDERC.2011.6044156

Notingher, I., 2007. Raman Spectroscopy Cell-based Biosensors. Sensors 7, 1343–1358. doi:10.3390/s7081343

Notley-McRobb, L., Death, A., Ferenci, T., 2006. The relationship between external glucose concentration and cAMP levels inside. Biochem. J. 1909–1918. doi:10.1099/00221287-143-6-1909

Nuntawong, N., Eiamchai, P., Wong-ek, B., Horprathum, M., Limwichean, K., Patthanasettakul, V., Chindaudom, P., 2013. Shelf time effect on SERS effectiveness of silver nanorod prepared by OAD technique. Vaccum 88, 23–27. doi:10.1016/j.vacuum.2012.08.006

Nuutinen, T., 2014. Optical nanostructures for biological fluorescence and Raman measurements Conceptions. University of Eastern Finland.

Oo, S.Z., Chen, R.Y., Siitonen, S., Kontturi, V., Eustace, D.A., Tuominen, J., Aikio, S., Charlton, M.D.B., 2013. Disposable plasmonic plastic SERS sensor. OSA 21, 18484–18491. doi:10.1364/OE.21.018484

Pan, C.T., Wu, T.T., Chen, M.F., Chang, Y.C., Lee, C.J., Huang, J.C., 2008. Hot embossing of micro-lens array on bulk metallic glass. Sensors Actuators, A Phys. 141, 422–431. doi:10.1016/j.sna.2007.10.040

Papukashvili, N., 2009. Entwicklung eines in vitro Systems zur Un- tersuchung der initialen Bakterienadhäsion an selbstanordnenden Monoschichten. Hamburg.

Paquet-Mercier, F., Aznaveh, N.B., Safdar, M., Greener, J., 2013. A Microfluidic Bioreactor with in Situ SERS Imaging for the Study of Controlled Flow Patterns of Biofilm Precursor Materials. Sensors 13, 14714–14727. doi:10.3390/s131114714

Paschotta, R., 2004. Noise of mode-locked lasers (Part II): timing jitter and other fluctuations. Appl. Phys. B 79, 163–173. doi:10.1007/s00340-004-1548-9

Paul, A., Carl, P., Westad, F., Voss, J.P., Maiwald, M., 2016. Towards Process Spectroscopy in Complex Fermentation Samples and Mixtures. Chemie-Ingenieur-Technik 88, 756–763. doi:10.1002/cite.201500118

Petrich, J.W., Martin, J.L., Houde, D., Poyart, C., Orszag, a, 1987. Time-resolved Raman spectroscopy with subpicosecond resolution: vibrational cooling and delocalization of strain energy in photodissociated (carbonmonoxy)hemoglobin. Biochemistry 26, 7914–23. doi:10.1021/bi00398a056

Petry, R., Schmitt, M., Popp, J., 2003. Raman spectroscopy--a prospective tool in the life sciences. Chemphyschem 4, 14–30. doi:10.1002/cphc.200390004

Philbrick, C.R., 1994. Raman lidar measurements of atmospheric properties. pp. 922–931.

Premasiri, W.R., Krieger, N., Associates, W.R., 2005. Characterization of the Surface Enhanced Raman Scattering (SERS) of Bacteria. J. Phys. Chem. B 109, 312–320. doi:10.1021/jp040442n

Premasiri, W.R., Lee, J.C., Sauer-Budge, A., Th??berge, R., Costello, C.E., Ziegler, L.D., 2016. The biochemical origins of the surface-enhanced Raman spectra of bacteria: a metabolomics profiling by SERS. Anal. Bioanal. Chem. 1–17. doi:10.1007/s00216-016-9540-x

Procházka, M., 2016. Surface-Enhanced Raman Spectroscopy. Springer-Verlag Berlin Heidelberg, Prague.

Prucek, R., Ranc, V., Kvitek, L., Panacek, A., Zboril, R., Kolar, M., 2012. Reproducible discrimination between Gram-positive and Gram-negative bacteria using surface enhanced Raman spectroscopy with infrared excitation. Analyst 137, 2866–2870. doi:10.1039/c2an16310a

Rajalahti, T., Kvalheim, O.M., 2011. Multivariate data analysis in pharmaceutics: A tutorial review. Int. J. Pharm. 417, 280–290. doi:10.1016/j.ijpharm.2011.02.019

Ravindranath, S.P., Wang, Y., Irudayaraj, J., 2011. SERS driven cross-platform based multiplex pathogen detection. Sensors Actuators B Chem. 152, 183–190. doi:10.1016/j.snb.2010.12.005

Renishaw, P., 2017. Brochure: inVia confocal Raman microscope.

Rodriguez, L.G., Lockett, S.J., Holtom, G.R., 2006. Coherent Anti-Stokes Raman Scattering Microscopy: A Biological Review. J. Int. Soc. Anal. Cytol. 69, 659–676. doi:10.1002/cyto.a.20299

Rodriguez-Fernandez, D., Langer, J., Henriksen-Lacey, M., & Liz-Marzán, L. M. (2015). Hybrid Au–SiO2 core–satellite colloids as switchable SERS tags. Chemistry of Materials. 27, 7 , 2540-2545. doi:10.1021/acs.chemmater.5b00128

Rojalin, T., Kurki, L., Laaksonen, T., Viitala, T., Kostamovaara, J., Gordon, K.C., Galvis, L., Wachsmann-Hogiu, S., Strachan, C.J., Yliperttula, M., 2016. Fluorescence-suppressed time-resolved Raman spectroscopy of pharmaceuticals using complementary metal-oxide semiconductor (CMOS) single-photon avalanche diode (SPAD) detector. Anal. Bioanal. Chem. 408, 761–774. doi:10.1007/s00216-015-9156-6

Rowland-jones, R.C., Berg, F. Van Den, Racher, A.J., Martin, E.B., Jaques, C., 2017. Comparison of Spectroscopy Technologies for Improved Monitoring of Cell Culture Processes in Miniature Bioreactors. Biotechnol. Prog. 33, 337–346. doi:10.1002/btpr.2459

Ryabchikov, Y. V., Popov, A.A., Sentis, M., Timoshenko, V.Y., Kabashin, A. V., 2016. Structural properties of gold-silicon nanohybrids formed by femtosecond laser ablation in water at different fluences, in: Proceedings of SPIE. pp. 1–6. doi:10.1117/12.2217777

Ryder, A.G., De Vincentis, J., Li, B., Ryan, P.W., Sirimuthu, N.M.S., Leister, K.J., 2010. A stainless steel multi-well plate (SS-MWP) for high-throughput Raman analysis of dilute solutions. J. Raman Spectrosc. 41, 1266–1275. doi:10.1002/jrs.2586

Ryll, T., Wagner, R., 1991. Improved ion-pair high-performance liquid chromatographic method for the quantification of a wide variety of nucleotides and sugar- nucleotides in animal cells. J Chromatogr 570, 77–88. doi:10.1016/0378-4347(91)80202-N

Schlücker, S., 2014. Surface-enhanced raman spectroscopy: Concepts and chemical applications. Angew. Chemie - Int. Ed. 53, 4756–4795. doi:10.1002/anie.201205748

Schmid, T., Messmer, A., Yeo, B., 2008. Towards chemical analysis of nanostructures in biofilms II : tip-enhanced Raman spectroscopy of alginates. Anal. Bioanal. Chem. 391, 1907–1916. doi:10.1007/s00216-008-2101-1

Schmid, U., 2009. Entwicklung chemometrischer Methoden für die Klassifikation von Bakterien mittels Mikro-Raman-Spektroskopie. Technischen Universität Braunschweig.

Schmidt, M.A., Kiefer, J., 2013. Polarization-resolved high-resolution Raman spectroscopy with a light-emitting diode. J. Raman Spectrosc. 44, 1625–1627. doi:10.1002/jrs.4385

Schmitt, M., Popp, J., 2006. Raman spectroscopy at the beginning of the twenty-first century. J. Raman Spectrosc. 37, 20–28. doi:10.1002/jrs.1486

Schneider, R.P., Ferreira, L.M., Binder, P., Bejarano, E.M., Slongo, E., Machado, C.R., Rosa, G.M.Z., 2005. Dynamics of organic carbon and of bacterial populations in a conventional pretreatment train of a reverse osmosis unit experiencing severe biofouling. J. Memb. Sci. 266, 18–29. doi:10.1016/j.memsci.2005.05.006

Sengupta, A., Mujacic, M., Davis, E.J., 2006. Detection of bacteria by surface-enhanced Raman spectroscopy. Anal. Bioanal. Chem. 386, 1379–1386. doi:10.1007/s00216-006-0711-z

Sibbald, M.S., Chumanov, G., Cotton, T.M., 1996. Reduction of Cytochrome c by Halide-Modified , Laser-Ablated Silver Colloids. J. Phys. Chem. B 100, 4672–4678.

Sim, S.T. V, Suwarno, S.R., Chong, T.H., Krantz, W.B., Fane, A.G., 2013. Monitoring membrane biofouling via ultrasonic time-domain reflectometry enhanced by silica dosing. J. Memb. Sci. 428, 24–37. doi:10.1016/j.memsci.2012.10.032

Šmídová, N., 2012. Optimization of surface-enhanced Raman scattering spectroscopy for study of biologically important biomolecules and their interactions. Charles University.

Smith, E., Dent, G., 2005. Modern Raman Sectroscopy - A Practical Approach. John Wiley and Sons, West Sussex.

Smith, G.E., 2009. The invention and early history of the CCD. Nucl. Instruments Methods Phys. Res. Sect. A Accel. Spectrometers, Detect. Assoc. Equip. 607, 1–6. doi:10.1016/j.nima.2009.03.233

Smith, Z. J., Knorr, F., Pagba, C. V., & Wachsmann-Hogiu, S., 2011. Rejection of fluorescence background in resonance and spontaneous Raman microspectroscopy. Journal of visualized experiments. 51, 1-5. doi:10.3791/2592

Smyth, C.A., Mirza, I., Lunney, J.G., Mccabe, E.M., 2013. Applied Surface Science Surface-enhanced Raman spectroscopy (SERS) using Ag nanoparticle films produced by pulsed laser deposition. Appl. Surf. Sci. 264, 31–35. doi:10.1016/j.apsusc.2012.09.078

Smythe, E.J., Dickey, M.D., Bao, J., Whitesides, G.M., Capasso, F., 2009. Optical Antenna Arrys on a Fiber Facet for in Situ Surface-Enhanced Raman Scattering Detection. Nano Lett. 9, 1132–1138.

Song, J.J., Eesley, G.L., Levenson, M.D., 1976. Background suppression in coherent Raman spectroscopy. Appl. Phys. Lett. 29, 567–569. doi:10.1063/1.89189

Sowoidnich, K., Kronfeldt, H.D., 2012. Shifted excitation Raman difference spectroscopy at multiple wavelengths for in-situ meat species differentiation. Appl. Phys. B Lasers Opt. 108, 975–982. doi:10.1007/s00340-012-5160-0

Sparén, A., Johansson, J., Svensson, O., Folestad, S., 2009. Transmission raman spectroscopy for quantitative analysis of pharmaceutical solids raman. Am. Pharm. Rev. 12, 179–192. doi:10.1211/jpp.59.2.0005

Sperling, R.A., Rivera, P.G., Zhang, F., Zanella, M., Parak, W.J., 2008. Biological applications of gold nanoparticles. Chem. Soc. Rev. 37, 1745–2140. doi:10.1039/b712170a

Stillhart, C., Imanidis, G., Kuentz, M., 2013. Insights into Drug Precipitation Kinetics during In Vitro Digestion of a Lipid-Based Drug Delivery System Using In-Line Raman Spectroscopy and Mathematical Modeling. Pharm Res. doi:10.1007/s11095-013-0999-2

Strachan, C.J., Rades, T., Gordon, K.C., Rantanen, J., 2007. Raman spectroscopy for quantitative analysis of pharmaceutical solids. J. Pharm. Pharmacol. 179–192. doi:10.1211/jpp.59.2.0005

Streefland, M., Martens, D.E., Beuvery, E.C., Wijffels, R.H., 2013. Process analytical technology (PAT) tools for the cultivation step in biopharmaceutical production. Eng. Life Sci. 13, 212–223. doi:10.1002/elsc.201200025

Strehle, K.R., Cialla, D., Rösch, P., Henkel, T., Köhler, M., Popp, J., 2007. A Reproducible Surface-Enhanced Raman Spectroscopy Approach . Online SERS Measurements in a Segmented Microfluidic System. Anal. Chem. 79, 1958–1963.

Suzuki, M., Niidome, Y., Terasaki, N., Inoue, K., Kuwahara, Y., Yamada, S., 2004. Surface-Enhanced Nonresonance Raman Scattering of Rhodamine 6G Molecules Adsorbed on Gold Nanorod Films. Jpn. J. Appl. Phys. 43, 553–556. doi:10.1143/JJAP.43.L554

Sylvestre, J., Poulin, S., Kabashin, A. V, Sacher, E., Meunier, M., Luong, J.H.T., 2004. Surface Chemistry of Gold Nanoparticles Produced by Laser Ablation in Aqueous Media. J. Phys. Chem. B 108, 16864–16869. doi:10.1021/jp047134

Szymborski, T., Witkowska, E., Adamkiewicz, W., Waluk, J., Kaminska, A., 2014. Electrospun polymer mat as a SERS platform for the immobilization and detection of bacteria from fluid. Analyst 139, 5061–5064. doi:10.1039/C4AN01137F

Tamarov, K.P., Osminkina, L.A., Zinovyev, S. V., Maximova, K.A., Kargina, J. V, Gongalsky, M.B., Ryabchikov, Y., Al-kattan, A., Sviridov, A.P., Sentis, M., Ivanov, A. V, Nikiforov, V.N., Kabashin, A. V, Timoshenko, V.Y., 2014. Radio frequency radiation-induced hyperthermia using Si nanoparticle-based sensitizers for mild cancer therapy. Sci. Rep. 4, 1–7. doi:10.1038/srep07034

Tamer, U., Boyacı, İ.H., Temur, E., Zengin, A., Dincer, İ., Elerman, Y., 2011. Fabrication of magnetic gold nanorod particles for immunomagnetic separation and SERS application. J. Nanoparticle Res. 13, 3167–3176. doi:10.1007/s11051-010-0213-y

Tang, C.Y., Kwon, Y.N., Leckie, J.O., 2009. Effect of membrane chemistry and coating layer on physiochemical properties of thin film composite polyamide RO and NF membranes. II. Membrane physiochemical properties and their dependence on polyamide and coating layers. Desalination 242, 168–182. doi:10.1016/j.desal.2008.04.004

Temur, E., Hakki, İ., Tamer, U., Unsal, H., Aydogan, N., 2010. A highly sensitive detection platform based on surface-enhanced Raman scattering for Escherichia coli enumeration. Anal. Bioanal. Chem. 397, 1595–1604. doi:10.1007/s00216-010-3676-x

Thomsen, C., Reich, S., 2000. Double Resonant Raman Scattering in Graphite. Phys. Rev. Lett. 85, 5214–5217. doi:10.1103/PhysRevLett.85.5214

Tian, Z., Ren, B., Li, J., Yang, Z., 2007. Expanding generality of surface-enhanced Raman spectroscopy with borrowing SERS activity strategy. Chem. Commun. 3514–3534. doi:10.1039/b616986d

Timegate Instruments Oy, F., 2015. Timegate Instruments specification of 532 Raman instrument [WWW Document]. URL http://www.timegate.fi/products/ (accessed 7.29.17).

Tung, K., Damodar, H., Damodar, R., Wu, T., 2012. Online monitoring of particle fouling in a submerged membrane filtration system using a photointerrupt sensor array. J. Memb. Sci. 407–408, 58–70. doi:10.1016/j.memsci.2012.03.013

Uusitalo, S., Hiltunen, J., Karioja, P., Siitonen, S., Kontturi, V., Myllylä, R., Kinnunen, M., Meglinski, I., 2015. Performance and flow dynamics studies of polymeric optofluidic SERS sensors. J. Eur. Opt. Soc.-Rapid 15043, 1–8.

Uusitalo, S., Kögler, M., Välimaa, A.-L., Popov, A., Ryabchikov, Y., Kontturi, V., Siitonen, S., Petäjä, J., Virtanen, T., Laitinen, R., Kinnunen, M., Meglinski, I., Kabashin, A., Bunker, A., Viitala, T., Hiltunen, J., 2016. Detection of Listeria innocua on roll-to-roll produced SERS substrates with gold nanoparticles. RCS Adv. 6, 62981–62989. doi:10.1039/c6ra08313g

Uusitalo, S., Kögler, M., Välimaa, A. L., Petäjä, J., Kontturi, V., Siitonen, S., Laitinen R., Kinnunen M., Viitala T., Hiltunen J., J. A., 2017. Stability optimization of microbial surface-enhanced Raman spectroscopy detection with immunomagnetic separation beads. Optical Engineering. 56, 3, 037102. doi:10.1117/1.OE.56.3.037102

Uusitalo, S., Popov, A., Ryabchikov, Y. V, Bibikova, O., Alakomi, H., Juvonen, R., Kontturi, V., Siitonen, S., Kabashin, A., Meglinski, I., Hiltunen, J., Laitila, A., 2017. Surface-enhanced Raman spectroscopy for identification and discrimination of beverage spoilage yeasts using patterned substrates and gold nanoparticles. J. Food Eng. 212, 47–54.

van den Berg, F., Lyndgaard, C.B., Sørensen, K.M., Engelsen, S.B., 2013. Process Analytical Technology in the food industry. Trends Food Sci. Technol. 31, 27–35. doi:10.1016/j.tifs.2012.04.007

Velusamy, V., Arshak, K., Korostynska, O., Oliwa, K., Adley, C., 2010. An overview of foodborne pathogen detection: In the perspective of biosensors. Biotechnol. Adv. 28, 232–254. doi:10.1016/j.biotechadv.2009.12.004

Vielma, J., Leung, P.T., 2007. Nonlocal optical effects on the fluorescence and decay rates for admolecules at a metallic nanoparticle. J. Chem. Phys. 126, 1–8. doi:10.1063/1.2734549

Virtanen, T., Reinikainen, S.P., Kögler, M., Mänttäri, M., Viitala, T., Kallioinen, M., 2017. Real-time fouling monitoring with Raman spectroscopy. J. Memb. Sci. 525, 312–319. doi:10.1016/j.memsci.2016.12.005

Vohnik, S., Hanson, C., Tuma, R., Fuchs, J.A., Woodward, C., Thomas, G.J., 1998. Conformation , stability , and active-site cysteine titrations of Escherichia coli D26A thioredoxin probed by Raman spectroscopy. Protein Sci. 35, 193–200.

Vonhoff, S., Condliffe, J., Schiffter, H., 2010. Journal of Pharmaceutical and Biomedical Analysis Implementation of an FTIR calibration curve for fast and objective determination of changes in protein secondary structure during formulation development. J. Pharm. Biomed. Anal. 51, 39–45. doi:10.1016/j.jpba.2009.07.031

Wagener, P., Schwenke, A., Barcikowski, S., 2012. How Citrate Ligands Affect Nanoparticle Adsorption to Microparticle Supports. Langmuir 28, 6132–6140. doi:10.1021/la204839m

Wang, J., Xie, X., Feng, J., Chen, J.C., Du, X.-J., Luo, J., Lu, X., Wang, S., 2015. Rapid detection of Listeria monocytogenes in milk using confocal micro-Raman spectroscopy and chemometric analysis. Int. J. Food Microbiol. 204, 66–74. doi:10.1016/j.ijfoodmicro.2015.03.021

Wang, Y., Ni, Z., Hu, H., Hao, Y., Wong, C.P., Yu, T., Thong, J.T.L., Wang, Y., Ni, Z., Hu, H., Hao, Y., Wong, C.P., Yu, T., 2010. Gold on graphene as a substrate for surface enhanced Raman scattering study Gold on graphene as a substrate for surface enhanced Raman. Appl. Phys. Lett. 97, 3. doi:10.1063/1.3505335

Wei, D., Chen, S., Liu, Q., 2015. Review of Fluorescence Suppression Techniques in Raman Spectroscopy. Appl. Spectrosc. Rev. 50, 387–406. doi:10.1080/05704928.2014.999936

Weidemaier, K., Carruthers, E., Curry, A., Kuroda, M., Fallows, E., Thomas, J., Sherman, D., Muldoon, M., 2015. Real-time pathogen monitoring during enrichment: a novel nanotechnology-based approach to food safety testing. Int. J. Food Microbiol. 198, 19–27. doi:10.1016/j.ijfoodmicro.2014.12.018

Weller, D., Andrus, A., Wiedmann, M., Bakker, H.C. Den, 2015. Listeria booriae sp . nov . and Listeria newyorkensis sp . nov ., from food processing environments in the USA. Int. J. Syst. Evol. Microbiol. 65, 286–292. doi:10.1099/ijs.0.070839-0

Wett, M., 2005. Foulingverhalten des Membranbelebungs verfahrens und Auswirkungen auf die Leistungsfähigkeit. Kassel.

Wilén, B.M., Onuki, M., Hermansson, M., Lumley, D., Mino, T., 2008. Microbial community structure in activated sludge floc analysed by fluorescence in situ hybridization and its relation to floc stability. Water Res. 42, 2300–2308. doi:10.1016/j.watres.2007.12.013

Willemse-Erix, D.F.M., Scholtes-timmerman, M.J., Jachtenberg, J., Leeuwen, W.B. Van, Horst-kreft, D., Schut, T.C.B., Deurenberg, R.H., Puppels, G.J., Belkum, A. Van, Vos, M.C., Maquelin, K., 2009. Optical Fingerprinting in Bacterial Epidemiology : Raman Spectroscopy as a Real-Time Typing Method ▯. J. Clin. Microbiol. 47, 652–659. doi:10.1128/JCM.01900-08

Wilson, R., Monaghan, P., Bowden, S.A., Parnell, J., Cooper, J.M., 2007. Surface-Enhanced Raman Signatures of Pigmentation of Cyanobacteria from within Geological Samples in a Spectroscopic-Microfluidic Flow Cell. Anal. Chem. 79, 7036–7041.

Witkowska, E., Korsak, D., Kowalska, A., Księżopolska-Gocalska, M., Niedziółka-Jönsson, J., Roźniecka, E., Michałowicz, W., Albrycht, P., Podrażka, M., Hołyst, R., Waluk, J., Kamińska, A., 2017. Surface-enhanced Raman spectroscopy introduced into the International Standard Organization (ISO) regulations as an alternative method for detection and identification of pathogens in the food industry. Anal. Bioanal. Chem. 409, 1555–1567. doi:10.1007/s00216-016-0090-z

Xie, C., Goodman, C., Dinno, M.A., Li, Y., 2004. Real-time Raman spectroscopy of optically trapped living cells and organelles. Opt. Eng. 12, 6208–6214.

Yang, D., Zhou, H., Haisch, C., Niessner, R., Ying, Y., 2016. Reproducible E. coli detection based on label-free SERS and mapping. Talanta 146, 457–463. doi:10.1016/j.talanta.2015.09.006

Yu, W.W., White, I.M., 2012. A simple filter-based approach to surface enhanced Raman spectroscopy for trace chemical detection. Analyst 137, 1168–1173. doi:10.1039/c2an15947c

Zappa, F., Tisa, S., Tosi, A., Cova, S., 2007. Principles and features of single-photon avalanche diode arrays. Sensors Actuators, A Phys. 140, 103–112. doi:10.1016/j.sna.2007.06.021

Zeman, E.J., Schatz, G.C., 1987. An accurate electromagnetic theory study of surface enhancement factors for silver, gold, copper, lithium, sodium, aluminum, gallium, indium, zinc, and cadmium. J. Phys. Chem. 91, 634–643. doi:10.1021/j100287a028

Zhang, C., Abdijalilov, K., Grebel, H., 2007. Surface enhanced Raman with anodized aluminum oxide films. J. Chem. Phys. 127, 44701. doi:10.1063/1.2752498

Zhang, D., Go, B., Barcikowski, S., 2017. Laser Synthesis and Processing of Colloids : Fundamentals and Applications. Chem. Rev. 117, 3990–4103. doi:10.1021/acs.chemrev.6b00468

Zhang, D., Xie, Y., Deb, S.K., Davison, V.J., Ben-Amotz, D., 2005. Isotope Edited Internal Standard Method for Quantitative Surface-Enhanced Raman Spectroscopy. Anal. Chem. 77, 3563–3569.

Zhang, Z.M., Chen, S., Liang, Y.Z., Liu, Z.X., Zhang, Q.M., Ding, L.X., Ye, F., Zhou, H., 2010. An intelligent background-correction algorithm for highly fluorescent samples in Raman spectroscopy. J. Raman Spectrosc. 41, 659–669. doi:10.1002/jrs.2500

Zhao, H., Wu, L., Zhou, Z., Zhang, L., Chen, H., 2013. Improving the antifouling property of polysulfone ultrafiltration membrane by incorporation of isocyanate-treated graphene oxide. Phys. Chem. 9084–9092. doi:10.1039/c3cp50955a

Zhao, X., Lin, C.-W., Wang, J., Oh, D.H., 2014. Advances in Rapid Detection Methods for Foodborne Pathogens. J. Microbiol. Biotechnol. 24, 297–312. doi:10.4014/jmb.1310.10013

Zhou, H., Yang, D., Ivleva, N.P., Mircescu, N.E., Niessner, R., Haisch, C., 2014. SERS detection of bacteria in water by in situ coating with Ag nanoparticles. Anal. Chem. 86, 1525–1533. doi:10.1021/ac402935p

Zhou, H., Yang, D., Ivleva, N.P., Mircescu, N.E., Schubert, S., Niessner, R., Wieser, A., Haisch, C., 2015. Label-Free in Situ Discrimination of Live and Dead Bacteria by Surface-Enhanced Raman Scattering. Anal. Chem. 87, 6553–6561. doi:10.1021/acs.analchem.5b01271

List of figures

Figure 13 – Comsol simulation results: (A) Fluid flow velocity profile inside the flow-cell shown as a top-view and as an isometric 3D projection. (B) Wall shear stresses inside the flow-cell shown as a top-view and as an isometric 3D projection.

Figure 14 – Detection of Adenine with online (blue curve) and offline SERS (red curve) by using Au NP SERS-sensing-area on PS-membranes. (A) Raw SERS-measurement data without off-set. (B) Normalized, scaled, smoothed and baseline-corrected SERS-measurement data.

Figure 15 – Long-term stability test of Au NP SERS-sensing-area during immersion in adenine solutions of different concentrations. SERS-spectra after 0 days (A), after 7 days (B), band changes after 7 days compared to 0 days (C) and after 13 days (D).

Figure 16 – SEM images of BD adhesion on NF-membrane without (left column; A, C, E) and with (right column; B, D, F) Au NP SERS-sensing-area at different sampling times 6 h (A and B), 16 h (C and D) and 26 h (E and F). BDs are visible as rod-shaped depositions.

Figure 17 – (A) Raw SERS-spectra of BD formed on SERS-substrate immobilized on MCE-membrane (red), SERS-spectra of BD-grow on MCE-membrane without SERS-substrate (blue) and LB as reference (green) separated with off-set. (B) SERS-spectra of BD in PBS drop on Au MCE membrane (blue), immersed in static pure LB-media (red) and LB as reference (green).

Figure 18 – Photograph of roll-to-roll patterned polymer webs and die-cut sheets before and after gold deposition.

Figure 19 –Schematic of a PDMS well on top of a patterned SERS substrate with IMS bound *L. innocua* and Au NPs. The integrated hydrophobic PDMS well concentrates the sample inside the well on top of the SERS substrate in a more consistent manner than a free droplet on top of the substrate would. Au NPs are located around the bacteria giving a stronger SERS enhancement. IMS beads bind the bacteria around them and concentrate them inside the excitation laser beam strengthening the SERS signal.

Figure 20 – (A) TEM image of IMS beads with gold nanoparticles. The scale in the picture is 500 nm. (B) SEM image of the IMS beads (Invitrogen dynabeads) on top of patterned SERS substrate.

Figure 21 – (A–C) TEM images of the different sized Au NPs: small, medium and large size Au NPs respectively. (D–F) The corresponding size distribution histograms calculated from TEM images of the Au NPs with Gaussian fit: small, medium and large size Au NPs respectively. Each histogram has been calculated from 100 particle sizes with ImageJ software. (G) UV-Vis spectrum for the small, medium and large size Au NPs.

Figure 22 – (A) concentration series of the IMS bound *L. innocua* ATCC 33090 with the Au NPs inside a PDMS well on top of a patterned SERS surface shows how the large Au NPs have the best separation ability between the smallest concentrations and the 0 reference. The results are an average of 18 spectrums. (B) A bar plot of the SERS intensity for the dominant *L. innocua* peak at 737 cm^{-1} for different concentrations with the Au NPs inside a PDMS well on top of patterned SERS surface clarifies the choice of large AuNP as the one to use for further studies for best sensitivity.

Figure 23 – (A) The effect of IMS concentration to the *L. innocua* ATCC 33090 SERS intensity with the Au NPs inside a PDMS well on top of patterned SERS surface. The cumulative effect of the IMS beads to the bacteria strengthens the SERS signal considerably. The intensity of 1×10^5 CFU ml^{-1} sample with IMS has 2 times stronger 737 cm^{-1} peak than the 1×10^6 CFU ml^{-1} sample without IMS. (B) The variation in SERS spectra of 1×10^5 CFU ml^{-1} *L. innocua* with IMS between 9 measured points.

Figure 24 – (A) IMS bound 1×10^7 CFU ml^{-1} *L. innocua* ATCC 33090 inside a PDMS well on top of patterned SERS surface. (B) IMS bound 1×10^7 CFU ml^{-1} 1 *L. innocua* ATCC 33090 with large Au NPs inside a PDMS well on top of a silicon wafer. (C) IMS bound 1×10^7 CFU ml^{-1} *L. innocua* ATCC 33090 with large Au NPs inside a PDMS well on top of a patterned SERS surface. (D) A bar plot of the SERS intensity for the dominant *L. innocua* peak 737 cm^{-1} for the cases presented in (A–C).

Figure 25 – (A) Baseline corrected SERS spectra from *L. innocua* ATCC 33090 with large Au NPs inside a PDMS well on top of patterned SERS surface with IMS beads. Detected with 20 × magnification with a detection limit between 1×10^7 CFU ml^{-1} and 1×10^6 CFU ml^{-1}. The peaks maintaining their height with lower concentrations are caused by cultivation media residuals, Au NPs, IMS beads and other disturbances coming from the sample matrix. (B) Comparison of baseline corrected Raman intensities for the culturing media, i.e., LEE broth, and the 0 CFU ml^{-1} sample. The reason behind the peaks remaining in the *L. innocua* spectrum as the sample concentration is lowered are the peaks originating from the culture broth and the buffer solutions used for IMS bead washing steps.

Figure 26 – Three SERS spectra of *L. innocua* were compared to confirm that the measured spectrum originates from the assumed bacteria. The literature reference has been borrowed from a publication by Luo, B. Steven et al. (2008) with a concentration of 1×10^8 CFU ml^{-1} *L. innocua* measured with CW 785 nm laser excitation with Ag NPs. The 785 nm CW-laser excitation with the in-house built device has been recorded from 1×10^6 CFU ml^{-1} IMS bound *L. innocua* ATCC 33090 with large Au NPs inside a PDMS well on top of a patterned SERS surface with IMS beads, detected with 40 × magnification. The 532 nm Time-gated pulsed laser excitation is a AgNP-enhanced SERS spectra of 1×10^6 CFU ml^{-1} IMS bound *L. innocua* ATCC 33090 placed on top of a glass slide and 40 × magnification (TG-SERS).

Figure 27 – (A) A normalised concentration series for LOD estimation. (B) An exponential fit for the normalised concentration series in logarithmic scale for the entire series and a linear fit for the small concentrations. (C) Comparison of the 737 cm^{-1} peak intensity for different concentration series with 5–10 ml dried IMS bound *L. innocua* ATCC 33090 samples placed with Au NPs into a 1–1.5 mm PDMS well on top of SERS substrate. (D) Comparison of baseline corrected Raman intensities for three of the concentration series. All figures are a mean of 9 measurement points with mean absolute deviations.

Figure 28 – HR-TEM images of Au-100 % (100 % Au) (A), Au-60 % (60 % Au/40 % Si) (B), and Au-30 % (30 % Au/70 % Si) (C) prepared by methods of femtosecond laser ablation in water, with corresponding size distribution.

Figure 29 – Normalized extinction (absorption + scattering) (A) and Raman (B) spectra from laser-synthesized Au-based NPs with different content of Au in their composition: Au-100 % (black), Au-60 % (red) and Au-30 % (blue).

Figure 30 – Normalized SERS spectra (upon 785 nm CW excitation) of 100 µM Rhodamine 6G (R6G) detected with different Au-Si compositions (Au-100 %, Au-60 % and Au-30 %) on top of a silicon wafer. The average SERS spectra were calculated from 18 points measured for each concentration.

Figure 31 – A) SERS spectra of 2 µl of dried 100 µM Rhodamine 6G (R6G) detected with different Au-Si composition in a 1.5 mm diameter PDMS well on top of a polymer-based Au coated SERS substrate. The average SERS spectra were calculated from 18 points measured for each concentration. B) Normalized with integration time SERS spectra of a concentration series of R6G detected using Au-60 % NPs and a polymer-based Au-coated SERS substrate. The average SERS spectra were calculated from 9 points measured for each concentration using 785 nm CW excitation.

Figure 32 – Normalized SERS spectra of IMS bead captured *L. innocua* (IMS LIN) detected using a polymer-based SERS substrate (green) and a combination of the substrate and Au-60 % NPs (red) using 785 nm CW excitation.

Figure 33 – SERS spectra of *E. coli* W3110 measured with time-gated Raman using 532 nm wavelength picosecond pulsed excitation with the use of Au-60 % NPs as Raman probes (red) and without them (green). For comparison we show Raman spectra without time gating (pink).

Figure 34 – Different spectroscopic set-ups: TG-Raman (TGM1) with pulsed green λ_{exc} = 532 nm laser, NIR-Raman (RXN1) with red λ_{exc} = 785 nm laser and confocal setting of CW-microscope (InVia) with orange λ_{exc} = 633 nm laser used in this work; each measurement without and with injection of Ag NPs into each microwell.

Figure 35 – Microwell with supernatant sample - symbolical representation of (A) Raman and (B) SERS measurement set-up in a single aluminium well.

Figure 36 – Normal Raman results with CW-Raman (RXN1), TG-Raman and CW-microscope (A-C) and with SERS measurement mode (D-F).

Figure 37 – Normalized (0-1) concentrations of A) glucose (1130 cm^{-1}), B) acetate (877–891 cm^{-1}), C) cAMP (731–736 cm^{-1}), and D) AMP (1320–1340 cm^{-1}), corresponding max. peak height measured by NIR-Raman (red triangles) and TG-Raman (green dots) in SERS mode except for acetate (Raman max. peaks). The yellow curve with squares refers to the actual HPLC concentration in mM per sample during the cultivation.

Figure S1 - Normalized extinction (absorption + scattering) UV-Vis spectrum of Ag-based NPs used for SERS detection

Figure S2 - Time-Gate (TG) raw-data as data cubes including SERS/Raman (x-axis), intensity (y-axis) and temporal signal as decay time (z-axis) of supernatant sample at beginning of the cultivation S0 (0h) and the end S21 (21h), SERS results (A, C, E) and Raman results (B, D, F). (A) – TG with SERS S0, (C) TG with SERS S21 resulting in 5-6 x higher raw-signal with clearly identifiable peaks compared to (B) TG without SERS which shows low fluorescence background for S0 and clearly increased fluorescence background for (D) at S21. The decay time in nanoseconds is set to cover the same range for all measurements up to 2 ns. (E) Overlay of SERS results and (F) overlay of Raman results.

Figure S3 - Integration of the regression coefficients for (A) AMP and (B) cAMP over the spectral range respectively with SERS on NIR-Raman.
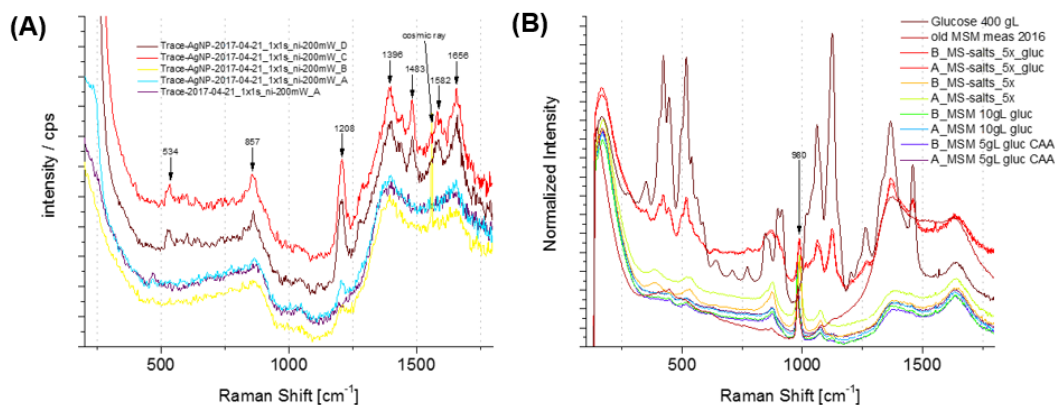
Figure S4 - Trace elements of MSM-medium: (A) with SERS and without including repetition measurements; (B) Pure glucose 400 g/L without SERS, MSM-medium with glucose and salts.

Figure S5 - (A) MgSO4 with SERS (red/black) and without (green/blue) including repetition measurements; (B) Thiamine with SERS (red/black) and without (green/blue) including repetition measurements; (C) Mineral salt medium (MSM) as stock-solution with nutrition components as mix before usage at cultivation – difference of SERS bands (red/black) and without SERS (violet), yellow and cyan spectra are the SERS measurements with decreased peaks after more than 1h after injection of the Ag NPs into the microwells.

Figure S6 - PLSR results including weighted regression coefficients (upper row) and predicted vs. reference plots (lower row) for (A) cAMP using the micro-Raman (RMSEC/RMSEC = 0.042/0.056), (B) cAMP using the NIR-Raman spectrometer (RMSEC/RMSEC = 0.0098/0.0187). Black-colored regression coefficients are considered significant, blue-colored not. Blue colors refer to calibration data and red colors to full cross validation in the regression plots.

Figure S7 – PLSR results for acetate from (A) NIR-Raman and (B) micro-Raman spectra using cross validation. Upper left: scores plot, upper right: weighted regression coefficients, lower left: explained variance and lower right: vs. reference plots (lower lane). Black-colored regression coefficients are considered significant, blue-colored not. Blue colors refer to calibration data and red colors to full cross validation in the regression plots.

Figure S8 - Exemplarily presentation of fluorescence background influence of sample S21 (21h of cultivation) with SERS and without – (A) TG-SERS (green/dark-green), NIR-Raman-SERS (red/dark-red) and micro-Raman-SERS-microscope (orange/pink) with repeated measurement; (B) TG-Raman (green/dark-green), NIR-Raman (red/dark-red) and micro-Raman (orange/pink) with repeated measurement. The sharp peaks at around (A) 1200 and 1300 cm^{-1} and (B) 1170 cm^{-1} in the micro-Raman spectra denote interfering's of the SERS/Raman detection by cosmic rays.

List of tables

Table 1 – Performance comparison for different SERS methods.

Table 2 – Comparison of the level of the interfering Raman-signal of different pure non-fouled filter-membranes determined with a confocal Raman-scanning-microscope.

Table 3 – Raman bands detected for L. innocua ATCC 33090.

Table 4 – Characteristics of Au-based NPs prepared by laser ablation of the gold target in deionized water or Si NPs colloidal solutions.

Table 5 – Tentative Raman/SERS band assignments with different spectroscopic settings (- not detectable; + detectable; ND out of spectral range).

Table 6 – Prediction of analyte concentrations based on Raman and SERS measurements.